Developing a BIPVT

Building Integrated PV-Thermal System

S. Garg

TU Delft

Delft University of Technology

SET3901

Graduation Project

Developing a BIPVT

Building Integrated PV-Thermal System

Author:

Shiwankar Garg (4576446)

Supervisors:

Prof. Ir. Arno Smets

Dr. Ir. Rudi Santbergen

Ir. Michiel Mensink

7th November 2018

Abstract

Photovoltaic Technologies in recent years have gained immense attention owing to reduced costs and increasing efficiencies. While decades of research in Photovoltaic Thermal (PVT) technologies, producing thermal and electrical energy simultaneously have brought these costs further down, improving a system's overall performance. PVT collectors consist of PV modules with a thermal absorber bonded/attached underneath them. Excessive solar radiation that is not converted into electricity by the panels is released as heat, causing their temperatures to rise. Rising PV panel temperatures have an adverse effect on their efficiency, particularly for building integrated photovoltaics, that generally lack sufficient ventilation for this heat release. Thermal absorbers for PVT systems, are designed specifically for absorbing the excess heat generated by PV modules. In practise, helping the panels perform better by effectively removing the heat present behind them, with the help of a heat transfer fluid.

This project has been a collaborative effort between the TU Delft, and Exasun BV, a solar panel manufacturer located in the Netherlands. At Exasun, the project has also benefited by being a part of a larger consortium project, the PVT inSHaPe, currently underway at the Solar Energy Application Centre (SEAC), in Eindhoven. PVT inSHaPe aims to realise zero energy buildings by integrating PVT systems with heat pumps alongside effective thermal storage. As a manufacturer, Exasun BV specialises in state of the art building integrated photovoltaic systems (BIPV). BIPV systems aim to integrate photovoltaic technologies seamlessly into building facades. In doing so, they forego essential thermal ventilation required for maintaining lower panel temperatures. Thus, a novel BIPVT design was developed in-house at Exasun, for extracting the excess heat of panels, and utilising it to match the domestic hot water and space heating demand for Dutch households.

A simple thermal model for concentrating PV-Thermal collectors, currently under development at the TU Delft was validated alongside widely used steady-state and quasi-dynamic thermal models. Individually calculated thermal efficiencies from the models were juxtaposed, with the simple thermal model recording an error of 1.65 % against the steady-state model, and an error of 9.21 % against the quasi-dynamic model. Once validated, the model was used further for system characterisation and performance evaluations of the design.

Various technology concepts have been tested extensively. However, further feasibility, reliability and optimisation studies need to be performed, in order to test the novel, cost-effective, and relatively maintenance free design in mind. The performance of PVT systems rely on high irradiance levels from the sun, and module temperatures. As space heating demands are higher during winter months, even after heat pump integration, the system is not effective enough to match the entirety of the load demand, and must be coupled with an auxiliary (electrical) heater, that can be powered by the PV system. Presumptive performance analysis carried out for a simulated household, revealed an average thermal efficiency of 10 % for the design, while recording a combined efficiency of 36 %. The stand-alone system was able to match over 55 % of the domestic hot water demand. When combined with a heat pump, the system is able to meet roughly 80 % of the hot water demand, while it is able to match almost 40 % of the complete thermal demand for a household.

Contents

List of Figures

List of Tables

Nomenclature

α	Absorption factor	%
β	Solar panel's temperature coefficient for electrical efficiency	
$\dot{V}$	Volumetric flow rate	kg/m^3
ϵ	Hemispherical emittance	%
η_e^{sys}	Annual electrical system efficiency	%
η_{th}^{sys}	Annual thermal system efficiency	%
η_E	Electrical efficiency	%
η_T	Thermal efficiency	%
η_C	Combined system efficiency	%
$\eta_{E,avg}$	Average electrical efficiency	%
η_{STC}	Electrical efficiency at standard test conditions	%
$\frac{\epsilon}{\alpha}$		0.98
$\frac{w}{W}$	Concentration factor for concentrating PV/Thermal collectors	-
ρ	Heat transfer fluid density	kg/m^3
ρ_p	Density of fluid to be pumped	kg/m^3
$\rho_{ref,liq}$	Liquid density of the heat pump's refrigerant	kg/m^3
σ	Stefan-Boltzmann constant	$5.67 \times 10^-8 W/m^2K^4$
τ	Rate of transmission	
θ	Incidence angle	deg
A_{eff}	Effective absorption factor for PV cells	%
b_1	Heat loss coefficient	W/m^2K
b_2	Wind speed dependence of heat loss coefficient	J/m^3K
b_o	Incident angle modifier for beam radiation	
b_u	Wind speed dependence of heat loss coefficient	s/m
c_1	Heat loss coefficient at zero-loss efficiency $(T_m - T_{amb})$	W/m^2K
c_2	Temperature dependence of heat loss coefficient	W/m^2K^2
c_3	Wind speed dependence of heat-loss coefficient	J/m^2K
c_4	Long-wave irradiance dependence of the heat losses	W/m^2K
c_5	Effective thermal capacitance	J/m^2K
c_6	wind speed dependence of zero-loss efficiency	s/m
c_p	Specific heat capacity for the HTF	$J/(kgK)$

$c_{p,ref}$	Specific heat capacity of the heat pump's refrigerant	J/kgK
E_e^{col}	Annual electrical yield for a system	kWh/y
E_{th}^{col}	Annual heat generated by the collector	kWh/y
E_{dhw}^{dem}	Annual domestic hot water demand	kWh/y
E_{sh}^{dem}	Annual domestic space heating demand	kWh/y
E_L	Long-wave irradiance	W/m^2
E_{sun}	Annual incident solar energy per m^2	kWh/y
E_{use}	Useful energy generated	W
F_R	Heat removal factor	-
G_b	Global beam radiation	W
G_d	Global diffuse radiation	W
G_{POA}	Global plane of array irradiance	W/m^2
G_{sun}	Irradiance at standard test conditions	W/m^2
G_{sun}	Solar irradiation corrected for long-wave irradiation	W/m^2
h_{ca}	Heat loss coefficient from cell to ambient	$W/m^{2o}C$
h_{cw}	Heat gain coefficient from cell to fluid	$W/m^{2o}C$
I_{mpp}	Maximum operating current	A
I_{SC}	Short-circuit current	A
$K_{\theta b}$	Incidence angle modifier for beam radiation	-
$K_{\theta d}$	Incidence angle modifier for diffuse radiation	-
m_{Ref}	Mass flow rate for the heat pump	kg/s
P_h	Hydraulic power required by a pump	kW
P_{ca}	Heat lost from PV cells to atmosphere	W
P_{cw}	Heat gained from PV cells to fluid	W
P_{Rated}	Rated output power at STC	W
P_{sc}	Heat absorbed from the sun to PV cells	W
Q_C	Heat extracted from the BIPVT	W
Q_i	Heat absorbed by the collector	W
Q_o	Heat lost by the collector	W
q_p	Flow rate	kg/s
Q_u	Useful heat gain by the collector	W
Q_w	Heat extracted by thermal storage tank	W
T_1	Heat pump evaporator outlet temperature	^oC
T_2	Heat pump condenser inlet temperature	^oC
T_3	Heat pump condenser outlet temperature	^oC

T_4	Heat pump evaporator inlet temperature	^oC
T_5	Storage tank inlet temperature (collector loop inlet)	^oC
T_6	Storage tank outlet temperature (collector loop outlet)	^oC
T_7	House inlet temperature (demand loop inlet)	^oC
T_8	House outlet temperature (demand loop outlet; mains)	^oC
T_c	PV Cell temperature	^oC
T_m	Mean collector temperature	^oC
T_w	Fluid temperature at each segment x	^oC
T_{amb}	Ambient temperature	^oC
T_{red}	Reduced temperature	$(m^2{}^oC)/W$
T_{stag}	Stagnation temperature	^oC
$T_{w,in}$	inlet water temperature for BIPVT	^oC
$T_{w,out}$	Outlet water temperature for BIPVT	^oC
U_L	Overall heat loss coefficient	$W/(m^2K)$
V_{mpp}	Maximum operating voltage	V
V_{OC}	Open circuit voltage	V
Y_f	Useful energy yield of a system	-
Y_r	Reference yield for a system	-
A	Aperture area of the collector	m^2
COP	Coefficient of performance	-
FF	Fill factor for a cell or module	-
g	Earth's gravitational constant	m/s^2
h	Differential head to be covered	m
l	Thermal adjustment length	m
m	Mass flow rate for the BIPVT	kg/s
Pr	Performance ratio	%
Q	Heat flow	W
SF	Solar Fraction	%
u	Wind speed	m/s
W	Concentration length for the PV collector	m
W	Work done by compressor of a heat pump	W
w	Width of the thermal absorber	m
x	Size of each segment of the thermal absorber	m

Chapter 1

Introduction

This chapter will provide some background into the photovoltaic-thermal industry, along with some information about the consortium project that this project has been a part off. The third section introduces the project definition, followed by thesis objectives.

1.1 Background

The fundamental behind a photovoltaic cell consists of converting incident sunlight into electricity. This conversion, termed as the photovoltaic effect, forms the basics of PV technology. Photovoltaic cells are semiconductor devices, wherein weakly bonded electrons (negatively charged) occupy the energy bands in the valence band of the semiconductor, whereas holes (positively charged) occupy the energy levels in the conduction band. Band gap energy, enforced on the valence electrons breaks these electronic bonds, thus making the electrons mobile, leading to their movement to the conduction band. This movement leads to the conduction of energy (electricity) in the form of a charge, through the material by free electrons. This band gap energy is supplied by incident photons on the photovoltaic cell, which constitutes the particles of light, coming from the sun [42]. Further in-depth information about the internal workings of a solar PV cell can be found in the work carried out by Hersch and Zweibel [36].

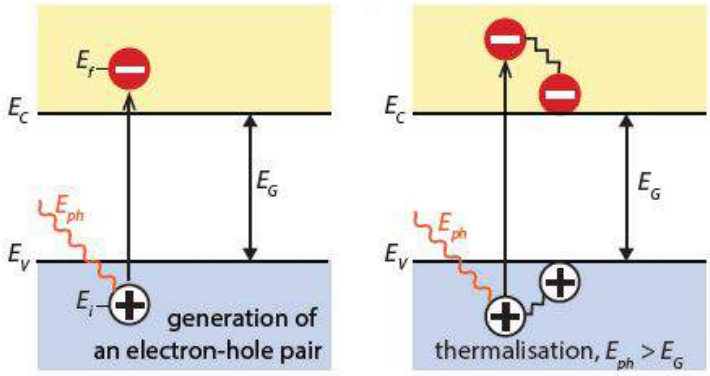

Figure 1.1: Photon Absorption illustration in a semiconductor, with bandgap E_g [42]

Solar energy has travelled a long way, from the photovoltaic effect to where it is today. Accounting for roughly 5% of the world's energy production, it is projected to rise to about 9% of the world's total energy production [58]. For 2011, solar power generation recorded an estimated LCOE of 0.14 €/kWh in the Netherlands, whereas wing recorded an estimate of 0.09 €/kWh [29]. True grid parity, will be achieved when solar electricity costs around utility prices, before capital subsidies. With storage included, covering for solar power's intermittency, there is still a long way to go before we can truly reach grid parity [41]. However, with its decreasing costs, solar energy is on track to being the largest energy provider for the future. Expected to be achieved between 2020 and 2030, in Northern Europe.

However, for over a century now, electricity has not been the only form of energy generation from solar energy. Solar thermal technologies have been primarily used for water heating purposes. They utilise the transfer of heat from solar radiation, running a thermodynamic system, essentially a generator. The first use of such a technology can be dated back to over a hundred years, as early as 1896 in the United States. However, the technology was still in its nascent stages then, and went through extensive advancements only recently, towards the later part of the 20th century [39]. Somewhat recently, towards the end of the 20th and the early start of the 21st century, solar photovoltaic technologies started getting integrated with solar thermal technologies, to effectively utilise the same area for two forms of energy generation. Various concepts and working designs have been developed for the same, which will be looked into further, at a later part in this report.

1.2 PVT inSHaPe Consortium Project

This project has been a collaborative effort between the TU Delft and Exasun BV for realising improved integration of PV-Thermal Systems into Dutch Households. Owing to the collaboration with Exasun BV, this project is also a part of the project consortium, *PVT inSHaPe*, consisting of a plethora of research partners such as TNO, Solartech, Dimark Solar, NRGTEQ, W/E advisers, Resource Solar, Conico Valves, TU Eindhoven and Solar Energy Application Centre (SEAC). The project deals with realising zero-energy buildings, by combining PV-Thermal systems with a heat pump. Done so, in order to cover household domestic hot water and space heating demands of a house/building.

At SEAC, PVT inSHaPe consortium project aims to design, realise and validate optimised PV/Thermal and Heat pump integrated systems. For which, the broad consortium of partners listed above have been working towards designing optimal systems. With Exasun, Energiedak and DimarkSolar providing and testing new PVT design concepts. Whereas based on their expertise in the particular area, TNO and Conico Valves are developing a heat pump and heat storage system respectively. Designed particularly for optimised PVT integration.

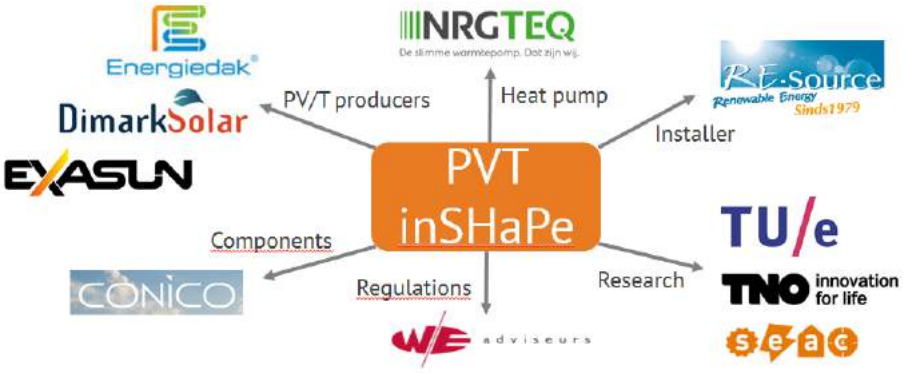

Figure 1.2: PVT inSHaPe Consortium Project

1.3 Project Definition

Currently, standard solar panel designs allow them to generate electricity with a panel efficiency of 20% at best. Meaning that roughly 80% of the incoming sunlight is not being converted into electricity. Rather, it is dissipated as heat. Therefore, combining a standard PV panel with a thermal collector at the back for harvesting this heat seems logical enough to improve the total energy harvested. The system should be able to generate both electricity and thermal energy simultaneously, in the same area.

A plethora of new houses have already disconnected themselves from the Dutch gas-grid, utilising ground-sourced heat pumps for their hot water requirements. In a PVT system, the heat pump would use solar-heated water.

Owing to high water temperatures, the heat pumps can reach a relatively high coefficient of performance (e.g., 5 kWh-thermal supplied per 1 kWh-electrical utilised). For an effective PVT system design, a PV Thermal panel, heat pump and a hot water storage facility is required. The proposed approach is to design a CAD model of the system on SolidWorks (CAD Software). After which, a new set of 50W Solar Panels will be manufactured, along with a new thermal absorber and mounting design. Experimental tests will be carried out on this design, to gain a sense of its thermal performance and provide possible optimisations, if required.

The data acquired from the roof setup would then be used to further validate a simple thermal model for photovoltaic-thermal collectors, currently under development at the TU Delft. The first expected outcome of this undertaking will be a thorough literature survey of the present technology, its recent advancements and appropriate components. Alongside the literature research, the roof setup will be located at SEAC's research facility, the SolarBEAT, at the TU Eindhoven campus. The setup will be monitored regularly using a dashboard. By the end, this project will answer the critical question of whether such a system (BIPVT) is technically feasible & whether the heat pump integration is necessary.

1.4 Motivation

The development of PVT/BIPVT systems can be considered a viable and necessary alternative for meeting electricity, domestic hot water and space heating demands for a household or residential building. In order to do so, consumption of various energy products in the residential sector of the European Union must be discussed. The residential sector, or simply put, households, use energy for various purposes such as space and water heating, cooking, lighting, electrical appliances and even space cooling in a few regions. A statistical study carried out by Eurostat [24] found that on average, for the entire European union, the majority of the energy demands in households were met by natural gas, covering roughly 37.1%, while electricity covered 24.5%. Whereas renewables accounted for almost 16% of this mix. Complete energy balances for the same can be found in Eurostat [23].

Distributed among countries, figure 1.3 depicts the share of fuels in the final energy consumption of a household, segregated based on end use [24]. As this project is based on developing a renewable space and water heating system for the Netherlands, the household use for the same is highlighted in figure 1.3. The highlighted content reveals that natural gas in Dutch households accounts for **72 %** of the final energy consumption. Highest among all other EU nations! With electricity accounting for almost 20% and renewables accounting for only 5% of this energy mix.

The household energy consumption realised above is understandable, since the Netherlands is the EU's largest natural gas producer. However, it is surprising since, in June of 2016, the then Dutch Minister of Economic Affairs announced further reductions in Dutch natural gas production. Capping the annual production at 24 billion cubic meters (bcm). With no scope for it to go up again. The production was most likely capped owing to a significant uptick in seismic activities in the northern part of the country, where most of the mining takes place [8]. With such a historic decision under implementation in the Netherlands, natural gas prices will keep on increasing, creating a void in the domestic space and water heating market. Luckily, there are a plethora of mature technologies available to fill this void, such as PVT or BIPVT collectors.

Owing to similar weather conditions and energy household requirements between the Netherlands and France, a well-known research blog harkin [33] conducted a study on their individual household heating markets, while providing some insights into future forecasts for the same. The study predicted a win for lower carbon-emitting technologies in the future. With such technologies accounting for more than a quarter of the household heating appliances by 2025 for the Netherlands. As well as significantly reduced gas boiler sales for the same. The evolution predicted by [33] can be seen in figure 1.4 below.

	Electricity	Derived Heat	Gas	Solid fuels	Oil & petroleum products	Renewables and Wastes
EU-28	**24.4**	**7.8**	**36.9**	**3.3**	**11.6**	**15.9**
Belgium	19.9	0.0	42.1	0.9	29.2	7.9
Bulgaria	41.0	14.4	2.6	6.7	1.2	34.1
Czech Republic	18.6	15.3	28.8	10.8	0.6	25.9
Denmark	19.8	37.7	13.9	0.0	5.2	23.4
Germany	19.6	7.9	39.4	0.9	20.6	11.6
Estonia	17.7	33.5	6.2	0.2	1.1	41.2
Ireland	25.4	0.0	21.1	13.7	38.1	1.7
Greece	40.1	1.2	7.7	0.0	29.5	21.4
Spain	39.8	0.0	23.1	0.5	18.3	18.4
France	34.4	3.1	30.3	0.1	14.4	17.7
Croatia	22.0	5.0	19.5	0.1	6.0	47.5
Italy	17.2	2.9	53.1	0.0	7.1	19.6
Cyprus	41.8	0.0	0.0	0.0	37.0	21.2
Latvia	13.5	32.3	9.3	1.0	4.5	39.4
Lithuania	16.6	32.4	10.1	4.0	3.3	33.6
Luxembourg	15.4	0.0	45.2	0.1	33.8	5.6
Hungary	15.3	8.0	45.7	2.0	1.0	28.1
Malta	69.5	0.0	0.0 :		23.9	6.6
Netherlands	19.8	3.0	72.0	0.0	0.4	4.8
Austria	24.2	12.7	19.1	0.3	16.3	27.4
Poland	12.6	19.7	17.6	33.4	3.0	13.8
Portugal	42.9	0.0	9.6	0.0	16.3	31.1
Romania	14.0	10.8	30.9	0.8	3.4	40.2
Slovenia	24.4	7.1	10.0	0.0	12.5	45.9
Slovakia	21.6	22.1	52.6	1.5	0.4	1.8
Finland	36.6	31.8	0.5	0.1	6.4	24.6
Sweden	51.3	34.9	0.4	0.0	0.3	13.0
United Kingdom	24.4	0.1	63.3	1.5	6.3	4.4

Figure 1.3: Share of final energy consumption in the residential sector by type of end-use [24]

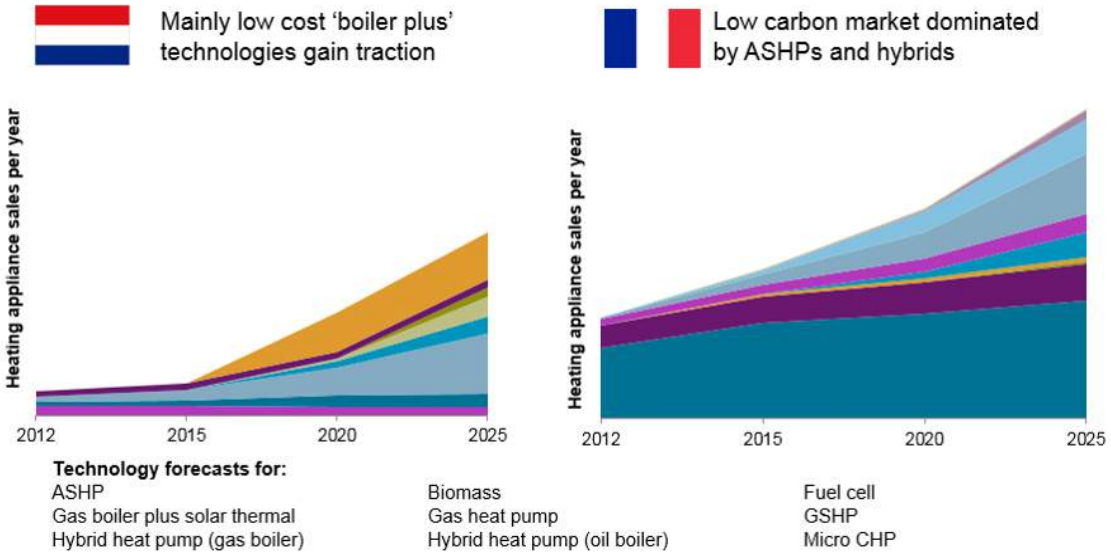

Figure 1.4: Evolution of the sales of heating appliances in the Netherlands & France till 2025 [33]

1.5 Thesis Objectives & Outline

This section will present the objectives of this project, along with what it aims to achieve upon its completion. Followed by an outline of what can be expected with the chapters to follow.

1.5.1 Objectives

The objectives for this thesis were defined by the results of the literature study presented in Chapter 2, based on the latest research and developments in the field of PV-Thermal systems. Along with the addition of research objectives formalised at the TU Delft and Exasun BV. The main focus areas of this work revolves around three essential objectives, listed below:

- Development, design and setup of an experimental BIPV-Thermal system.
- Validation of a new thermal model being developed for concentrated photovoltaic collectors.
- Heat pump integration necessity
- Yearly & Daily design characterisation
- Further design recommendations and improvements

1.5.2 Thesis Outline

Dealing with the design and development of a BIPVT system, chapter 2 of this project provides an overview of various solar thermal technologies currently available, in use and a few of it's novel concepts. It further briefs upon PVT & BIPVT systems. While discussing about heat pumps, their general working and various types, it also touches upon thermal storage systems, their various types and a few novel concepts. The chapter will also briefly discuss various types of thermal heat transfer fluids, as well as parameters for selecting the right kind for respective applications.

Chapter 3 provides further discussions and explanations on BIPVT technologies, & their integration benefits. The chapter describes the solar panels to be used for the experimental setup, their characteristics as well as production methods. At the end of which, the BIPVT design developed in-house at Exasun will be discussed, along with the various components used for the same. Providing reasons behind various design choices as well.

Mentioned at the start of this chapter, an experimental setup for the BIPVT design was installed at the SolarBEAT testing facility, located on the roof top of the Vertigo building at the TU Eindhoven campus. Chapter 4 will dive into describing the testing facility, BIPVT system installed on a demo roof and the various setup characteristics. The chapter will also provide a complete setup installation report, ending with an overview of the entire system and the components to be integrated with it.

Chapter 5, defined various heat flows through an individual PVT absorber, followed by a description of three thermal models, namely, a simple thermal model for concentrating PVT collectors, the steady state thermal model and the quasi-dynamic thermal model. The models used for heat pump and stratified thermal storage tank calculations will be discussed as well.

The simple thermal model discussed in chapter 5 is currently under development at the PVMD group of the TU Delft. Thus, using the data obtained from the experimental setup, this model was validated in chapter 6. The chapter defined various testing parameters for the models discussed in the previous chapter. Following which, the results from the models were juxtaposed on a graph, further validating the simple thermal model's validity.

Once the simple thermal model was validated in chapter 6, it was used to characterise the BIPVT design, details of which follow in chapter 7. The design's performance was characterised for an entire year, first, for a m^2 area the same, following which, simulations were carried out for a demo house with a roof area of $30m^2$. Considering such a presumptive analysis, varying performance analysis was conducted as well, identifying the system's performance with varying inlet conditions.

With the model validated and the system design successfully characterised, chapter 8 provides conclusions for this project, along with some key economic aspects to bear in mind. Followed by recommendations for further design improvement and system optimisation.

Chapter 2

Technology Review

2.1 Solar Thermal Technologies

Solar Thermal Technologies currently in use by consumers will be discussed further. Primarily, solar water heating systems consist of three collector designs: unglazed or glazed flat plate, parabolic trough and evacuated tube collectors. However, on a domestic scale, only flat plate and evacuated tube collectors are used. Whereas industrial scale hot water requirements can be met by parabolic trough collectors, as they are viable for high-temperature applications, and can also be used for electricity generation. A schematic of the pertinent collector technologies can be found in figure 2.1, representing the unique characteristics of each design [22].

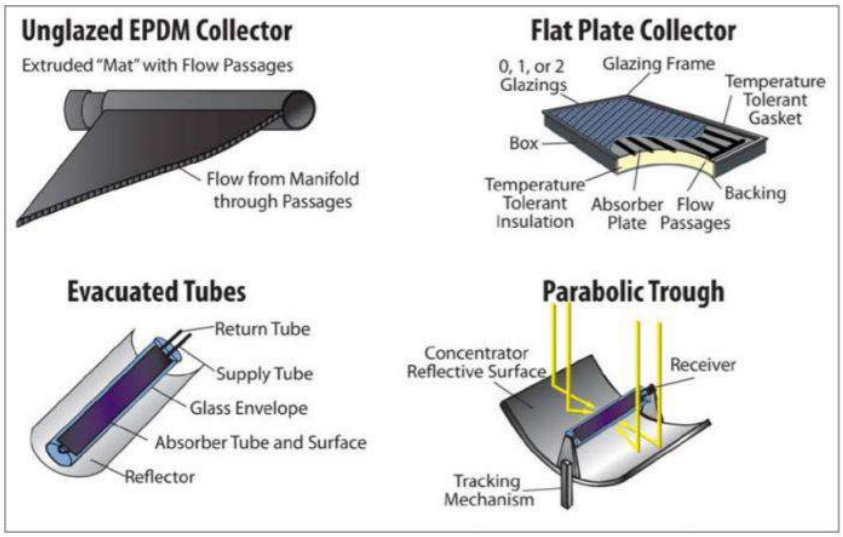

Figure 2.1: Primary solar thermal technologies [22]

Unglazed flat plate collectors are generally used for heating pools or supplying domestic hot water requirements for households. They consist of a dark absorber plate (metal or plastic) with the omission of a cover. However, recent advancements in unglazed collectors have seen them being implemented with/under photovoltaic systems for improved efficiencies and improved collector area utilisation. Conventional glazed flat-plate collectors, based on earlier designs of the technology, are generally housed in an insulated box with glass covers, containing either thin copper pipes or a thin copper plate, absorbing solar irradiance. Depending on design and application requirements, these collectors can be single or double glazed (referring to the number of glass covers on top of the collector). Owing to good thermal and structural properties, the collector housing is generally constructed of aluminium.

Evacuated tube collectors (ETCs) are probably the most advanced in their design, as they aim to overcome most of the thermal limitations of the glazed/unglazed flat plate collectors. The metallic absorbers for these collectors, are housed in a vacuum sealed glass tube casing. Each collector contains a few (exact number dependent on design and load requirements) interconnected glass tubes, with a reflector at the bottom for increased effectiveness. Although the costs for such collectors are high and the collectors themselves are fragile, the technology is quite mature and constitutes over 90% of the United States' flat-plate collector' market [22].

This project aims to focus on Photovoltaic-Thermal integrated collectors, which in simpler terms are solar modules

atop a glazed/unglazed flat plate collector. These designs will be discussed further in section 2.2.

2.2 PV-Thermal Technology

Stated in the previous chapter as well, solar energy is mainly harvested with the help of two matured technologies. That is, solar photovoltaic technologies, for electricity and solar thermal technologies, for thermal energy generation. In recent years, Photovoltaic Technologies have gained immense traction owing to their reduced costs, alongside increasing efficiencies. However, photovoltaics have serious challenges that still need to be overcome, such as high capital costs, relatively low conversion efficiencies, intermittent nature as an energy source and large installation area requirements. With decades of research in Photovoltaic-Thermal (PVT) integrated technologies, producing hot water and electricity simultaneously, the large area requirements for solar systems (at industrial/household level) can be curbed. While providing a better return on investments, and curbing CO2 emissions even further, at the same time. On a rudimentary level, PVT collectors consist of a PV module with a thermal collector bonded/attached/fixed on it's back.

The solar radiation that the module is unable to convert into electricity, is one of the main causes of high module temperatures. In PVT systems, this heat should effectively be absorbed by the thermal collector at the back of the module. The technology and its concepts may not be new or revolutionary as such, with the two of them being clubbed together (inefficiently) back in the mid-1970's [61]. It is widely known that solar module efficiencies reduce with high panel temperatures. Thus, an important aspect for this integration back in the 1970's, was to improve on the electric efficacy of the panels, utilising thermal collectors to extract excess heat energy produced by them. However, further feasibility, reliability and optimisation studies need to be performed in order to test novel, cost-effective, and relatively maintenance-free designs.

Since the technology depends solely on high irradiation levels of the sun and PV module temperatures, the systems are still not effective enough but are sufficient to supply low-grade thermal heat. This low-grade thermal output can be used in domestic households for space heating and hot water heating, as well as in industries for process heating or pre-heating, and even for crop drying in rural areas. As the systems perform better in the summer, owing to higher radiation levels, they are implemented with an electric auxiliary heat source (powered by the solar modules) for providing on tap demand during the winter months. Owing to this, a significant improvement PV-Thermal systems are incorporating nowadays is the coupling of an external heat pump [55].

2.3 Types of PVT Collectors

PV-Thermal collectors can be classified into two main categories based on the respective heat transfer techniques used by them, and further divided within these categories. The divisions are discussed further as follows,

2.3.1 Conventional PVT Systems

As the name suggests, conventional PV-Thermal systems rely on heat transfer fluids such as air and water for heat transfer.

Air based PV/T System

In such systems, atmospheric air is allowed to pass through the PV surface, comprising of various configurations, depending on application requirements. The systems can be set up in either active or passive mode, utilising forced or natural air convection heat transfer respectively. Naturally, passive systems are less costly than their active counterparts but lack reasonable efficiencies at the same time. The systems can also be configured to be single or double pass, as well as single glass (unglazed) or double glass (glazed) with different configurations [55].

It was seen that system efficiency improved with increased mass flow rate, cell density and collector length. With parametric studies conducted by [31], double pass parallel flow systems showcased the best performance in terms of produced electrical and thermal energy.

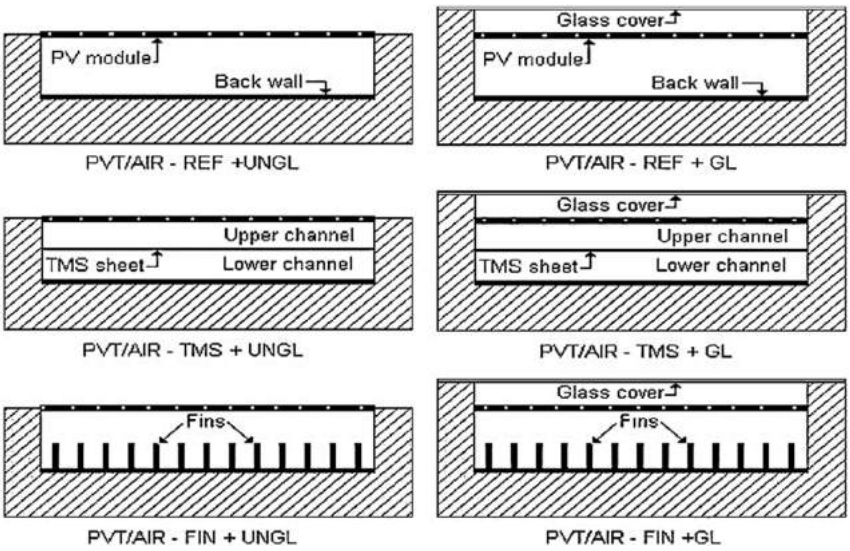

Figure 2.2: Various Air Based PVT Configurations [55]

Figure 2.2 showcases various configurations of PV-Air type systems, developed by Tonui and Tripanagnostopoulos [57]. These include unglazed (UNGL), glazed (GL), thin aluminium sheet (TMS), finned (FIN), & single air channel (REF) configurations.

Water based PVT System

A reasonable amount of research has gone into developing efficient water-based PVT systems. These systems addressed the main issues of air-based systems, which limit their efficient working at high temperatures. Such as their low heat carrying capacity, low thermal conductivity and density. Using water as a heat transfer medium does add the extra costs of using additional water heat exchangers but is negated by the system's superior thermal performance. While they also provide improved electrical efficiencies for the solar panels [55]. Various configurations of PVT were studied by Fraisse et al. [28] for building applications. Ranging from a separate PV and thermal system, covered hybrid PVT system, uncovered hybrid PVT system and another covered PVT system with low glass emissivity, as illustrated in figure 2.3. The tests performed by Fraisse et al. [28] observed that uncovered collectors recorded the highest annual cell efficiencies, followed by a normal PV system and then the covered PVT system, with it performing 28% lower than the standard cell efficiency.

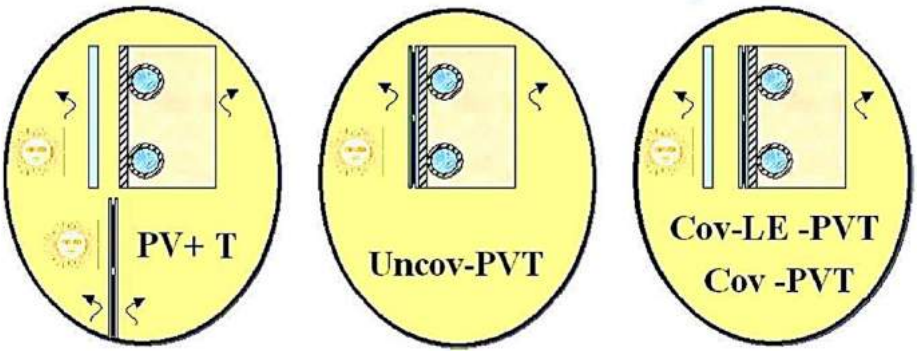

Figure 2.3: Water Based PVT Configurations studied by Fraisse et al. [28]

Another group of researchers Yazdanifard et al. [62], performed a series of numerical simulations on water-based

flat plate collectors, with/without glazing. The analysis considered the effect of several crucial parameters on the system, such as incident solar radiation, collector length, pipe diameters, packing factor, number of pipes, etc. The analysis also included considerations for laminar and turbulent flow regimes. The study showed that when it came to thermal performance, the glazed system performed better, whereas when it came to increased electrical performance, the unglazed system performed better, reinforcing what was learnt earlier from Fraisse et al. [28]. As expected, the total energy and exergy efficiencies increased for both the systems with increasing solar radiation and packing factor. Compared to glazed systems, unglazed systems seemed to have a higher optimum mass flow rate requirement. Coming to the flow regime through the systems, turbulent flow was found to produce higher total efficiency, whereas a higher exergy efficiency was realised with the laminar flow regime [62].

Bifluid based PVT System

A bifluid PVT system is one in which two fluids are used in a single PVT system. Although a niche category, fluid (air and water based) systems are considered to be the most developed PVT techniques yet. However, they have not panned out on a large scale. Generally, water and air were used in such systems, in order to produce hot air, hot water and electricity simultaneously, while overcoming the thermal limitations of simple air-based systems. Some research has also been performed coupling water with other fluids [55] as well.

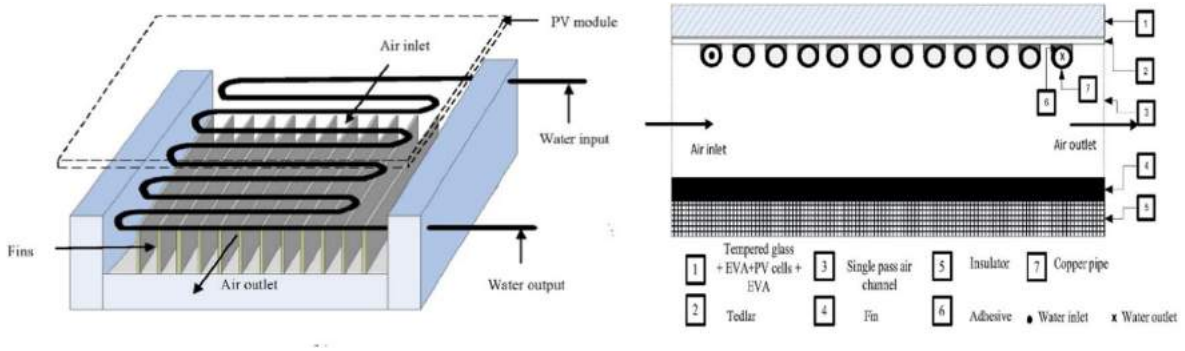

Figure 2.4: Bifluid Based PVT System studied by Jarimi et al. [43]

Figure 2.4, showcases a schematic design tested by Jarimi et al. [43], who studied it's numerical and indoor experimental performance. An important observation made by these group of researchers was that as the fluid flow of one fluid increased (water/air), the thermal efficiency of the other fluid flow (air/water) decreased. The study further had two modes of operation, the water mode and air mode. Air mode maintained a constant air flow rate while varying the water flow, and the water mode kept a fixed water flow rate while varying the air flow rate. System's efficiency was found to be better in air mode than in water mode, i.e. with a fixed (optimised) air flow rate and a varying water flow rate (air mode) [43].

2.3.2 Novel PVT Systems

Requiring particular system outputs, or learning and overcoming the thermal limitations of previous designs has led to the evolution of PV-Thermal technology. Evolving the system design over recent years, implementing a variety of heat transfer fluids other than air and water. These novel concepts which will be discussed in more detail, include design integrations such as anti-freeze liquids, heat pipes, nanofluids, and phase change materials.

Uncovered flat plate PVT

Uncovered PVT collectors can provide low-grade thermal heat to the heat source part of a heat pump. Improving the heat pump's coefficient of performance (COP). They, however, can also be used as a primary source of domestic hot water load, but only when solar irradiation is high. Reasons for the same were provided in section 2.3.1. They can also be used to supply regenerative heat to a heat pump for domestic cooling/heating. The differences in

supplying direct heat and regenerative heat will be discussed in section 2.4. Although, it is important to note that for all the drawbacks that an uncovered PVT system has, it also has some benefits over covered/glazed PVT systems. Such as their improved electrical performance and lower stagnation temperatures. A study, performed by Zondag et al. [63], implemented an uncovered PVT system as the regenerative source of a groundwater heat exchanger heat pump. The study showed that an uncovered PVT system, of $25m^2$ roof area, was able to fully cover building related electricity and heat consumption costs. It also showed that such a system had an effective payback period two-thirds the time of a side by side PV system.

A few important considerations arise when designing such systems. Heat transfer fluid flow in the absorber should be from bottom to top. Cold water inlet at the bottom, and a hot water outlet at the top. With a forced water circulation pump at the bottom, pushing water up. It is used thus, in the form of a thermosyphon system. Based on the simple principle that hot water rises. Such a configuration also helps the hot water stratify better in the tank, improving thermal efficiency [7]. Such systems are best used with a spectrally selective absorber. Two necessary properties that such an absorber should have are,

- High absorptivity for solar light (high absorption coefficient).
- Low emissivity for long-wave thermal radiation.

PVT systems based on nanofluids

The term nanofluids refer to fluids such as water, glycol and oil containing smaller than 100 nanometer (nm) sized nanoparticles, that can greatly alter the properties of the fluid, such as increasing its thermal conductivity. The term was first introduced by Chol and Estman [11], and has been used widely in various sectors ever since. With their increased thermal conductivity, researchers have been working on implementing nanofluids as a heat transfer fluid or an optical filter in solar technologies. Over decades of research, the right kind of nanofluids have proven themselves by significantly enhancing the performance parameters for PVT systems. The crucial properties that allow these fluids to perform the way they do are listed below [55],

- Type of fluid used.
- Particle size (ranging from 5 to 50 nanometer).
- Respective function of the fluid.
- Particle's concentration.
- Base fluid that it is based upon.

An investigation was conducted by Ghadiri et al. [32] on the overall performance of a PVT system, and its changing effects by implementing *'Ferrofluids'*. The authors of the study performed indoor experiments with the help of a solar simulator. The fluid was kept under a constant and alternating (50Hz frequency) magnetic field, in order to investigate its results on system performance. By using nanofluids, system performance enhanced significantly. With the system's overall efficiency improving by up to 45 and 50% under constant and alternating loads, respectively. Keeping in mind a 3 wt% quantity for the ferrofluids in the base fluid which was water.

A fairly recent, comparative study conducted by Al-Waeli et al. [5], compared the use of three nanofluids, Al_2O_3 (Aluminium oxide), CuO (Copper oxide) and SiC (Silicon carbide). The study found SiC to improve the system's performance the most, at 4.8%, while also remaining the most stable fluid compared to the rest. Assessing by a 4 wt% nanoparticle content in the base fluid. The study also found that a lower volume fraction resulted in greater fluid stability. Whereas, owing to the fluid's improved thermal conductivity, helped them maintain a lower temperature than water, thereby increasing the generated power as well.

PVT systems based on heat pipes

Figure 2.5 showcases a heat pipe, which works on the principle of carrying heat from one part of the section, the evaporator, to another part of the pipe, the condenser, without the help of an external power source. The system's working fluid absorbs heat from its surroundings in the evaporator section, converting it into the vapour phase. This vapour reaches the condenser section by passing through the adiabatic section. This flow takes place without the use of an external power source owing to a pressure difference in the adiabatic section. This vapour is released as heat in the condenser section, converting back into liquid and returning to the evaporator section, with the help of wick, that utilises capillary action [47]. Heat pipes have a large application base ranging from cooling of consumer electronic goods (laptops) to cooling industrial processes. When used for a PVT system, it extracts the heat generated at the back of a solar panel.

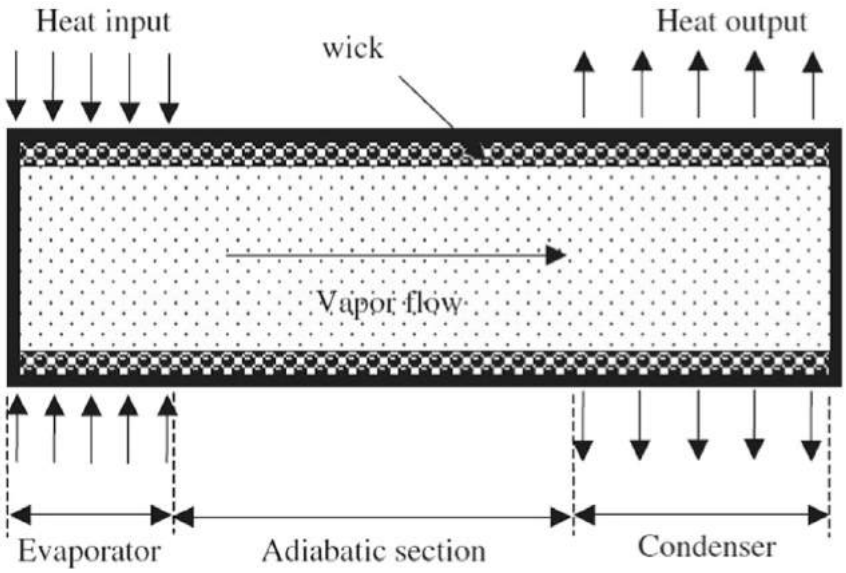

Figure 2.5: Heat pipe schematic [47]

One notable study on the research front for such systems was performed by Gang et al. [30]. The study developed a copper-based heat pipe PVT system, using water as a working fluid. Indoor and outdoor experiments conducted on the design took place under exceedingly controlled environments, after carrying out simulated hot water generation and finite difference electricity studies. The studies showed a 7.7% water temperature improvement when using an aluminium alloy baseboard compared to the then conventional Tedler-Polyester-Tedler (TPT) baseboard.

PVT systems based on phase change materials (PCM)

Applications of phase change materials are known to many as they are being used and developed for various other technologies. Such as hot water systems, fuel cells, batteries, automobiles and a plethora of other industrial cooling or storage applications. Using RT25 and paraffin wax as a phase change material, Huang et al. [37] developed and validated a numerical model, along with experiments for a PV/PCM system. The researchers analysed the system with and without fins, their research confirming a significant improvement in the thermal management of the PV/PCM system with fins.

Further effects of phase change materials on thermal management of the same PV/PCM system were evaluated in a later study by Huang et al. [38]. With an aluminium container, RT25(liquid) and GR40 (solid) PCMs were tested with three independent designs, based on the number of aluminium fins, strip matrix, and soft iron wire matrix. Experimental tests showed the RT25 PCM out-performing the granular GR40 PCM, which could not maintain efficient thermal control. Whereas, RT25 was able to maintain the surface temperature of the PV/PCM system depicted in figure 2.6. Hasan et al. [34] reported Capric-palmitic acid (C - P) and Salt Hydrates (such as

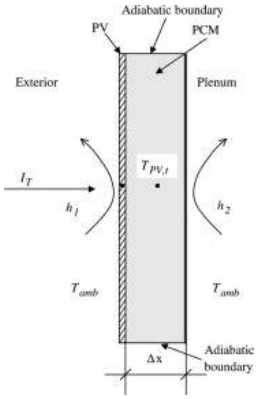

Figure 2.6: Schematic diagram of the heat transfer in a PV/PCM system [38]

$CaCl_2$) to be thermally and financially viable enough to be used for thermal management of PV systems in hot climates.

Rosenthal et al. [53] developed four different PCM configurations, to study PV temperature regulation by a PCM. The configurations are illustrated in figure 2.7. Configuration *a* consisted of bulk PCM (a single slab). Configuration *b* consisted of thick aluminium fins. Configuration *c* comprised of an aluminium honeycomb structure, utilised as a honeycomb, while configuration *d* had the PCM encapsulated in a water bath. The main aim of this study was to experimentally evaluate thermal heat dissipation of four different PCM configurations.

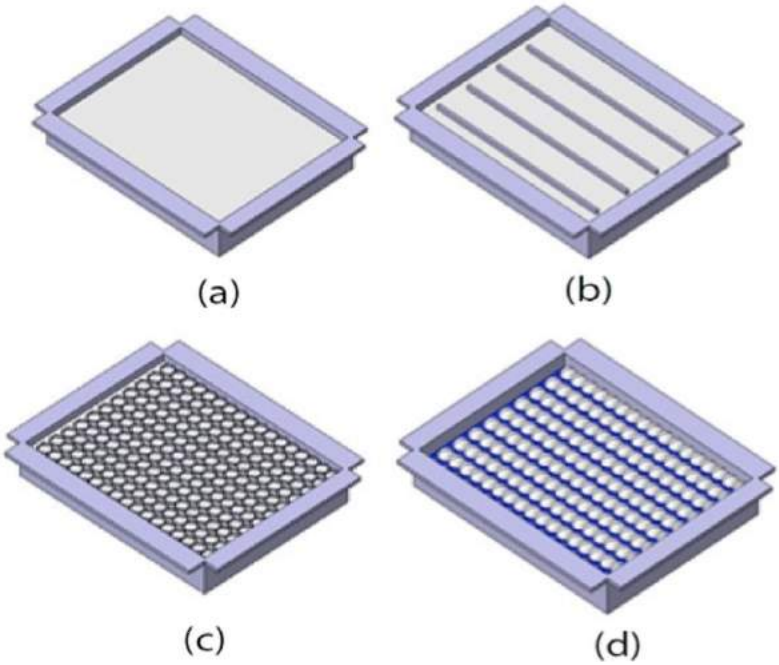

Figure 2.7: PCM Configurations - Case a: Bulk; Case b: Finned; Case c: Honeycomb; Case d: Encapsulated [53]

2.4 Heat Pumps

The sections below aim to provide a brief outlook into heat pumps, their working, general classification, and applications.

2.4.1 Working Principle of a Heat Pump

Heat pumps work on a similar principle and cycle as a refrigerator, offering an energy-efficient alternative to furnaces and air conditioners. They can be used for heating, by moving heat from a cool space to a warmer space, and for cooling, to remove heat from a cool space into a warmer space. It is important to note the distinction between 'moving' and 'generating', since heat pumps move heat rather than generate it. Owing to this, they can provide an equivalent amount of space conditioning, at a little less than a quarter of the cost of conventional heating/cooling appliances [50].

Heat pumps are generally closed-loop systems, with a refrigerant as working fluid. Figure 2.8 depicts a cycle of the heat pump that the refrigerant takes. This cycle starts at the evaporator which accepts heat from the heat source that can be sourced from different mediums. These mediums will be discussed later. The heat obtained helps turn the refrigerant in the heat pump into a cold vapour, as the refrigerant has a low boiling point. The vapour then passes through a compressor, controlled and powered electrically, that compresses the cold vapour into high-pressure hot vapour. The hot vapour passes through a condenser (heat exchanger), giving away the refrigerant's heat to a heat sink. Which in turn converts the refrigerant into a warm liquid. The warm liquid is passed through an expansion valve, in order to regulate its temperature and pressure, giving a cool liquid again. Obtaining this cool liquid, the process can be performed over and over again.

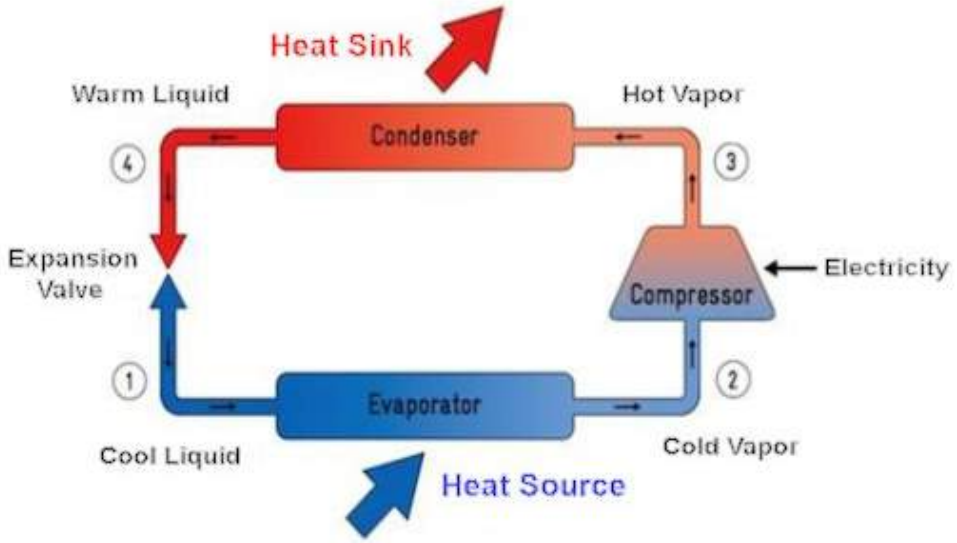

Figure 2.8: Heat pump working. A machine that "moves" heat. [Energy]

2.4.2 Thermodynamic cycle

Figure 2.9 provides an illustration of the thermodynamic cycle of a heat pump, also referred too as a Log P-h diagram. With its enthalpy plotted against pressure. Points 1 to 4 in figure 2.9 represent the change in enthalpy (in kJ/kg) & pressure (in Bar) for the refrigerant circulating in the heat pump, while the stages between those points refer to processes occurring within the heat pump [9], listed below. Heat pump calculation equations will be presented later in section 5.7.1.

- $1 \rightarrow 2$: Compressor.
- $2 \rightarrow 3$: Condenser.
- $3 \rightarrow 4$: Thermal expansion valve (TEV).
- $4 \rightarrow 1$: Evaporator.

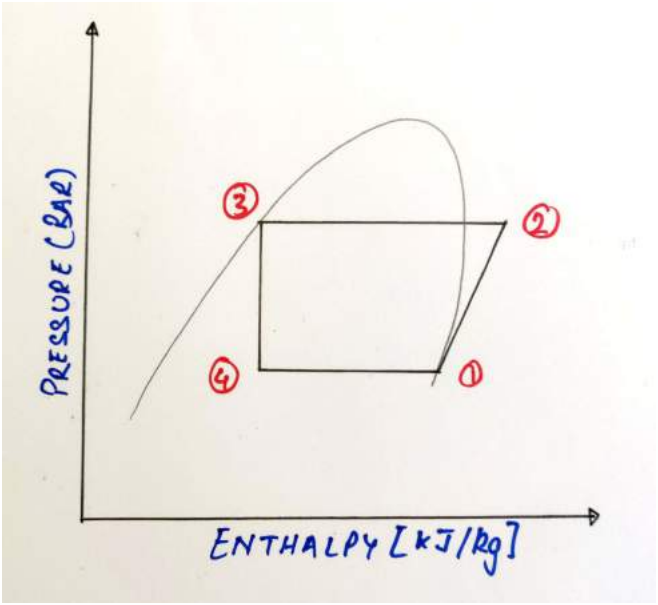

Figure 2.9: Thermodynamic cycle for an ideal Heat pump

2.4.3 Heat Pump Classification

Heat pumps can be classified based on the medium they use to collect heat. Such as air-to-air, water source, and geothermal. Collecting heat from air, water or the ground respectively. Currently, air-source heat pumps have been the most commonly used domestic option, with the potential of reducing electricity consumption for heating by up to 50% [50].

Geothermal based heat source

Although requiring intensive capital investment and a myriad of other prerequisite conditions such as land area and type, geothermal (ground-source) heat pumps are able to achieve high heat transfer efficiencies between a dwelling and the ground, or a nearby water source. The capital-intensive costs can be negated by the fact that they cost less to operate and can almost supply the domestic hot water load of a house to its entirety. Used effectively, they can reduce the energy heating bill of a house by up to 60% [50]. Geothermal systems can be found in a variety of configurations. Some of its vital distinctions are an open or closed loop system, with a vertical or horizontal heat ex-changer underground, or a pond/lake based system. Figure 2.10 depicts the various configurations that such systems are available in.

Water based heat source

The third type of classification deals with coupling a heat pump with a water/fluid based heat source. This heat source mostly consists of solar assisted systems. Systems such as flat plate solar thermal collectors, thermodynamic and photovoltaic panels. Thermodynamic panels are different wherein they act as the evaporator side of a heat

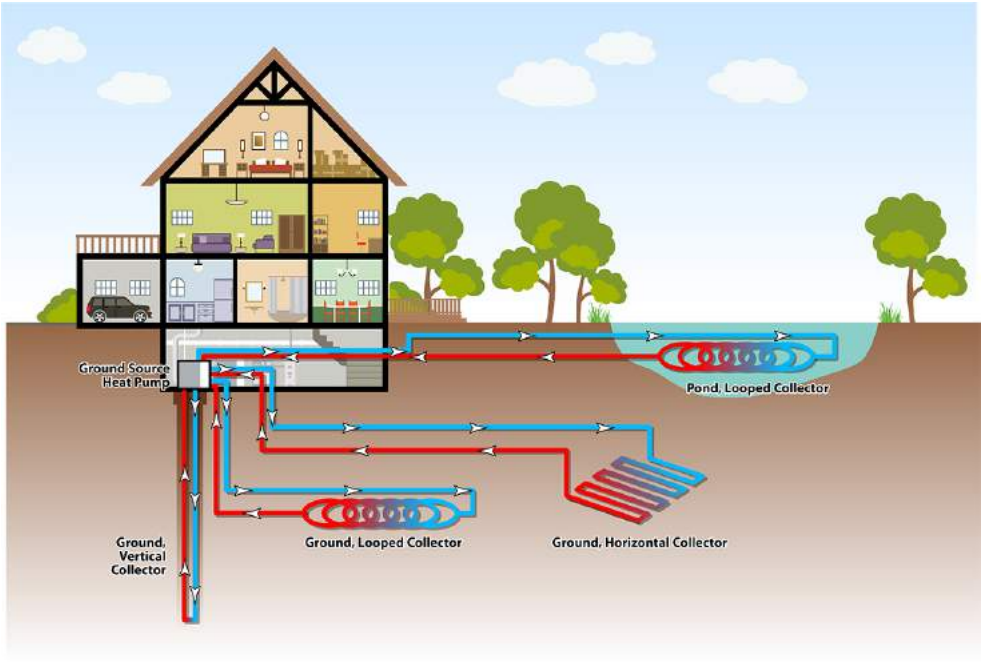

Figure 2.10: Geothermal heat pump configurations [13]

pump, with solar irradiation acting directly as the heat source, providing heat to the refrigerant. They can be used constantly for the entirety of the day. In most cases, they are efficient enough to provide domestic hot water load for an entire dwelling.

This project involves the design and further development of photovoltaic panels, integrated with a solar thermal system, coupled with a heat pump. Section 2.4 will provide further in-site for the same.

Direct Expansion Solar Assisted Heat Pumps (DX-SAHP)

DX-SAHP are also more commonly known as thermodynamic panels. The working of a heat pump involves an evaporator, supplied by a heat source. This has been discussed earlier in section 2.4.1. Thermodynamic panels have recently been developed to provide hot water for both domestic and commercial usage. They are more formally known as solar assisted heat pumps. The main idea behind such a panel is that they directly act as the evaporator to a heat pump. Using an application-specific refrigerant as the heat transfer fluid. Since such systems directly use a refrigerant, they send out a liquid htf at approximately -22^oC. Flowing through the panel, the HTF absorbs the surrounding heat, turning into gas at -15^oC. The gas after which, exits the panel entering the compressor unit of a heat pump, with its regular cycle continuing [40].

With such a working principle, the panels are touted to work with diffused irradiation and relatively cold climates as well. They can even be fitted at the side of a house, providing the entirety of the domestic hot water load for a household. However, such systems are still under development, with a relatively complex design, but an even more challenging system integration requirement, and high installation costs.

2.4.4 Heat Pump coupled with a PV-Thermal system

Ground source heat pumps have been used extensively to meet domestic hot water demands and space heating requirements. But in order to do so, requires installers to dig fairly deep trenches into the ground to access a reasonable temperature gradient for the heat pump' evaporators. PVT systems can be coupled with heat pumps as well, to avoid extensive installation costs, while providing hot water and space heating demands for a household. These systems have been discussed earlier in section 2.2. Coupling such systems, show optimal performance for

various configurations. Glazed or covered PVT systems need not be coupled with a heat pump as they are capable of providing a portion of the domestic hot water demand on there own. However, a covered system lowers the electrical yield of photovoltaic panels. Unglazed systems, on the other hand, producing low-grade heat, can effectively supply heat on the source side of a heat pump. Such a design aims at improving the electrical yield while maintaining an effective coefficient of performance for the heat pump in use [15]. Studies have shown that when designed proportionately, such systems can even provide better payback periods than regular photovoltaic systems [63].

The main benefits of unglazed systems are their relatively lower capital costs, easier installation, better electrical performance and reduced effective absorber area. Since the thermal loop is integrated below the photovoltaic panels. However, unlike ground sourced heat pumps, such systems cannot work year long, owing to a lack of solar radiation in the winter months. Thus, they are unable to completely match the load requirements of a house and need to be coupled with an auxiliary heater to meet the demand during winter months. When combining PVT collectors and heat pumps, there are three primary configurations that they can be divided into. These configurations are given as follows [15]:

Series

Wherein, the PVT collector acts as the main or one of the sources to a heat pump. Since unglazed PVT collectors are known for having low thermal efficiencies, they are coupled with heat pumps in a series configuration, where the heat produced from the collectors is utilised directly on the source side of a heat pump. Owing to their design, the thermal efficiency of unglazed PVT collectors rely heavily on the collector area, solar irradiation, and fluid inlet temperatures [20]. Thus, when temperatures are low (low solar insolation), the system is unable to supply the required heat, causing inefficiencies in heat pump operation, or no production at all. Therefore, an additional auxiliary (electrical) heater is required to balance out times with no production.

Parallel

Where, the collector and the heat pump can independently supply heat, to either the house or a storage tank. PVT systems can create heat parallel to heat pumps. Which can be supplied directly to the thermal storage. However, it is crucial for system control to be optimised as it can destroy or potentially waste generated heat. It is considered more suitable for covered (glazed) PVT collectors.

Regenerative

Where the heat generated by the PVT is used to regenerate the main heat source (ground or other) for a heat pump. Used commonly for energy roofs in the Netherlands. As an option, it can also be used for PVT systems. As regeneration temperatures are low, PVT efficiencies are high. In some cases, the PVT system's thermal generation can first be used directly, and then for regenerative purposes, for optimal performance.

With the configurations described above, a PVT system can be exclusive of a configuration, while combinations of the same are possible as well, depending on system design and requirements.

2.5 Thermal Energy Storage

Thermal energy storage (TES) plays an important role in various engineering applications. One such pertinent application relevant to our case is the storage of heat collected by solar thermal or heat pump systems. Particularly, storing the excessive heat produced by solar thermal systems during periods of bright sunshine. This can be stored and utilised during the night or at other instances of high demand [35]. Heat storage, particularly for water, can be categorised by its duration [25]. Such as,

- *Short-term storage*: comprise of a storage capacity between 1.5 to 2.0 times the daily hot water demand. Used extensively for solar hot water systems. Even for a short period, the storage tanks require a generous amount of insulation to avoid ambient losses.
- *Mid-term storage*: aim to cover heat demands for three to five days. Can be used for solar-combined heating systems and solar supported district heating schemes. A storage tank of 800 to 1500 litres should be sufficient to provide mid-term storage to a single household family, residing in a low-energy home.
- *Seasonal Storage*: can be a viable solution for places located towards the northern latitudes. Ideally, such storage solutions should provide a heat capacity of six to four months, depending on the household and duration of heating season.

The industry utilises two main types of thermal energy storage techniques. They are sensible and latent heat storage. Sensible heat storage varies the amount of energy stored in the storage medium by raising or lowering its temperature. Making it desirable for the storage medium to have a high specific heat capacity, long-term stability under thermal cycling, and a low-cost [35].

2.5.1 Types of TES

The two main forms of TES mentioned above have been described briefly below.

Sensible Heat Storage

In sensible heat storage systems, the temperature of the storage material rises when energy is absorbed and drops when it is lost. With the benefit of effectively having an unlimited number of charge and discharge cycles, over the lifespan of the storage. Sensible heat storage can further be classified on the basis of the heat storage media that it uses. The two main distinctions that it entails are liquid media storage and solid media storage. Liquid media storage refers to storage mediums such as water, molten salts, oil-based fluids etc. While, solid media storage refers to storage mediums such as rocks, metals and other elements [35]. The most common material used by domestic storage tanks for heat storage is water. This technology will further be discussed in section 2.5.2.

Latent Heat Storage

Melting 1 kg of ice into water requires 80 times more energy than raising the temperature of liquid water by 1^oC. Latent heat storage is based on a similar principle, wherein it uses the energy stored in a substance when it changes from one phase to the other. As is the case from ice to water. The materials used for the same are termed as phase change materials (PCM), i.e. they store large amounts of energy in their phase change. With decades of research being performed for thermal energy storage options, latent heat storage is particularly attractive as it offers a high energy storage density, and can potentially store heat as latent heat of fusion, at a constant temperature. As a technology, it also holds the key for efficient and reasonably priced seasonal thermal storage, using appropriate phase change materials (PCM).

2.5.2 Domestic Hot Water Storage

A domestic hot water (DHW) storage tank is an insulated tank, that accepts hot water from an external heating device. It is designed to store hot water for a short period of time, a couple of days at the maximum. Utilising any type of solar thermal technology, heat pump, or a conjunction of the two, for meeting domestic hot water and space heating demand, requires the addition of a DHW storage tank. Used mainly for residential buildings, some tanks are equipped with a water heater inside the tank for when a heat pump or solar thermal collector is unable to match the demand load [27]. Domestic hot water tanks can be stratified into horizontal, thermally

uniform water layers. A model for the calculation of these stratified layers will be presented in section 5.7.2. Un-pressurised plastic water tanks can be used as a cheap alternative for long-term water storage as well, but do require a significant amount of insulation. A few important aspects must be considered while specifying and deciding on a thermal storage system [52].

- The design of the heating system should be matched to the calculated peak heat load.
- When including solar heating, ensure that there is extra capacity within the store to accommodate fluctuations.
- Where a biomass boiler is being used, consider sizing the storage to provide for the heat capacity generated in a load.
- Consider designing not only for short-term anticipated capacity but possible future extensions to the system.
- Consider stratification of water temperatures within the storage, particularly where low-grade heating is provided. The effective separation between the hot water at the top of the tank and the cooler water at the bottom can increase the time between charges.
- Ensure that there is adequate insulation for the storage (100mm + PU foam)
- Ensure that there is adequate pipework insulation, otherwise, a fair amount of heat can be lost to the ambient.

2.6 Heat Transfer Fluid (HTF)

Most forms of thermal systems, dealing with the transfer of heat, such as refrigerants, heat pumps or solar thermal collectors, use some form of a heat transfer fluid to transfer heat between different stages. The section below will provide further insight into these fluids, the parameters affecting their selection, along with the popular types utilised.

2.6.1 HTF Parameters

Heat pumps comprise of heat transfer fluids running in a closed loop within the system and PVT systems comprise of heat transfer fluids running via tubes below the photovoltaic panels. Similar in principle, yet both the systems utilise different HTFs, owing to dissimilar design requirements. With system design, it is important to choose the correct heat transfer fluid, with the appropriate design aspects and considerations in mind. Some important parameters to consider before choosing an appropriate HTF can be found below [of Energy].

- Coefficient of expansion (fractional change in length).
- Viscosity or fluid resistance; should be kept as low as possible to avoid resistive pipe losses.
- Thermal capacity or the ability to store/transfer heat; should be as high as possible (better thermal performance).
- Freezing point of the material; particularly important for colder climates, as freezing of the HTF in winter can cause severe system issues.
- Boiling point of the fluid; an important consideration parameter for warmer climates.
- Flash point of the fluid.
- Corrosiveness and stability of the fluid; a vital property for consideration, specially when using metal pipes.

For the BIPVT system, keeping the above parameters in mind, and considering for colder climates (i.e. the Netherlands), the HTF used should have a low freezing point. Boiling point is not much of a concern as the summers are only moderately warm in the Netherlands. The fluid should have low viscosity and high specific heat, to transfer as much heat as possible with the least resistance, i.e. with minimal effort required by the pump. Discussed earlier in section 2.4, heat pumps exclusively utilise refrigerants, owing to their low boiling points and high latent heat of vaporisation.

2.6.2 Types of HTF

The section below will provide brief insights into the various types of heat transfer fluids that can be used for either a solar thermal system or other forms of thermal systems, such as heat pumps [of Energy]. After which, the particular HTF used for the experimental setup will be discussed.

Air

Air, under operation does not freeze, cannot boil and is non-corrosive. However, owing to its low thermal capacity, it provides a relatively lower thermal performance when used in a system. It tends to leak out of collectors, dampers and ducts as well.

Water

If it can meet design requirements, water can act as an inexpensive and nontoxic HTF. It has a high specific heat as well as a low viscosity (easy to pump). However, issues can arise when using water as it has a relatively low boiling point, and a high freezing point. Meaning that it cannot be used in very hot and sub-zero climates. Along with that, if water is not maintained at a neutral pH (acidic/alkalinity) level, it can be corrosive to components it comes under prolonged contact with. High mineral content water (i.e. "hard" water) can cause mineral deposits in the collector tubing and system's plumbing.

Antifreeze mixtures

Antifreeze mixtures are liquid mixtures with water as its main base. These mixtures are mixed with a varying amount of propylene or ethylene glycol (depending on application). As their name suggests, this is done so in order to reduce the mixture's freezing point so that they can be used in colder climates. They can comprise of 50/50, 60/40 or even 70/30 water/glycol ratio. Using ethylene or propylene depends upon the application of the fluid. Ethylene glycol is very toxic and should not be used for domestic hot water heating applications, in case of any leaks. Thus, propylene glycol is widely mixed with water and used for PVT systems. These materials need to be changed every 3-5 years, as they degrade over time. They are generally part of a pressurised system, and should be serviced by qualified professionals.

Hydrocarbon oils

Hydrocarbon oils consist of synthetic, paraffin, or aromatic refined mineral oils. Such oils require more energy to be pumped since they have a higher viscosity and lower specific heat than water. However, they are inexpensive, and have a lower freezing point.

Refrigerants or Phase Change Fluids (PCF)

Refrigerants, or phase change fluids (PCFs), are most commonly used as HTFs in refrigerators, air conditioners and heat pumps. Having a low boiling point and a high heat capacity enables a small amount of refrigerant to transfer a large amount of heat quite efficaciously. They respond relatively quicker to solar heat as well, and can be used in direct expansion solar assisted heat pump systems (DX-SAHP) as well, making them more effective on cloudy days than other HTFs.

Refrigerants do not solely work on increasing temperatures. Rather, heat is absorbed when the refrigerant boils and changes its phase from liquid to gas. The now-gaseous refrigerant releases this heat when it condenses back into liquid in a heat exchanger. Owing to environmental concerns such as leakage of chlorofluorocarbons (CFCs) and hydro chlorofluorocarbons (HCFCs) from such systems, popular refrigerants such as R134a or Freon-22 (R22) have now been banned by various governments. HTFs such as methyl alcohol or ammonia are now coming into use as refrigerants.

Silicones

Silicones have their fair share of pros and cons when it comes to their utilisation as HTFs. They have a low freezing point, high boiling point, are non-corrosive and long-lasting. But because they have a high viscosity, and low heat capacity, more energy is required for their pumping. They also leak relatively easily, even through microscopic holes in a solar loop.

Chapter 3

BIPV-Thermal System Design

PVT systems have been discussed thoroughly in chapter 2. The main design criteria for this report is to install and test an unglazed BIPV-Thermal system which will provide low thermal heat to the evaporator side of a water-water heat pump, for improved thermal performance (COP). Whereas when the supply (solar radiation) is high and so is the heating demand, the system can also be used to supply domestic hot water load (DHW) for a household. It is best to have a spectrally selective absorber for the thermal collectors used in such systems. The main requirements for the same are listed below.

- High absorptivity for solar light
- Low emissivity for long wave thermal radiation

3.1 Building Integrated Photovoltaics

Mounting solar panels on the roof of a house is not the most aesthetically viable approach for domestic installations. It is also one of the most significant obstacles shunting the growth of the domestic solar industry. Building integrated photovoltaic (BIPV) systems have gained a considerable amount of traction in the recent past. With them projected to become one of the fastest growing solar industry segments, with a capacity growth upwards of 50% in the next few years [16]. BIPV technologies have a few recognised methods for their integration techniques, given as follows,

1. Panel integration into the building envelope ($BIPV$):

   Involves replacement of roof shingles/wall cladding/facade panels with PV panels. Significantly more advantageous than the general 'add-on' strategy. Such techniques require considerable architectural and aesthetic design integrations. They can lead to higher overall performance for the system while enhancing its durability.

2. Thermal collector integration into panels ($BIPVT$):

   This technique involves the integration of thermal absorbers below the integrated panels. Capturing excess solar energy that escapes, as useful heat. It is effectively a PVT system underneath, which have been discussed extensively in chapter 2.

3. Building applied Photovoltaics ($BAPV$):

   Such techniques apply solar panels as part of the architectonical composition of the building, and not as a construction component. No vital building components (shingles, facade panels, etc) are removed during their setup.

3.1.1 BIPV-Thermal Concept

As a manufacturer, Exasun deals solely in BIPV systems. Although the systems are aesthetically appealing and seamlessly integrate into buildings, they have a few known issues. Currently, solar panels are able to extract almost 20 % of the absorbed solar insolation, with the rest being reflected back into the environment or absorbed as heat. This heat absorption causes panel temperatures to rise, directly affecting panel efficiencies. The high-temperature

drop in performance is particularly important for BIPV systems, as there is a general lack of ventilation beneath the panels. Causing a higher than average rise in ceiling temperatures for the modules. This excessive heat generation can be extracted with the help of a thermal absorption system beneath the BIPV. Such a system termed a BIPVT is capable of converting solar into electrical energy, while simultaneously converting the same into thermal energy. This waste heat collection can be utilised in meeting domestic hot water load and space heating demands of a household.

3.1.2 Integration Benefits

One of the biggest advantages of PVT systems over stand-alone PV and solar thermal systems is that they can achieve a higher total energy yield per unit area of the surface. Useful for areas, especially in colder climates having a combined demand for electricity and heat. Such cases, as well as areas where roof surface area is a major limiting criterion can be beneficiaries of a PVT system [54]. Although initial capital costs may be higher, studies have shown that such a system can have a better payback period [63] when compared to a similarly sized PV system.

Owing to improved area utilisation, PVT systems can also have reduced labour (installation) costs, as well as reduced BOS (Balance of a System) costs overall. The BOS costs refer to system costs such as wiring, inverters, switches, charge controllers, metering system etc. In fact, BIPVT systems can have even lower BOS costs compared to non-integrated installations [16]. Whereas, using an unglazed system over a glazed one, improves on the system's electrical performance, by cooling down the PV [64]. Some of the key benefits that BIPVT systems can have over common non-integrated systems can be found below [16].

- Sunscreen, providing power generation.
- Reduced carbon footprint of the building.
- Aesthetically appealing.
- Innovative design.
- Acoustic & Thermal insulation, providing better comfort for the tenants.
- Increases building value.
- Sustainable and environmentally friendly.
- Unglazed systems specially, help improve electrical efficiency of the panels.
- Can effectively help households becoming net-zero energy buildings (NZEBs), helping them benefit from subsidies by the government.

3.2 Solar Panels

The basic working of photovoltaic cells has been discussed earlier in Chapter 1.1. This section aims to discuss the novel photovoltaic panels designed, used and produced by Exasun BV.

3.2.1 Exasun' 50W PVT Panel

The project undertaking with Exasun involved various design requirements and restrictions. Currently, Exasun produces glass-glass PERC-Mono-crystalline Silicon - Metal Wrap Through solar modules. As the company deals mainly with building integrated systems, it is important to have panels of various sizes to fit different rooftops. The unglazed PVT system designed, having a single pass through the tube beneath the panels required a new

panel to be designed, with smaller dimensions. Owing to which, a new size of panels was produced, consisting of two series of 5 cells each. Using ten such mono-crystalline high-efficiency cells, the panel was rated at a peak output of 50W. The panel's characteristics and I-V curve can be found in the table 3.1 and figure 3.1 below. The complete panel data sheet can be found in appendix E.

Characteristic	Value
Pmax (W)	50
Voc (V)	6.64
Isc (A)	9.93
FF	0.76
Efficiency	20.2
Vmpp (V)	5.34
Impp (A)	9.36

Table 3.1: Solar panel's electrical characteristics

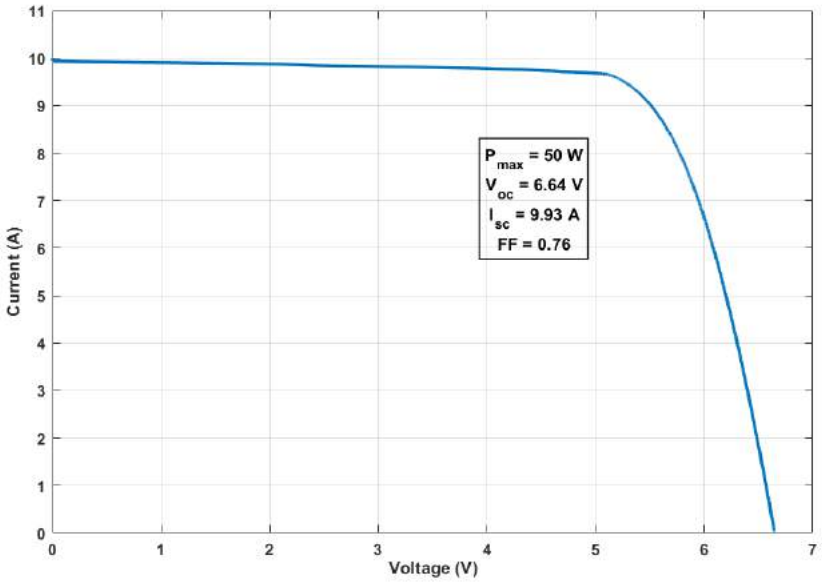

Figure 3.1: Exasun 50W PVT Panel: I-V Curve

A computer-aided design render of the 50W panels can be found in figure 3.2. Under confidentiality restrictions, in-depth details cannot be mentioned about the design or the production process. However, a brief overview of the steps involved can be found in section 3.3.

3.2.2 Silicon Cells: Metal Wrap Through Technology

Solar panel production nowadays is based on screen printed H-patterned silicon solar cells. A process and technique that suffers from severe front shading and surface resistance losses, caused by the presence of external contacts (bus-bars) on the front surface. Using Metal Wrap Through technology, these contacts can be transferred to the rear surface, while using industrial production techniques. The MWT-PERC combined approach, with PERC representing the passivated emitter and rear cell technologies, have shown cell efficiencies higher than 20% [12]. A data-sheet for the MWT cells currently used by Exasun can be found in section E.2.

The front charge on an MWT cell is collected at the back, as stated above. However, this charge is transferred at the back of the cell using a wrapped-through metal electrode connected with the back contact through a channel which runs through the cell, called a 'via' [12]. Such a cell's cross-section can be seen in figure 3.3. The benefits of MWT cells over H-pattern cells are that since most of the front grid is removed, there is no bus-bar, resulting in

Figure 3.2: Exasun's 50W PVT Panel Render

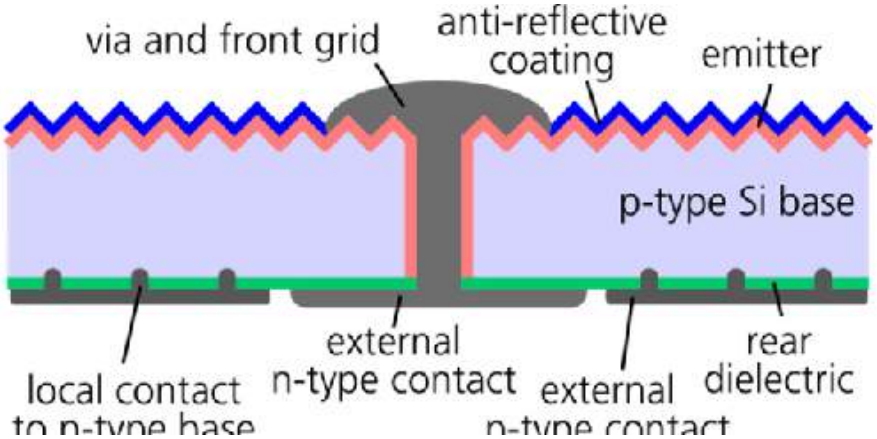

Figure 3.3: MWT-PERC cell side cross-section [12]

fewer shading losses, higher efficiencies owing to higher cell area, and in general a more aesthetic cell appearance. Higher efficiencies, result in a higher output, along with outstanding module reliability, and low cell breakage rate. The only downside to such a technology are its slightly higher costs, which can be negated by a higher yield [60].

3.2.3 MWT-PERC Panels Layers

The following section will briefly brush through the various layers of an MWT-PERC solar cell

Glass-glass Module

The solar panels produced by Exasun are of a special kind, i.e. as most manufacturers use a Glass-back sheet (aluminium/polymer-based) panel, Exasun produces Glass-Glass (GG) encapsulated modules particularly for BIPV roofs. With extended tests carried out by researchers, it has been found that GG configuration modules are the most effective solution in providing protection to the cells, along with good mechanical stability. The GG configuration provides lower production costs as well since, with added stability, a metallic frame around the module is no longer required [10].

Back-conductive Sheet

MWT-PERC cell technologies require a conductive back sheet for collecting front and rear charges. For the same, Exasun designs optimised conductive back sheets for its panels in-house. They consist of a low-cost copper coated aluminium foil, as well as a mechanical pattern instead of wet chemical etching. These conductive back sheets sit below the cells, connecting them together.

Encapsulant

An encapsulant, as the name suggests, is used to provide adhesion between PV cells, top glass, the bottom surface (glass or aluminium), and all other components in between. Such an encapsulant needs to adhere to various physical properties. It needs to be stable at elevated temperatures, and have a high resistance for UV exposure. It should be optically transparent while having low thermal resistance [Education.org]. Thus, with these properties in mind, the most commonly used encapsulant material has been Ethyl Vinyl Acetate (EVA). It is processed in thin sheets and can be applied to the top and rear surface of a solar panel. When solar panels have been stacked, i.e. its various layers placed accordingly, the panel goes through a lamination step. This crucial step, also a bottle-neck in the production process, heats the EVA up to 150 ^{o}C. Thus, polymerising the EVA and bonding the panel together [Education.org]. The exact encapsulant used by Exasun is a confidential material, however, a few of its basic properties can be found in the table 3.2 below

Property	Value
Thermal Conductivity (W/mK)	0.2
Optical transmission	91%
Density (g/cm^3)	0.88
Thickness (mm)	0.46

Table 3.2: Encapsulant's properties

3.3 Panel Manufacturing

This section aims to provide the basic panel production steps taking place at Exasun. An overview description of the same is presented. These steps remain the same for any MWT-PERC or back contact silicon solar modules. A panel cross section of the PVT panels can be found in figure 3.4 below. Note that the aluminium profile and tube are attached to the installation of the project and play no role in the panel production. It is also important to note that figure 3.4 is not an accurate representation of the final design, owing to confidentiality restrictions. The production steps given below are performed in the order presented.

Encapsulant cutting & Tabbing

The utility of an encapsulant was discussed in section 3.2.3. The encapsulant cutting step deals with cutting large sheets of the encapsulant into desired dimensions, depending upon the panel's requirements. Simultaneously,

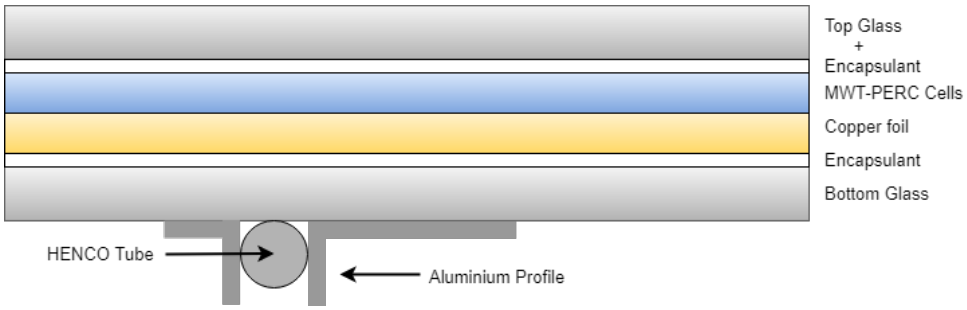

Figure 3.4: MWT Solar Panel cross-section

another step takes place in the production process, i.e. tabbing. Which refers to soldering of tabs to the conductive back layer. This is done in order to connect the bypass diode and junction box to the back layer.

Bottom Stacking

As solar panels are comprised of various layers, bottom stacking refers to the alignment and stacking of all the layers below the PV Cell. The stacking starts from bottom to top. In the case of Exasun, producing glass-glass panels, the bottom-most layer is glass. For the PVT panels produced at Exasun, the bottom stack consisted of the bottom glass cleaned with isopropyl alcohol (IPA), a layer of encapsulant and the conductive back layer. This is not an automated process as employing a production worker for such a job is more economical and effective.

Stencil Printing

The bottom stacked panel is passed through a stencil printer. This is another vital step in the production process, wherein a specifically designed stencil is placed atop the bottom stack. After which, the machine rolls over conductive paste through the stencil on the required points of the conductive back layer. This is an automated process as high accuracy is required for placement of the paste.

Cell Placement

Running on an automated assembly belt from the stencil printer, the bottom stack is passed through a pick and place machine. Called so, as the pick and place individually pick up solar cells, placing them appropriately on the bottom stack. The conductive paste mentioned in section 3.3 now comes into use as it bridges the gap and connects the conductive back layer with the solar cells. Mentioned earlier, the pick and place is an automated process, as cell placement needs to be as accurate as possible. This is achieved through the help of computer vision. If the cells are not placed correctly, the panel may not function at all. Such inaccuracy can lead to severe economic losses. However, the machine is manned by a production worker for quality control and in case of emergencies.

Top stacking

Top stacking is based on a similar concept as bottom stacking. Layers comprising the solar panel above the PV cells are placed by hand in the top stack. For Exasun's PVT panels, the top stack is fairly straightforward, consisting of a layer of encapsulant and the top glass cleaned by IPA. After top stacking, the two glasses are tapped together on the sides, temporarily holding them in place. After which, they are carried forward to the lamination process discussed next.

Lamination

Panel lamination is easily the most crucial and complicated production step, as well as the most time-consuming process of the entire assembly. Owing to which, it is also the toughest bottle-neck in panel manufacturing. Solar panel lamination is carried out in a vacuum membrane laminator, consisting of a single heating plate. It is important to note that the entire lamination process takes place under constant vacuum. The process takes place in three crucial steps, explained below [10].

- Step 1: Removing impurities:
  Once the module has been loaded onto the laminator, air and other volatile organic compounds (VOC) are removed by vacuum, while the module, placed up, is being heated. The panel is heated up till the point of encapsulant softening.
- Step 2: Adhesion:
  Now that the impurities have been removed, and the encapsulant has been softened, a flexible membrane, (generally made of silicon) is pressed against the module. This step helps ensure optimal adhesion of the components inside the module.
- Step 3: Cooling:
  For the final step, a controlled cooling mechanism terminates the chemical reactions induced for module lamination, while cooling it down naturally. After the final lamination step, the module can move forward in the production process.

Lamination temperatures and their determination are a bit tricky as it depends on various factors. Such as the encapsulant used, type of cells used, module configuration and lastly, size of the panel as well as the laminator. The temperatures generally range around 150 ^{o}C. An important side note, if the VOCs are not properly removed in the lamination process, it can give rise to bubbles in the final module [10]. A solar panel's lifetime is not determined by the limits of the solar cell it uses, but rather by moisture ingression into the laminate [46]. Thus, choosing the right encapsulant is essential.

J-Boxing

After lamination is complete, the modules are taken out and allowed to cool down further. They are then checked for bubbles that may have risen due to the presence of VOCs during the lamination. Owing to quality restrictions, any module with bubbles will eventually be disposed off, and not processed further. After they cool down, the junction boxes are attached to the panels, using the tabs sticking out of the laminated module. These tabs were discussed in section 3.3. The junction box is also moisture sealed using a special adhesive (kit). This procedure is commonly known as J-boxing. Owing to the intricate nature of the kit application, the junction box is attached to the panel manually, i.e. by a production worker.

Flashing

After the junction box has been attached, the panels will now be passed through a flasher. Sourced via Eternal Sun, a flasher is a solar simulator, capable of mimicking the AM1.5 spectrum. Each individual solar panel produced, is flashed a few times, in order to assess the panel's quality. Panels not performing up to a certain standard are set aside. These panels will be disposed of, or recycled. Since each panel is flashed and characterised individually, they are done so, manually by a production worker.

There can be a plethora of reasons for a non-performing panel. Some of the important and controllable ones are listed as follows,

- Faulty conductive back layer.

- Faulty cells.
- Inaccurate conductive paste printing.
- Inaccurate cell placement.
- Presence of VOCs in the laminator.
- Inaccurate lamination settings, etc.

Back railing

As the name suggests, refers to the placement of mounting structures/back rails on the back of the panel. The mounts are installed using an adhesive (kit). Done so, also because there is no other effective way of mounting BIPV GG solar panels lacking a metal side frame.

3.4 BIPVT Design Concept & System Components

This section will provide further insight into the design concept, and system components used for the BIPVT system, along with a justification for their selection.

3.4.1 Design Concept

As a solar panel manufacturer, Exasun BV deals majorly with BIPV systems. Figure 3.5 below, provides a concept render of the eventual BIPVT system from the manufacturer. While utilising the solar panels mentioned in section 3.2.1. Whereas the sections ahead will discuss the various system components. Chapter 4 will discuss the experimental setup utilised for characterising the BIPVT system.

3.4.2 Thermal Absorber

The thermal absorber or collector for most thermal systems comprise of appropriate materials or pipes with the highest possible thermal conductivity. The most common ones for the same are considered to be copper and aluminium. With a thermal conductivity of 385 and 205 [W/mK] respectively, at room temperatures [Nave]. However, utilisation of such metals is accompanied by their own issues. Such as increased investment costs, maintenance issues due to corrosion, difficult material handling (pipe bending), special tool requirements, etc. All such issues, usually dealt with, due to improved thermal performance for a system.

A thorough study conducted by Patterson et al. [51] used various materials to understand the difference in heat transfer rates between the materials, for the same type of solar thermal collector. Patterson et al. [51] used a wide range of piping materials such as steel, copper, PEX (cross-linked high-density polyethylene), CPVC (Chlorinated polyvinyl chloride), PE (polyethylene) and PVC (polyvinyl chloride) in their study. With thermal conductivities ranging from as high as 401 [W/mK] (copper) to as low as 0.14 [W/mK] (CPVC). The study proved that for solar thermal collectors, materials should not be chosen by there ability to conduct heat to a fluid within a tubing. Since, using the varied materials, statistically indicated no difference between the materials and their ability for heat transfer. Thus, based on the findings in the study above, a multilayer pipe produced by HENCO was utilised for the BIPVT system. The pipe consists of PE-Xc/Aluminium/PE-Xc layers, giving it some remarkably versatile properties. The datasheet and physical properties for the same can be found in appendix E, in figure E.3. The 16 mm outer diameter pipe was chosen for the BIPVT, meeting design considerations. The main reasons for choosing these particular pipes can be found below.

- They have the best properties of both materials (plastics and metals).

Figure 3.5: House with a BIPVT roof

- Can withstand pressures of up to 16 bar, with maximum working temperatures of 16 ^oC.
- As light as plastic piping.
- Flexible and easy to bend, retaining their shape after bending.
- Can be used for both heating and cooling purposes.
- A 100% oxygen and water vapour diffusion tight.
- Almost entirely corrosion-resistant.

3.4.3 HTF used

As the test setup and further BIPVT systems will be placed in the Netherlands, a heat transfer fluid with a low freezing point, relatively high boiling point, and low viscosity was required. These parameters, their effects, and other such heat transfer fluids have been discussed in section 2.6. A water and propylene glycol mixture were used for the BIPVT system, as it met the necessary design requirements. Specifically, TYFOCOR-LS HTF was used for the BIPVT, supplied and manufactured by TYFO (Treat Your Fuel Oil) Chemie GmbH, a heat transfer fluid supplier from Ha mburg, Germany. The particular manufacturer was used for their high-quality products. Their product, the TYFOCOR-LS HTF is a ready-to-use heat transfer fluid, specially designed for solar thermal systems, dealing with high thermal loads. Providing frost protection up till -28 ^oC. The HTF's thermophysical properties can be found in appendix E. Whereas it's characteristics can be found in the table 3.3 below.

Table 3.3 depicts water content of the HTF between 55 - 58 %. As the content is quite low, a refractometer was used to further dilute the water/glycol mixture, to a 70/30 mix respectively. The concentration for the same can be found in figure 3.6, whereas the fluid's chemical properties, can be found in table 3.4 below. The highlighted properties in the table were the ones that were eventually used for the experiment and its further calculations.

Property	Value
Appearance	clear, red-fluorescent liquid
Boiling point	102 - 105^oC
Frost protection	-28^oC
Density (@ 20^oC)	1.032 - 1.035 g/cm^3
Viscosity (@ 20^oC)	4.5 - 5.5 mm^2/s
Refraction	1.38 - 1.384
pH value (@ 20^oC)	9.0 - 10.5
Water content	55 - 58%
Flash point	none
Reserve alkalinity	$>$ 12 ml 0.1 m HCl

Table 3.3: Tyfocor-LS HTF thermophysical properties

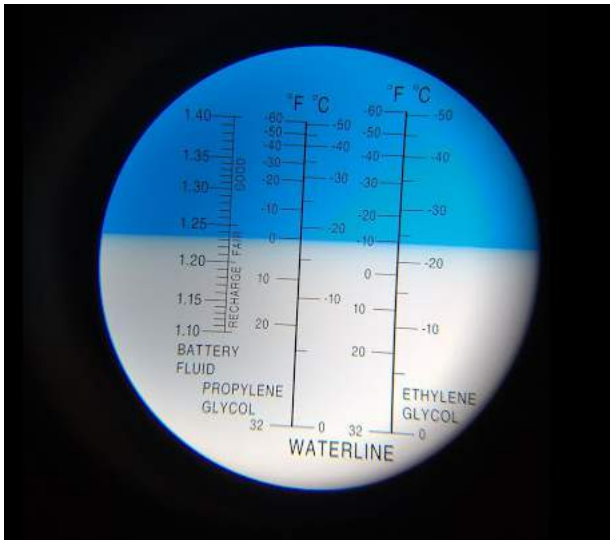

Figure 3.6: Water diluted polypropylene concentration determination, using a refractometer

Glycol percentage (by mass)	**Freezing point** (^oC)	**Specific mass** (kg/m^3)	**Specific heat** (J/kgK)
0	0	1000	4186.8
10	-3	1008	4103.064
20	-8	1017	4019.328
30	**-14**	**1026**	**3914.658**
40	-22	1034	3747.186
50	-34	1041	3558.78
60	-48	1046	3370.374

Table 3.4: Tyfocor-LS HTF chemical properties

3.4.4 Mounting system

Mounting systems for solar PV setups are a crucial design choice, relying on the system and geographic requirements. Particularly for BIPVT systems, as they aim to integrate such systems into a building or house. Exasun as a solar PV manufacturer, specialises in BIPV systems and their effective building integrated mounting. For this project, and the BIPVT system, specialised aluminium mounting structures were designed. These structures can be mounted (drilled) directly onto the roof of an installation. An aluminium block on the solar panels, attached with in unbreakable seal attaches into the mounting structure, holding the panels in place. The concept was discussed earlier in section 3.3 as well. As the company solely manufacturers glass-glass BIPV modules, they rely on some innovative mounting structures, developed in-house at the company. Since these are proprietary designs,

one cannot dive into their details, owing to confidentiality restrictions.

3.4.5 Alucobond

Aesthetic differences between figures D.1 and D.3, helps one ascertain the importance of facade panels. Especially for BIPV systems, aiming to integrate efficaciously into a building. For these purposes, an appropriate and aesthetically matching facade panel was used, provided by 3A Composites GmbH. 3A Composites have been manufacturers and suppliers of a wide variety of high-quality aluminium composite panels, along with other materials such as plastics, foam boards and even wood. Mainly for architectural applications, as well as for visual communication, and the transport industry. Of the plethora of materials on offer by 3A, the one utilised for this experimental setup was ALUCOBOND. For aesthetic materials, these panels offer a wide variety of processing options, such as cutting, punching, contour cutting, bending, roll bending, routing & folding, riveting, and screwing. Giving access to a host of possibilities for facades. Technical data sheet for the same can be found in appendix E figure E.5.

Chapter 4

Experimental Setup

4.1 SolarBEAT Test facility

Stated earlier in chapter 3, an experimental setup was installed at the SolarBEAT facility, situated on the roof of the Vertigo building at TU/e. PV Thermal systems have a myriad of thermal and electrical performance parameters that need to be evaluated. Providing reliable measurements for the variables involved is the main purpose for the experimental test facility at the TU/e. This chapter and the sections ahead will dive further into the design, characteristics and choices made for the setup. Figure 4.1 below provides an aerial view of the various dummy buildings at the SolarBEAT facility.

Figure 4.1: Solar Beat test roof at TU/e

Figure 4.2a below provides a view of the base support structure, upon which the system will be mounted. The dummy building also houses other PVT setups from EnergieDak and Dimark solar, adjacent to Exasun's system. Dimensions for the dummy building are, 6.6 x 6.9 meters, whereas the dimensions for the experimental setup for this thesis are 1.64 x 6.12 meters. Which is roughly 10 m^2. The same can also be found in figure 4.2b. Figure 4.2b also showcases various sensors, such as the pyrgeometer, windmeter and pyranometer. More will be mentioned about them in section 4.2.2. Before the setup was installed, computer aided design models of the same were created to get a better sense of the design and accurate dimensions. These CAD models can be found further in appendix D.

(a) Base structure of the SolarBEAT test roof facility

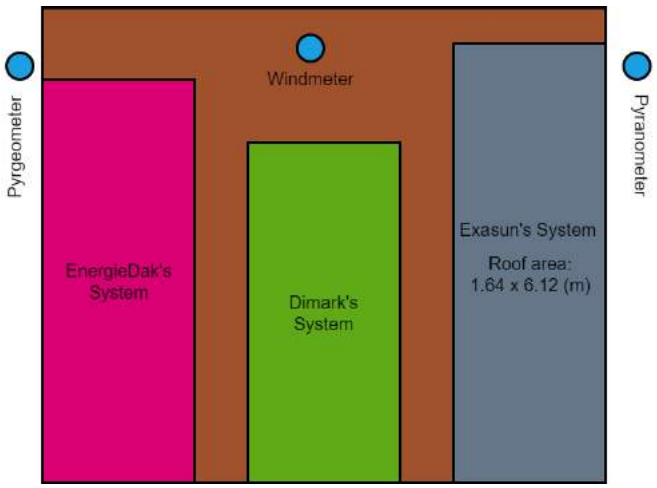

(b) Roof facility dimensions

Figure 4.2: base structure for the setup along with dimensions

4.2 Setup Characteristics

Exasun's 50W PVT panel dimensions are 0.82 x 0.4 meters. With the 10 m^2 experimental roof, 34 such panels could be installed, as can be seen in figure D.3. With the top and bottom rows stacked with facade panels. The setup's characteristics can be found in the table 4.1 below.

Component	Value
Roof area	10 m^2
Effective collector area	8.92 m^2
No. of panels	34 x 50 W
Rated electrical output	1700 W
Pipe length	41.7 m
Pipe diameter	16 mm (OD) 12 mm (ID)
HTF used	Water/Glycol (70/30) mixture
Effective HTF volume	0.02 m^3

Table 4.1: Experimental Setup Characteristics

Flow for the absorber was set from bottom to top. That is a cold fluid inlet at the bottom and a hot fluid outlet at the top. With a forced water circulation pump at the bottom driving the fluid upwards. Such a configuration utilises the thermosyphon effect on fluids, wherein hot water rises owing to the reduced liquid density at higher temperatures. It is also used as it helps the fluid stratify better in the storage tank, improving thermal efficiency [7].

4.2.1 Panel connections

With 34 panels to be connected, 6 power optimizers (or, charge controllers) were available for maximum power point tracking (MPPT). Thus, a string of 6 panels each, are connected to 5 power optimiser' in series. Whereas the final string of 4 modules is connected in series to the last optimiser. Schematic view of the panel connections for both can be seen in figures 4.3a and 4.3b respectively.

Solar Edge, P405 power optimiser was provided by SEAC. Datasheet for the same can be found in appendix E.

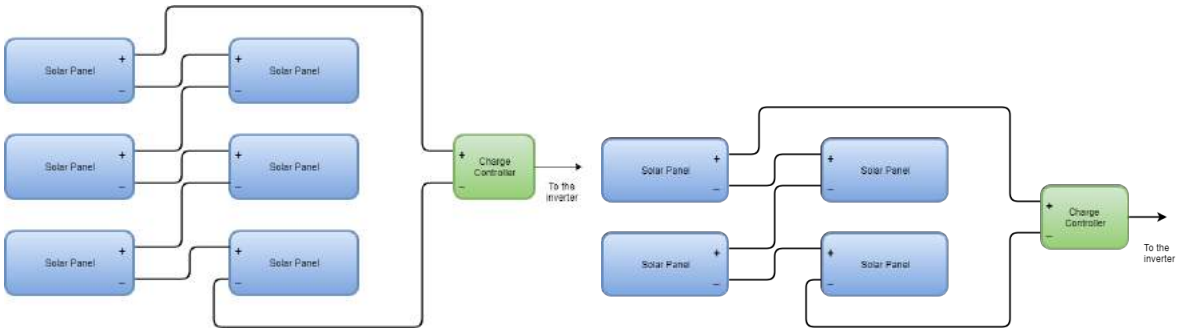

(a) Panel connection for five module sets; 6 modules connected in series

(b) Panel connection for the last module set; 4 modules connected in series

Figure 4.3: Experimental Setup panel connections

In order to ascertain panel connections and their compatibility with the charge controllers, table 4.2 provides an overview of the rated current and voltage capacity for the solar edge power optimizers, along with the maximum voltage and current values for the panels connected in series. Figure 4.4a displays a solar edge P405 power optimiser, whereas figure 4.4 adjacent to it displays the optimiser connections located right below the experimental setup, inside the dummy building.

Component	**Current (A)**	**Voltage (V)**
Power Optimiser	$I_{max} = 10$	$V_{max} = 125$
50W Panel	$I_{sc} = 9.94$ $I_{mp} = 9.34$	$V_{oc} = 6.65$ $V_{mp} = 5.31$
6 panels in series	$I_{mp} = 9.34$	$V_{mp} = 31.86$
4 panels in series	$I_{mp} = 9.34$	$V_{mp} = 21.24$

Table 4.2: P405 Power optimiser connections

The end of the string connection is split after reaching the power optimiser, with one pair feeding the SolarEdge inverter, and the other to the Yokogawa data acquisition unit, for measuring maximum power point voltage (V_{MPP}). Each string's maximum power point current (I_{MPP}) is determined by measuring voltage drop on a MurT manganin shunt resistor. The 1.7 kW of rated electricity that is generated, is fed directly into the local grid with the help of the inverter. The feed-in electricity is read with the help of an Upp power meter as well.

4.2.2 Sensors

Numerous sensors were installed and used for accurate monitoring of the thermal and electrical performance of the system. They were installed for measuring the temperature of the fluid flow at various locations along the setup (Tempco PT100), while a flow meter was installed as well to measure and control flow rate for the system (Krohne Optiflux 110). Three such PT100 temperature sensors were installed at bends in the fluid tubing for the system, ensuring that they remain pointed towards the flow, and measure the temperature of the mainstream fluid, rather than measuring for a stagnant fluid layer. This particular sensor placement can be seen in figure 4.5.

Sensors were also put up on the dummy building at the SolarBEAT for measuring environmental parameters as well. Incident solar irradiance was measured using an EKO MS 802 Pyranometer, installed at the same plane as the solar panels, with the same 35 ^{o} tilt angle. A Gill WindSonic anemometer was used for measuring the wind speed and its direction, while long-wave irradiance was measured using an EKO CGR-2 pyrgeometer. These sensors were placed on the same dummy building as the experimental setup, as can be seen in figure 4.2b. Two T-type thermocouples were placed on the back side of the solar panels, for monitoring the back temperatures of the PV panels. While measurements for the setup were performed every 5 seconds, a minutely average of the same is stored by using Yokogawa MW100s, a data acquisition unit. A daily aggregate of this data is uploaded to SEAC's data server every night. After which, the data is accessible online, via the online dashboard mentioned in section 4.4.

(a) Solar Edge P405 Power Optimiser

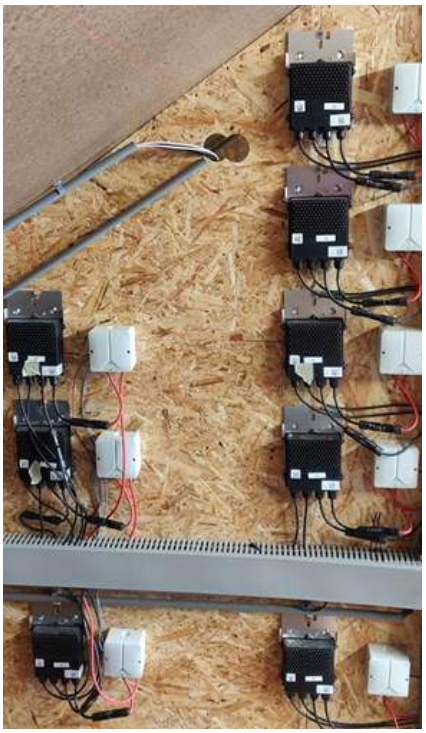

(b) Power Optimiser/Charge controller connections inside the dummy building

Figure 4.4: Power optimiser connections

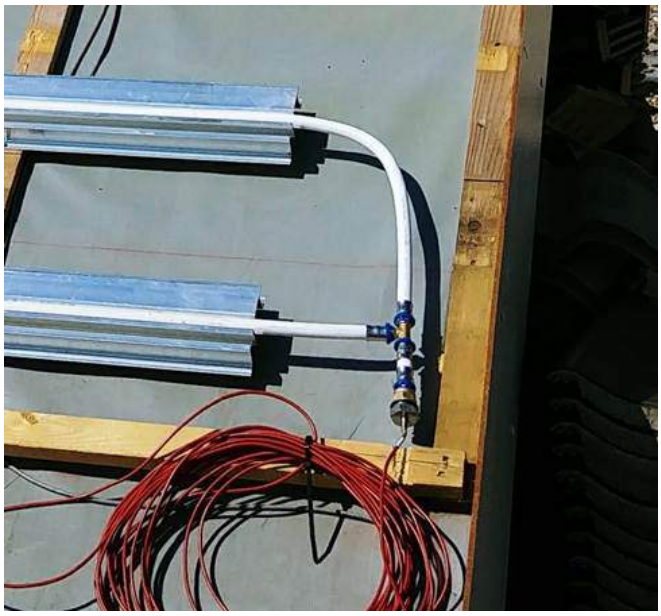

Figure 4.5: PT100 temperature sensor placement along the fluid flow

4.2.3 Thermal Fluid System

The thermal collectors of the experimental setup were connected to the thermal loop system of SolarBEAT. This thermal loop system is crucial for design characterisation, as it can provide the required inlet temperatures, at specific flow rates for the working fluid, to the experimental setup. For the BIPVT system, a controlled and stable supply of thermal fluid is ensured by the SolarBEAT facility, owing to a set of thermal loops running in a

laboratory below the testing facility. These set of thermal loops are able to control the temperature of cooling liquids. Using a set of pumps to transport the working fluid through a heat exchanger, and on to the dummy building's piping framework. This framework is situated inside the dummy building, providing the working fluid to the BIPVT system. The inlets and outlets for the BIPVT collector, as well as the thermal loop, can be seen in figure 4.6.

A water/glycol mixture ranging from 7 ^oC to 60 ^oC can be supplied by the thermal loop system. With inlet temperature control for the collectors being accurate up to 0.1 ^oC. A single pump, visible in figure 4.6 controls the total flow rate for the BIPVT. An aquifer thermal energy storage system is present at the TU/e, accepting the excess heat generated from the setup. Naturally, the inlet and outlet temperatures for the system are measured as well with the help of PT100 temperature sensors, discussed earlier in section 4.2.2.

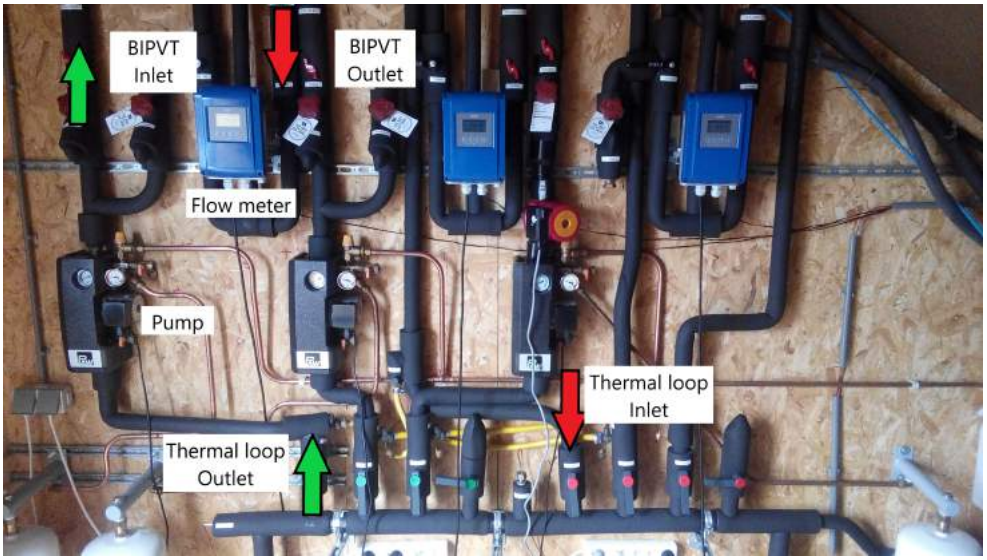

Figure 4.6: Thermal fluid framework under the dummy roof

4.3 System Installation

The installation process for the BIPVT will be discussed further. Installed at the SolarBEAT, the wooden structure of the dummy roof is illustrated in figure 4.2a. For reference sake, the setup had to be installed in a space of 6.12 x 1.64 meters. Each solar panel to be installed dimension's at 0.4 x 0.82 meters. Keeping in mind facade panels to be installed at the edges of the system, space had to be optimised for installing a maximum number of panels. Thus, seventeen rows with two adjacent panels in each row optimised this space, installing 34 such panels. Design render for the same is presented in appendix D, figure D.3.

4.3.1 Initial preparations

Before the installation could begin, the entirety of the facade panels covering the roof had to be disassembled and stored separately. Although these are not visible in figure 4.2a, the horizontal wooden beams visible in the figure had to be replaced, as the spacing between them was not optimal for the design in mind. Supporting beams were drilled again onto the roof, atop the vertical beams. Maintaining a spacing of 0.34 meters from the base for the first beam. Identical spacing requirements were kept for the rest. It was found to be most convenient to place this supporting structure bottom to top. As they also act as a supporting step for placing the next row above. It was important that these horizontal beams be placed at the right distance from each other, at the right angle and level. Since the structure not only acts as a step for installing higher up, it also acts as a reference plank upon which the mounting structure of the panels had to be placed.

Initials preparations for the setup also included transport for the items to be installed from Exasun's manufacturing facility in Ypenburg, Den Haag, to the SolarBEAT at TU/e. Such as,

- 36 x Exasun's 50W PVT panels (back railed and flashed).
- 2 x 25 meter HENCO pipes.
- 18 x Mounting (aluminium) profiles.
- 18 x Wooden planks for installation requirements (1.5 meter in length).
- A plethora of crimp connections for pipes, along with their crimping tool.
- 5 x Alucobond panels (1.65 x 0.6 meters).
- Various tools borrowed from Exasun' production hall.
- Few extra wooden planks for unforeseen requirements.

4.3.2 Mounting structure

Mounting profiles for the BIPVT discussed earlier in section 3.4.4, comprise of 6000 series extruded aluminium blocks. The profiles were cut to a length of 1.38 meters each, in order to fit in the required space. Stated in the list above, 18 such profiles were placed on the dummy building, with a spacing of 0.34 meters between each other. Equivalent to 6.12 meters. These aluminium profiles were placed right above the aforementioned horizontal planks, which acted as reference planks for the profiles. This helped in a speedy installation of the mounting structures, that were directly drilled on to the vertical wooden beams visible in figure 4.2a. Special aluminium piercing screws were used to pierce through the aluminium blocks.

4.3.3 Thermal pipes

Once the mounting profiles were in place, it was time for the placement of the thermal absorber pipes. The HENCO pipes that were used have been described earlier in section 3.4.2, along with the various reasons as to why those specific pipes were chosen for the system. Since the HENCO pipes are delivered in a coil, they had to be straightened out with the help of a pipe straightener, illustrated in figure 4.7a before they could be installed. Installation of the thermal pipes required the utilisation of specific tools, as well as special pipe connection crimping pieces to allow the connection of temperature sensors. These specific tools are illustrated in figure 4.7. With continuous pipes, temperature sensor connections had to be made with the help of T-piece brass press links, viewable in figure 4.7d. While figure 4.7b displays the crimping tool required to crimp the pieces in question. The particular press link pieces were chosen as they can withstand pressures up to 10 Bar and water temperatures up to 95 ^oC. Once crimped, the connection of the temperature probe was followed by a 16 mm to 0.5-inch female fitting crimp piece. Each row comprised of a 1.64-meter long pipe, with 17 such rows. The pipes were bent 90^o at the end of each section, and then bent inwards again after a distance of 0.22 meters, with the help of a pipe bender. A 60 mm pipe bender was utilised and can be viewed in figure 4.7c. The complete pipe installation, fluid flow direction, thermal fluid low input/outlet, temperature sensors, as well as the inlet for various sensors and solar panel cables into the dummy building are illustrated in figure 4.8.

4.3.4 Panel installation & Connections

Once the pipes were in place, solar panel installation and connection could begin. The installation began by placing the panels bottom to top. Since the way the panels lock on to the mounting structure and are fixed in place by the panel above, it was soon realised that installing bottom to top was not the most optimal strategy. Along with that, while placing the panels bottom to top, there was no supporting frame for the installer to rest on, to place the panels appropriately and perform necessary connections.

(a) HENCO Pipe straightener

(b) Pipe fitting crimping tool

(c) 60 mm Pipe Bender

(d) T-piece Brass press link 16mm fitting

Figure 4.7: Specific installation tools

Thus, the installation began placing the panels top to bottom. Utilising the mounting profiles as stepping stones for better support and easier installation. Figure 4.9a displays the installed panels on the dummy roof. Connections between the solar panels, forming a string was discussed in section 4.2.1. Figure 4.9b illustrates the strings, as they were installed top to bottom, along with the respective optimiser connected with them.

4.3.5 System checks

Since the PVT inSHaPe project that this thesis is a part off will continue up till December of 2019, a few system checks had to be performed on the system, in order to ensure flawless operation. Before the solar panels were installed, an open loop with water was run throughout the system for a few hours, checking for water leakages. The check was reasonably straightforward and was performed with the help of a bucket filled with water. The BIPVT thermal loop's inlet and outlets, including the system pump, were connected to pipes and placed inside this bucket, forming an open loop. An image of this rudimentary system check can be seen in figure 4.10.

While checking for water leakages, one such leakage was found throughout the piping system. Originating from a crimp fitting below the solar panels. However, it was fixed easily with the help of epoxy resin. Once the system was confirmed water and airtight, the solar panels were connected. As each panel comes flashed from Exasun, the voltage output of each string was double checked and re-wired if the connections were found to be faulty. Once that was complete, the strings were connected to their respective power optimizers, and output at the inverter was double checked.

4.3.6 Final setup

With the panels installed and system checks taken care off, the sides of the installation had to be closed off for a proper BIPVT setup. As is visible in figure 4.9a. This was done so with the help of alucobond A2 fixtures, discussed earlier in section 3.4.5. These fixtures compliment the design and appearance of the PVT solar panels and were utilised for covering off the system on all sides. An image of the complete installation can be found in

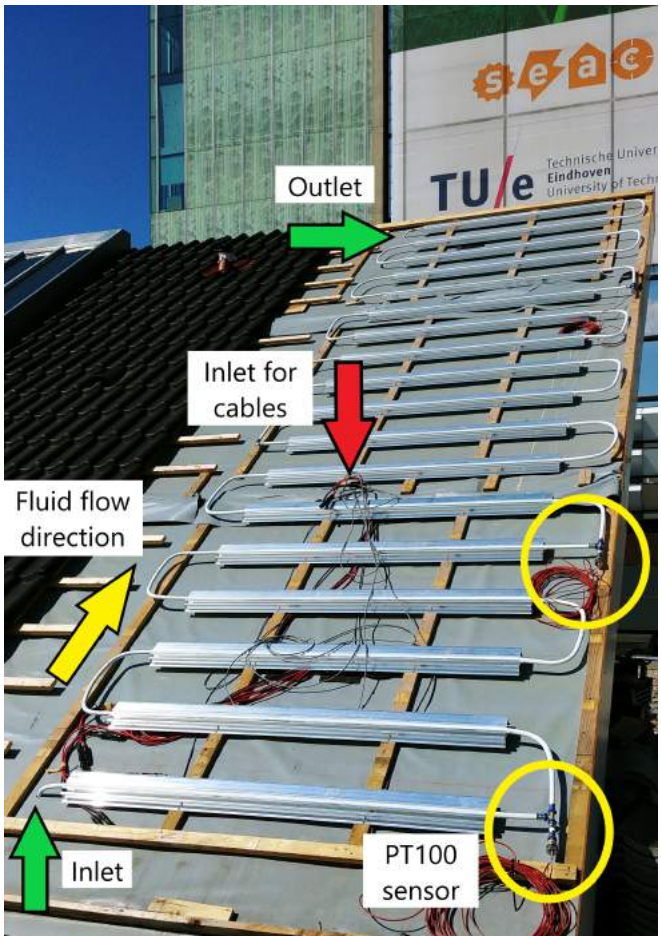

Figure 4.8: Mounting structures and pipes atop the dummy roof

figure 4.11. The design can also be referred back to the final CAD render found in appendix D, figure D.3.

After the installation was complete, it covered a space of 6.6 x 1.9 meters, with a slight increase in its width by 0.13 meters on either side. The extra height and width were a result of alucobond facade panels required to cover the edges of the system on all sides.

(a) Solar panels installed atop the dummy roof

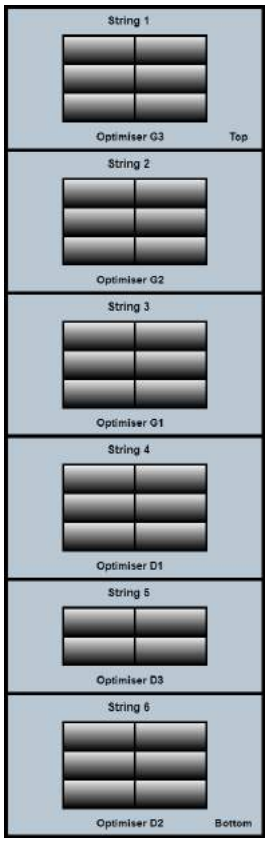

(b) Solar panel strings with the respective optimiser connected

Figure 4.9: Solar panels installed at the SolarBEAT

Figure 4.10: Thermal loop system checks

Figure 4.11: Completed BIPVT setup

4.4 Online Dashboard

Figure 4.12 provides a look at the dashboard accessible online. Provided by SEAC, the dashboard showcases data acquired by sensors and experimental setup. It displays the following vital parameters,

- Irradiance received at the test facility (Eindhoven, NL) [W/m^2]
- Ambient temperature surrounding the test facility (T_{amb}) [^oC]
- Temperature sensor readings of HTF temperatures for the system (T_{in}, T_{mid}, T_{out}) [^oC]
- Controlled flow rate for the setup [litres/hour]
- Thermal output (Q) of the system [W]
- Thermocouple readings of the PV panels [^oC]
- Electric output of the system [W]
- Performance ratio, along with the total electric energy harvest, as well as the top and bottom thermal energy harvest [kWh]

Figure 4.12: Online dashboard

4.5 System Overview

This section will provide an overview of the system and its various connections after the BIPVT. Such as, the heat pump loop, collector loop with thermal storage, & demand loop with a simulated household. Figure 4.13 provides an illustrated view of the system beyond the BIPVT, taking various temperatures into consideration as well. The figure also illustrates the electricity generated via the BIPVT, passing through an inverter that converts it to AC and forwards it to the house or sends excess to the grid. Various system temperatures denoted by a T are shown in figure 4.13, listed below. All temperatures are considered to be recorded in ^oC.

- $T_{w,in}$: BIPVT water inlet temperature
- $T_{w,out}$: BIPVT water outlet temperature
- T_1: Heat pump evaporator outlet temperature
- T_2: Heat pump condenser inlet temperature
- T_3: Heat pump condenser outlet temperature
- T_4: Heat pump evaporator inlet temperature
- T_5: Storage tank inlet temperature (collector loop inlet)
- T_6: Storage tank outlet temperature (collector loop outlet)
- T_7: House inlet temperature (demand loop inlet)
- T_8: House outlet temperature (demand loop outlet; mains)

The collector loop shown in figure 4.13 portrays the loop between the heat pump and the thermal storage tank, while the demand loop portrays the one between the thermal storage tank and the house. The demand loop outlet, i.e. T_8 is considered to be replenished by the mains, assumed to have a constant temperature of 10 ^oC [54]. For simplification, the collector loop outlet, i.e. T_6 is assumed to be the same as T_8 as well, at 10 ^oC. Further discussions regarding the heat pump and thermal storage will continue in section 5.7.

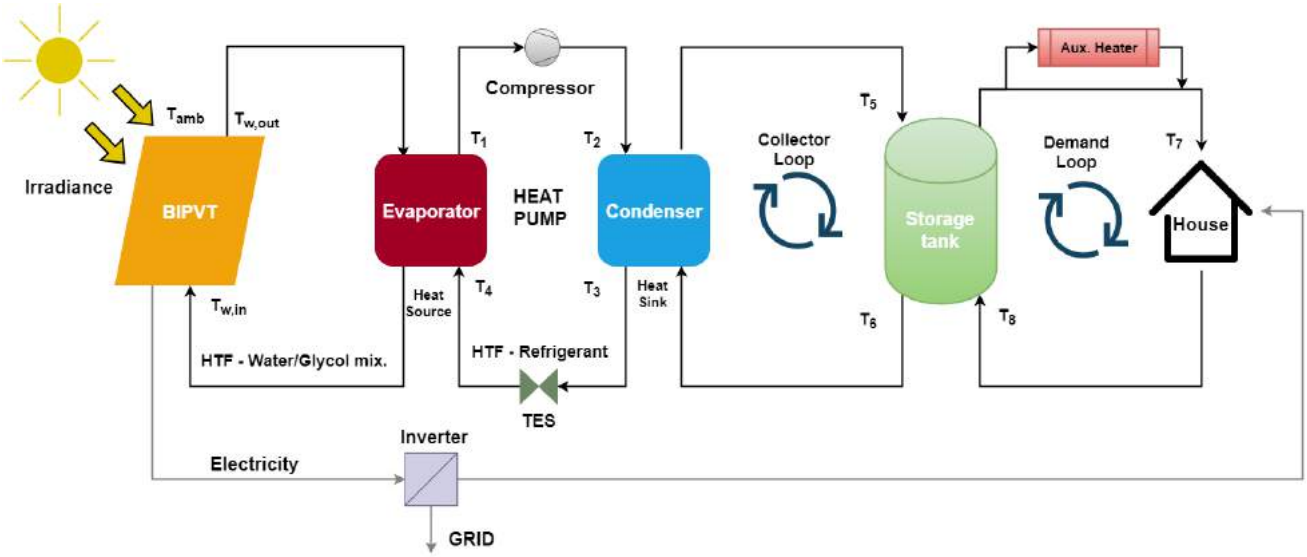

Figure 4.13: BIPVT/Heat pump System Overview

4.5.1 Household thermal energy demand

Figure 4.14a below depicts a standard hot water demand curve for a household of four people, calculated for each hour of the day. The left side of the y-axis depicts hot water demand in kg/h, while the right side of the y-axis depicts the same in kWh. Extracted from Santbergen [54], the withdrawal pattern consists of a demand of 117 litres of water per day, at 60 ^oC. Correcting for heat loss in water pipes running between the collector & demand loop, an effective withdrawal of 140 litres can be assumed, at a constant temperature of 60 ^oC. This hot water demand can be assumed constant for the entirety of a year. Thus, by repeating the pattern for the same, an annual energy demand of 2960 kWh (10.6 GJ) needs to be met. This energy demand can further be extrapolated to calculate the daily, hourly demand for water in Wh, in order to better understand the energy required, and for simpler comparison with the BIPVT system output. With hot water demand mentioned, the space heating

demand needs to be mentioned as well. Since PV/Thermal systems are designed to match both. Space, or room heating demand, naturally, exists mainly in the winter months, with an annual heat demand of 2990 kWh (10.8 GJ) [54]. Comparable in numbers, with hot water demand. The space heating demand, extracted by Santbergen [54] can be found in figure 4.14b.

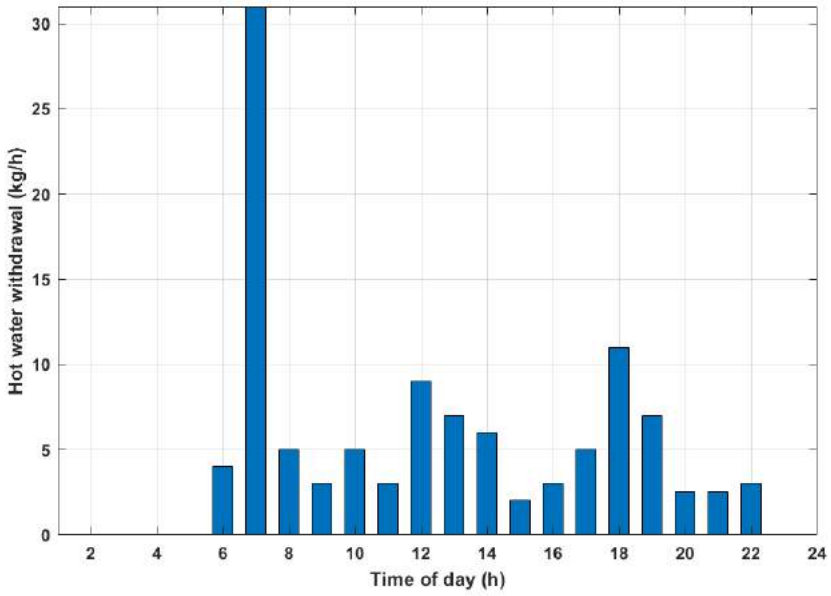

(a) Daily heat demand for domestic hot water on an hourly basis [54]

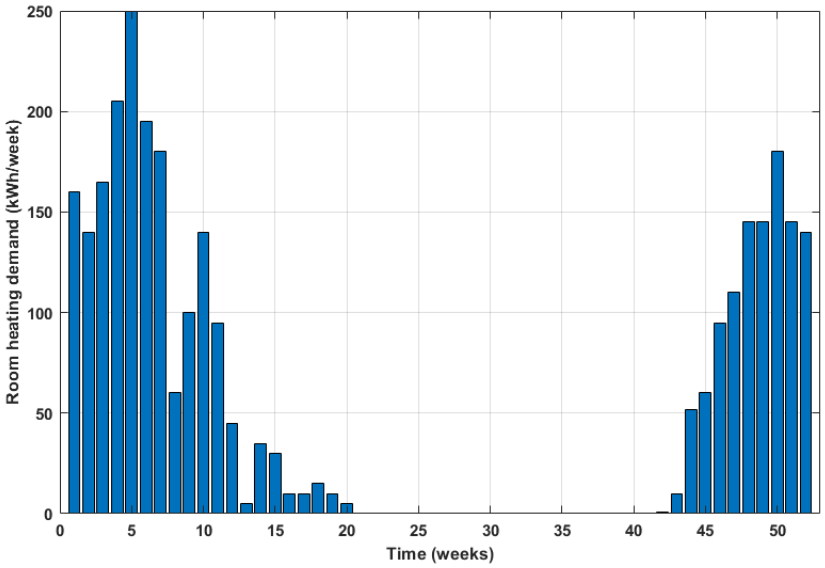

(b) Space heating demand for a household on a weekly basis [54]

Figure 4.14: Thermal energy requirements for a household of 4

4.5.2 System Sizing

A BIPVT system present atop a demo house visualised in figure 3.5 will later be simulated, with its results presented in section 7.3. These simulations will include calculations for an integrated heat pump, as well as a local thermal storage tank. Models and equations for the same will be defined later in chapter 5. The thermal

storage described in figure 4.13, required to be sized for matching domestic hot water demand needs for a household of four. Although the space heating demand is considered for the calculations, thermal storage for the same will not be considered, as it is out of the scope for this project.

The demo roof visualised in figure 3.5 considers a roof of 30 m^2, with an effective collector area of $28.9m^2$. Comprising of thermal pipes 72 meters in length. The domestic hot water demand mentioned above predicts a daily demand of roughly 140 litres per day. The storage tank volume is chosen such that it can contain heat demand for the following day or two. In practise, storage volumes of 200 to 300 litres per day are encountered [54]. Thus, a storage tank volume of 250 litres will be considered for these specific house simulations. For further calculations, the tank will be considered as a stratified thermal storage tank. Calculation model for the same is described in section 5.7.2. Although not considered, seasonal space heating demand for the system could be met by an underground heat storage tank sized at $40m^3$.

Control strategy

A simple control strategy was implemented while implementing the stratified thermal tank model, in order to maximise the thermal yield for the system, while maintaining the tank's temperature levels within a certain range. System was sized for meeting domestic hot water demands with a thermal storage tank of 250 litres. The water extracted from this tank should be heated to at least 60^oC, in order to avoid contamination from Legionella pneumophila bacteria. Illustrated in figure 4.13 as well, an auxiliary (electric) heater needs to be present in order to guarantee this temperature level for domestic hot water demand, for times of low irradiance or when the heat pump is unable to match the load. The collector loop for the thermal storage tank allows to be charged by the heat pump within the temperature range of 40 to 95 ^oC. Maintaining an upper limit so as to not overheat the storage. While this storage tank is said to reach its stagnation temperature when the entirety of the tank is at 60^oC.

Out of the scope of this project, a further control strategy could be developed to charge the space heating thermal storage tank when the domestic hot water tank has reached its stagnation temperature. This would also allow for greater flexibility with the system sizing. The collector could effectively be oversized, yet be able to maintain enough energy for meeting space heating demand in the winters.

Chapter 5

Thermal Models

Researchers at the Photovoltaics and Materials Department of the TU Delft, have been working on a simplified thermal model for characterising concentrating PV-Thermal collectors. This project aims to verify and validate the model being developed at the TUD, with the help of experimental values gathered from the experimental setup presented in chapter 4. This model is explained further in section 5.2. Once the model in question has been verified, it will be used to further characterise and optimise the BIPVT system currently under development at Exasun.

Mentioned in ISO 9806:2017 norms as well, the two main approaches considered for analysing the thermal performance of solar collectors are the Steady-state and Quasi-Dynamic methods. The quasi-dynamic method allows a wide range of operating and ambient conditions for the testing of a thermal collector. Whereas the steady-state method determines collector parameters at high irradiance levels ($> 650\ W/m^2$) and clear sky conditions. Owing to an extended parameter set, the quasi-dynamic method is more accurate in characterising thermal collectors. These methods will be discussed further in sections 5.3 & 5.4. Once solved, these published and proven methods will then be used to validate the model being developed at the TU Delft.

5.1 Heat flow through BIPVT Panels

The BIPVT design under analysis comprises of unglazed, non-insulated thermal absorbers, present below solar panels. Their thermal performance can be analysed with the help of various energy flows associated with the collector. Figure 5.1 depicts the entirety of heat flows coming in and moving out of the collector. As well as the lateral and horizontal conductive heat flows in the panel layers. With respect to unglazed collectors performing at low operating temperatures, all energy flows need to be considered as they might have a significant impact on collector performance.

The amount of solar radiation received by a collector can be defined as a product of the solar radiation incident on the surface area of the collector. However, a portion of this incident radiation is reflected back to the sky and is not absorbed further owing to the collector being an unglazed absorber. Thus, a conversion factor is used to indicate the percentage of solar rays actually absorbed by the collector. Which is a product of the rate of transmission (τ) of the cover, and the absorption factor (α) for the absorber [56]. Hence, equation 5.1 can be used to depict the amount of heat generated or solar radiation absorbed by a collector.

$$Q_i = G_{sun}\,(\tau\alpha)\,.A \tag{5.1}$$

Where, G_{sun} represents incident solar irradiance, and A represents aperture area for the collector. As the collector absorbs more and more solar radiation during sun hours, it absorbs more heat. Eventually, reaching a point where it is hotter than the surrounding ambient air. This is when the absorbed heat is lost to the atmosphere by convection and radiation. Occurring on either side of the collector, illustrated in figure 5.1. This heat loss (Q_o) depends on the overall heat transfer coefficient for the collector (U_L), as well as its temperature gradient with respect to ambient air. The plethora of heat transfers, i.e. radiation, convection and conduction are illustrated in figure 5.1 form the overall heat transfer coefficient. This rate of heat loss can be depicted by equation 5.2 [56].

$$Q_o = U_L A\,(T_m - T_{amb}) \tag{5.2}$$

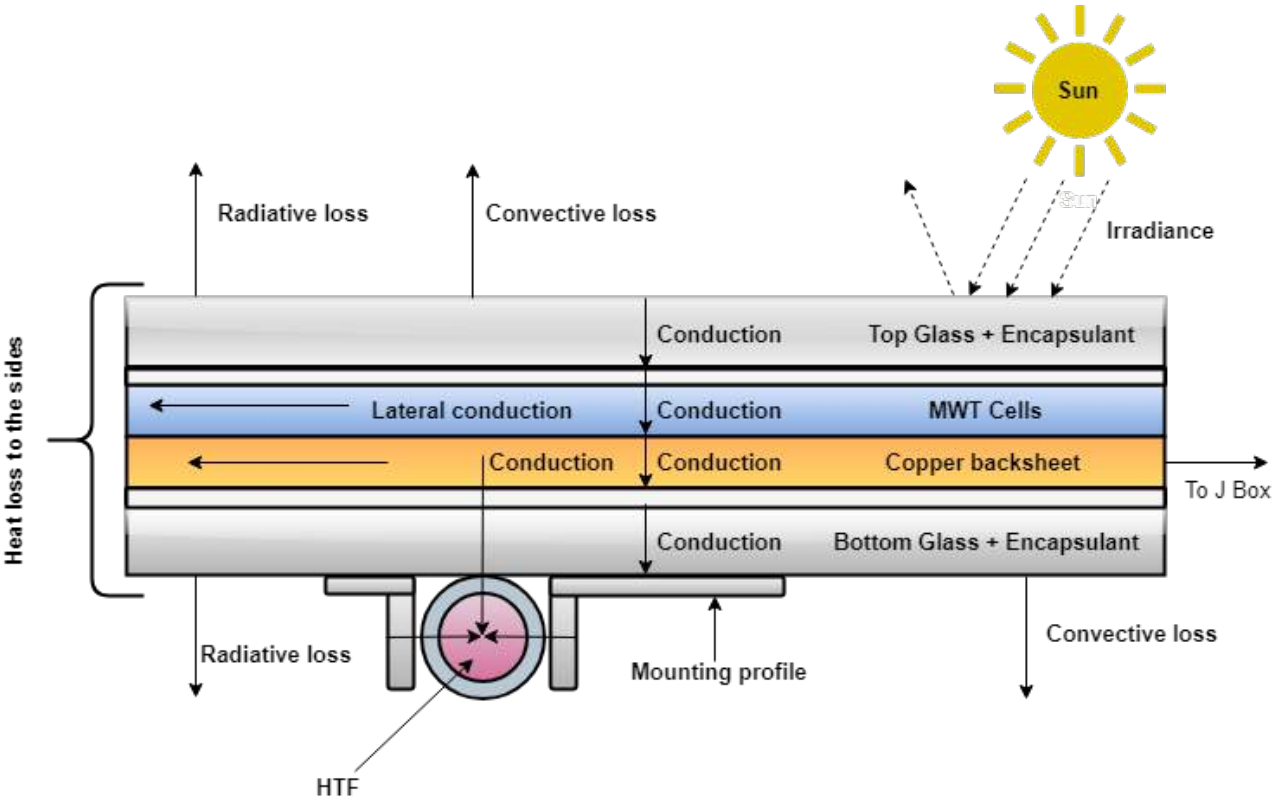

Figure 5.1: Heat flow diagram of the uncovered solar collector

Term T_m in equation 5.2 is the collector average temperature (average fluid inlet and outlet temperature), whereas T_{amb} depicts the ambient temperature. Thus, the useful energy extracted or absorbed by the collector can be defined as the difference between the energy absorbed, and the energy lost, in steady state conditions, depicted in equation 5.3. Useful energy denoted as Q_u can also be measured by the amount of heat carried away by the heat transfer fluid when it passes through the absorber [56]. As depicted in equation 5.3. Where $T_{w,out}$ and $T_{w,in}$ depict outlet and inlet temperatures respectively, while m and c_p are the mass flow rate of the system (in kg/s), and specific heat capacity for the heat transfer fluid (in J/kg^oC), respectively.

$$Q_u = Q_i - Q_o = G_{sun}\,(\tau\alpha)\,.A - U_L A\,(T_m - T_{amb}) = mc_p\,(T_{w,out} - T_{w,in}) \tag{5.3}$$

A quantity relating actual useful energy gain of a collector, to the useful gain of the entire collector, if it were at the fluid inlet temperature, is considered more convenient than defining the collector's average temperature T_m. This quantity is known as the collector's "heat removal factor (F_R), expressed by equation A.1, found in appendix A. Appendix A also includes an equation for the actual useful energy heat gain presented in equation A.2, also famously known as the **"Hottel-Whillier-Bliss equation"**. Whereas equation A.3 describes the instantaneous energy efficiency for a collector.

5.2 A Simple Model for concentrating PV/Thermal Collectors

5.2.1 Goal of the model

The goal for this thermal model is to calculate thermal efficiency curves for concentrating photovoltaic thermal solar collectors, that will eventually help in further investigating various design parameters and their impact on collector efficiency and slope. This model is also an extended simplification of an analytical model presented

by Duffie and Beckman, for flat-plate solar thermal collectors [18]. It has been mentioned several times that the BIPVT design comprises of an unglazed absorber, which is non-concentrating, Thus, the model that will be described ahead will be adopted for a non-concentrating, solar thermal collector.

With the instantaneous efficiency of a flat-plate collector described in equation A.3, performance characteristics of a solar collector can be approximated and better understood by plotting (η) against reduced temperature (T_{red}). Reduced temperature can be defined as the ratio between temperature gradient of collector inlet and ambient temperature, by the solar radiation. Expressed also in equation 5.4. Thermal efficiency deteriorates with higher reduced temperature values, as more heat is lost to the ambient [54]. A linear curve can be interpolated when plotting collector efficiency and reduced temperatures together.

$$T_{red} = \frac{(T_{w,in} - T_{amb})}{G_{sun}} \tag{5.4}$$

An example for the same can be seen in figure 5.2, that illustrates typical thermal efficiency curves for various types of solar thermal collectors, such as unglazed (blue), flat-plate (green), and evacuated tube collectors (red) [59]. Slope of the linear curves in figure 5.2 represent the rate of heat loss for the collectors [56]. For example, collectors having cover sheets (glazed/flat-plate/evacuated), have lesser heat loss than with the ones without (unglazed), thus having less of a slope. As is also visible in figure 5.2, with unglazed collectors performing really well at low inlet temperatures, reaching almost 87% in efficiency. However, their efficiency drops with increasing inlet temperatures, and increasing reduced temperatures. For the same reasons, and a lesser slope, evacuated tube collectors can be used for high-temperature applications, whereas flat-plate collectors also work well for intermediate heating temperatures, between 20 to 70 ^oC.

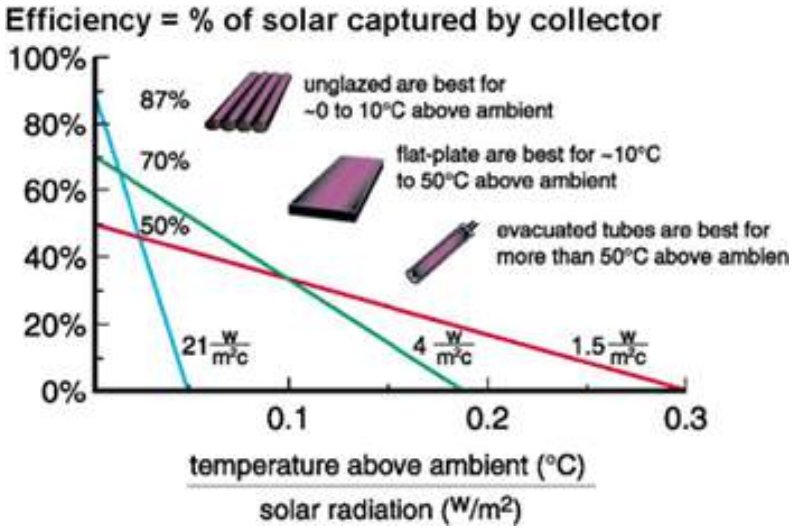

Figure 5.2: Typical thermal efficiency curves for unglazed, flat-plate and evacuated tube solar thermal collectors [59]

$$\eta_{th} \equiv \frac{m.c_p.(T_{w,out} - T_{w,in})}{A.Gsun} \tag{5.5}$$

Figure 5.3 represents a cross-section schematic of the thermal absorber for the BIPVT, wherein L represents receiver length. The width of the collector will be defined as the width of two solar cells, that form the two rows of cells in the 50W panels used. The model will focus on heat transport in the receiver length L, conceptually dividing it into smaller, segments of length dx. Terms $T_{w,in}$ and $T_{w,out}$, shown in the schematic 5.3, represent inlet and outlet temperatures for the collector. The collector efficiency is expressed in equation 5.5.

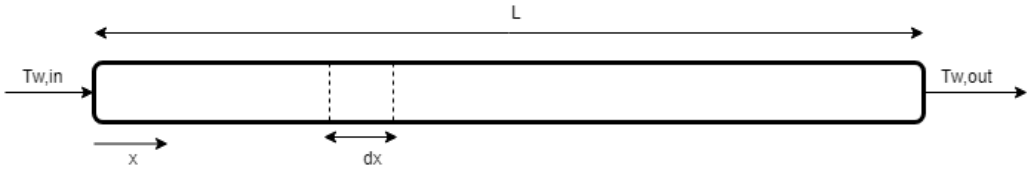

Figure 5.3: Thermal absorber schematic

5.2.2 Heat flows

Thermal fluid entering each segment dx in schematic 5.3, is considered to have an unknown temperature $T_w(x)$, as well as an unknown cell temperature $T_c(x)$. For each of these segments, three main heat flows were considered:

- Solar radiation incident on the absorber [Coefficient G_{sun} in W/m^2]
- Heat loss from cell to ambient [Coefficient h_{ca} in $W/(m^{2o}C)$]
- Heat gain from cell to fluid [Coefficient h_{cw} in $W/(m^{2o}C)$]

Considering these three heat flows, both coming in and flowing out, is an oversimplification of the overall heat transfer coefficient U_L defined earlier. It is done so, in order to get a better understanding of how the heat flows within the system.

The myriad of heat flows occurring in the panel layers and thermal absorber, illustrated in figure 5.1, form an overly complex amalgamation of thermal coefficients. With the heat flows considered, G_{sun} accounts for the incoming solar radiation. Coefficient h_{ca} accounts for the entirety of the heat lost to the atmosphere, including various radiative and convective heat losses occurring on the front, back and sides of the collector. Coefficient h_{cw} accounts for the heat gained by the thermal absorber. These coefficients can be solved manually. However, with questionable accuracy. Owing to the various panel layers, and complex design surrounding the thermal absorber. Due to which, the model will be solved using a **bottom-up approach**, wherein the coefficients will be determined by experimental values derived from the test setup.

These heat flows can be expressed and calculated in watts as well. The first heat flow, describing solar radiance, absorbed and converted into heat by PV cells can be expressed by equation 5.7 given below.

$$P_{sc} = A_{eff} G_{sun} W dx \tag{5.6}$$

Where, A_{eff} indicates the effective absorption factor for the particular cell (indicating the fraction of incident solar radiation converted into heat). As the current model is being developed for concentrating collectors, W corresponds to the width of the concentrating mirror. Since no such mirror is required, or present for an unglazed collector, it will not be considered. The second heat flow, corresponding to the heat lost from PV cell to ambient is approximated by equation 5.7, given below.

$$P_{ca} = (T_{cell} - T_{amb})\, h_{ca} w dx \tag{5.7}$$

Where T_{cell} is the cell temperature. The last heat flow describes the desired flow of heat from the PV cells to the heat transfer fluid flowing through the thermal absorbers. Expressed in equation 5.8. With T_w representing water temperature at that particular segment.

$$P_{cw} = (T_{cell} - T_w)\, h_{cw} w dx \tag{5.8}$$

5.2.3 Model Description

Considering steady state conditions and utilising the claw of conservation of energy, $P_{sc} = P_{ca} + P_{cw}$. The above set of equation from 5.6 to 5.8, are solved by the model, yielding a relation for calculating cell temperatures for a collector, at specific segments. Expressed in equation 5.9.

$$T_{cell} = \frac{T_{amb}h_{ca} + A_{eff}G_{sun}\frac{w}{W} + T_w h_{cw}}{h_{ca} + h_{cw}} \tag{5.9}$$

Equation 5.9 introduces a new term w/W, referred as the concentration factor for concentrating collectors. When evaluating for a non-concentrating, unglazed collector, this factor is considered as 1. The maximum attainable temperature above ambient for a solar collector is defined as its stagnation temperature. Which is expressed further in equation 5.10 below.

$$T_{stag} \equiv T_{amb} + \frac{A_{eff}G_{sun}\frac{w}{W}}{h_{ca}} \tag{5.10}$$

For every point x along the length of the receiver, an analytical expression for water temperature is obtained, expressed in equation 5.11 below.

$$T_w(x) = T_{stag} + (T_{w,in} - T_{stag})\, e^{-x/l} \tag{5.11}$$

Where, l is defined as the thermal adjustment length. Equation 5.11 makes it clear that as x increases, i.e. the further we move along collector length L, T_w asymptotically increases and approaches T_{stag}. Thus, thermal adjustment length l, determines the distance required for T_w to 'reach' T_{stag}. It is expressed in equation 5.12 below.

$$l \equiv \frac{mc_p}{w}\left\{\frac{1}{h_{ca}} + \frac{1}{h_{cw}}\right\} \tag{5.12}$$

The water outlet temperature $T_{w,out}$, can be determined by inputting x = L in equation 5.11. Substituting the same into equation 5.5, gives the desired thermal efficiency expression, expressed in equation 5.13 below.

$$\eta_{th} = \left[\frac{A_{eff}}{h_{ca}} - \left(\frac{T_{w,in} - T_{amb}}{G_{sun}}\right)\frac{w}{W}\right]\frac{mc_p}{wL}\left\{1 - e^{-L/l}\right\} \tag{5.13}$$

Equation 5.13 can be simplified a little, by not considering the concentration factor $\frac{w}{W}$. Thermal efficiency equation considered for the BIPVT can be found in equation 5.14 below.

$$\eta_{th} = \left[\frac{A_{eff}}{h_{ca}} - T_{red}\right]\frac{mc_p}{wL}\left\{1 - e^{-L/l}\right\} \tag{5.14}$$

Equation 5.14 confirms that thermal efficiency is indeed a linear function of the reduced temperature T_{red}. Further simplifications to the efficiency equation can be performed for some special cases. Efficient solar thermal designs can assume that the heat transfer from cell to water is significantly higher than the heat lost to ambient ($h_{cw} \gg h_{ca}$). However, this is not the case for unglazed collectors, hence it cannot be considered. For sufficiently high flow rates, it can be assumed that the thermal adjustment length l, far exceeds the length of the receiver L (l »>

L). The thermal efficiency expressed under this assumption is stated in equation 5.15 below.

$$\eta_{th} = \frac{A_{eff} h_{cw}}{(h_{ca} + h_{cw})} - \frac{T_{red}\,(h_{ca} h_{cw})}{(h_{ca} + h_{cw})} \tag{5.15}$$

5.2.4 Electrical Model

The thermal model under development at the TU Delft not only calculates for thermal efficiency, but it also helps predict the cell temperatures throughout the length of the receiver, expressed in equation 5.9. It is well known that increasing cell temperatures negatively affect a panel's electrical efficiency. The same can be expressed by equation 5.16.

$$\eta_E = \eta_{E,STC}\,(1 - \beta\,\{T_{cell} - 25\}) \tag{5.16}$$

With $\eta_{E,STC}$ representing the panel's electrical efficiency at standard test conditions (STC), β depicts the panel's temperature coefficient for electrical efficiency.

5.3 Steady-State Model

Further validation of the simple thermal model described above is only possible if it can be validated along with other perspective models used for characterising solar thermal collectors. The steady state thermal analysis model has been well defined and works best for sunny climates. Described in ISO 9806 norms, as well as de Jong [15], thermal efficiency in steady state analysis is calculated using equation 5.17. While, equation 5.18 represents a performance equation for unglazed collectors.

$$\eta_{th} = \frac{Q}{AG_{sun}} = \frac{\rho.c_p.\dot{V}\,(T_{w,out} - T_{w,in})}{AG_{sun}} \tag{5.17}$$

Where, Q is the heat flow for the system (in W), ρ represents the density of the heat transfer fluid (kg/l), and $\dot{V}$ is the volumetric flow rate (in l/s).

$$\frac{Q}{A} = \eta_{0,th} G_{sun}(1 - b_u u) - (b_1 + b_2 u)\,(T_m - T_{amb}) \tag{5.18}$$

Where, η_0 is the zero-loss, or peak collector efficiency for the system (η at $T_m = T_{amb}$), u is the wind speed (in m/s), while b_u is the wind speed dependence of the zero-loss efficiency. The other two important coefficients are, b_1, which is the heat loss coefficient, and b_2 is the wind speed dependence of the heat-loss coefficient. The pyrgeometer, mentioned earlier in section 4.2.2, was used for calculating long-wave irradiation (E_L). After which, the values were used for correcting the irradiance values obtained from the pyranometer. Irradiance correction was performed with the help of equation 5.19.

$$G_{sun} = G_{POA} + \frac{\epsilon}{\alpha}\left(E_L - \sigma T_{amb}^4\right) \tag{5.19}$$

Where, $\frac{\epsilon}{\alpha}$ is defined as the ratio of emissivity and absorptivity, considered to be 0.98 [15], in case the values are not readily available. σ is the Stefan-Boltzmann constant. G_{POA} is considered as the global irradiance in plane-of-array (in W/m^2). Equation 5.18 can be substituted into equation 5.17, yielding the desired efficiency

relation for steady state thermal analysis. Presented in equation 5.20 below.

$$\eta_{th} = \frac{Q}{AG_{sun}} = \eta_{0,th}(1 - b_u u) - (b_1 + b_2 u)\,(T_R) \tag{5.20}$$

It is important to note that equation 5.20 defines again thermal efficiency for the system as a linear relation with the reduced temperature. Coefficients η_{th}, b_u, b_1 & b_2 were fitted using a least squares method, applied to equation 5.20.

A vital parameter to note here is that the steady state model, and the quasi-dynamic model described in the next section, define reduced temperature differently. The simple thermal model, described in the previous section, defines reduced temperature as a temperature gradient between the inlet temperature and the ambient temperature, illustrated in equation 5.4. However, the steady-state and quasi-dynamic thermal performance models described by ISO norms 9806 [4], define reduced temperature as the temperature gradient between the average collector temperature and the ambient temperature. Illustrated further in equation 5.21 below.

$$T_R = \frac{T_m - T_{amb}}{G_{sun}} \tag{5.21}$$

The overall extracted power for the steady state model is presented in appendix B, illustrated by equation B.1.

5.4 Quasi-Dynamic Model

The Quasi-dynamic thermal analysis has become the standard for testing solar collectors around the globe. With q uasi-dynamic analysis standard for liquid heating collectors described in ISO 9806 norms, as well as EN 12975 norms for the European union. This method takes into account the dependency of wind speed, long-wave irradiation, effective thermal capacitance of the collector, angle of incidence over the testing period [26], as well as during changing weather conditions. Allowing for a wider range of test conditions, it is for more suitable for outdoor testing calculations than when compared with the steady state method described earlier in section 5.3. Acceptable time periods for steady-state and quasi-dynamic analysis model measurements on a clear day is illustrated in figure 5.4. Depicting that steady-state measurements can be performed for a very short period of the day, whereas quasi-dynamic measurements can be obtained over the entire day [26].

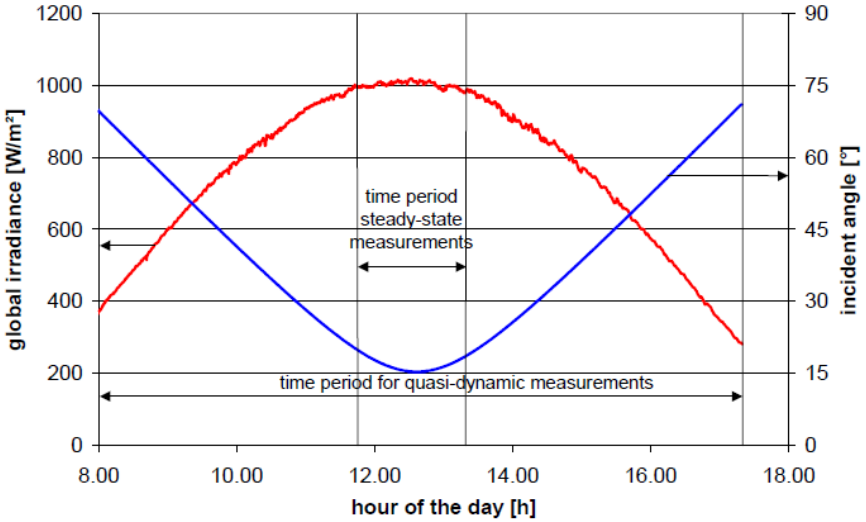

Figure 5.4: Acceptable time periods for steady-state and quasi-dynamic analysis methods [26]

Thermal efficiency gain per unit area of the collector, described in the quasi-dynamic thermal model can be found in the following equation 5.22.

$$\frac{Q}{A} = \eta_0 K_{\theta b}(\theta) G_b + K_{\theta d}(\theta) G_d - c_1 (T_m - T_{amb}) - c_2 (T_m - T_{amb})^2 - c_3 u (T_m - T_{amb}) - c_4 (E_L - \sigma T_{amb}^4) - c_5 \frac{dT_m}{dt} - c_6 u G_{sun} \quad (5.22)$$

Where, the zero-loss efficiency (η_0) is defined in equation B.4. The basic modelling for the incidence angle modifier (IAM) for direct beam irradiation ($K_{\theta b}(\theta)$) is defined in equation B.5. While $K_{\theta d}$ represents the incidence angle modifier for diffuse radiation. θ depicts the incident angle, G_b and G_d are the beam and diffuse irradiances. Further discussions about the zero-loss efficiency and incidence angle modifier are presented in appendix B. Alongside the mathematical model equation for calculating the thermal output of a collector, for quasi-dynamic testing, presented in equation B.3. The necessary coefficients presented in equation 5.22 are explained below [26]:

- c1: Heat loss coefficient at zero-loss efficiency $(T_m - T_{amb})$ $[W/(m^2K)]$
- c2: Temperature dependence of heat loss coefficient $[W/(m^2K^2)]$
- c3: Wind speed dependence of heat-loss coefficient $[J/(m^2K)]$
- c4: Long-wave irradiance dependence of the heat losses $[W/(m^2K)]$
- c5: Effective thermal capacitance $[J/(m^2K)]$
- c6: wind speed dependence of zero-loss efficiency, a collector constant [(s/m)]

However, equation 5.22 can be simplified further, since for the BIPVT installation, influence of the direct and diffuse radiations on the collector, as well as the impact of the incidence angle on the same has not been evaluated, as it is beyond the scope of this project. Therefore, the simplified quasi-dynamic performance equation can be found below, in equation 5.23.

$$\frac{Q}{A} = \eta_0 G_{sun} - c_1 (T_m - T_{amb}) - c_2 (T_m - T_{amb})^2 - c_3 u (T_m - T_{amb}) - c_4 (E_L - \sigma T_{amb}^4) - c_5 \frac{dT_m}{dt} - c_6 u G_{sun} \quad (5.23)$$

The above equation can also be substituted into equation 5.17, for the desired thermal efficiency equation of the quasi-dynamic thermal analysis. Presented below, in equation 5.24.

$$\eta_{th} = \eta_0 - c_1 \frac{(T_m - T_{amb})}{G_{sun}} - c_3 u \frac{(T_m - T_{amb})}{G_{sun}} - c_5 \frac{dT_m}{dt} - c_6 u \quad (5.24)$$

5.5 Electrical Coefficients

This section provides a brief overview of the various terms and parameters used for evaluating the electrical performance of a PV cell, or module, or system.

5.5.1 Module Parameters

Important electrical module parameters are given in the equations below. Where, V_{mpp} & I_{mpp} are the voltage and current at the maximum power points. Whereas, V_{OC} & I_{SC} are the open circuit voltage and short circuit current for a module, respectively. Equation 5.26 defines the maximum operating power point for a given module. Equation 5.27 represents the fill factor (FF) for a module. A measure of quality, FF compares a module's maximum power to its theoretical power.

$$P_{Rated} = V_{OC} \times I_{SC} \tag{5.25}$$

$$P_{mpp} = V_{mpp} \times I_{mpp} \tag{5.26}$$

$$FF = \frac{(V_{mpp} \times I_{mpp})}{(V_{OC} \times I_{SC})} \tag{5.27}$$

Equations 5.28 & 5.29 represent the power output efficiency for a module, and its average module efficiency, respectively. These equations were obtained from Amin et al. [6].

$$\eta_{output} = \frac{P_{mpp}}{P_{rated}} \times 100 \tag{5.28}$$

$$\eta_{E,avg} = FF \times \frac{(V_{mpp} I_{mpp})}{A G_{sun}} \tag{5.29}$$

5.5.2 Performance Ratio

Utilising the electrical output of the PV obtained from experimental results, a performance ratio for the modules can be evaluated as well with the help of equation 5.30 below. Equations 5.31 & 5.32 represent the useful yield of a PV system, and the reference yield for the same [17].

$$Pr = \frac{Y_f}{Y_r} = \frac{E_{use}.G_{STC}}{P_{Rated}.G_{sun}} \tag{5.30}$$

$$Y_f = \frac{E_{use}}{P_{Rated}} \tag{5.31}$$

$$Y_r = \frac{G_{sun}}{G_{STC}} \tag{5.32}$$

5.6 Solar fraction & System Efficiency

Solar fraction, denoted as SF, is defined as the fraction of heat supplied by the collector, to the amount of heat required. Denoted by equation 5.33.

$$SF = \frac{E_{th}^{col}}{E^{dem}} \tag{5.33}$$

Where, E_{th}^{col} denotes the annual heat generated by a collector, whereas E^{dem} denotes the annual heat demand for a household. The annual heat demand comprises of two components, the annual domestic hot water demand (E_{dhw}^{dem}) and annual space heating demand (E_{sh}^{dem}). The annual thermal energy demands for the households were discussed earlier in section 4.5.1.

The annual thermal system efficiency can be defined by equation 5.34.

$$\eta_{th}^{sys} = \frac{E_{th}^{col}}{E^{sun}} \tag{5.34}$$

Where, E^{sun} is the annual incident solar energy on the collector, assumed as 1100 $kWh/y/m^2$ of a collector. The annual electrical system efficiency can be defined by equation 5.35.

$$\eta_{e}^{sys} = \frac{E_{e}^{col}}{E^{sun}} \tag{5.35}$$

Where, E_e^{col} is the annual electrical yield for a system. Note that the equations defined and described above were extracted by Santbergen [54].

5.7 Heat Pump & Thermal Energy Storage

The collaboration of this project with the PVT inSHaPe consortium project was discussed earlier in section 1.2. The system overview discussed in section 4.5 corresponds to the next stage of this project that will be implemented later, under collaboration with companies such as NRGTEQ & CONICO Valves, specialising in heat pumps and thermal storage systems. This section provides an overview of the heat pump to be implemented by NRGTEQ, as well as a stratified thermal storage model [54].

5.7.1 Ideal Heat Pump

Basic heat pump calculations were carried out in order to ascertain the necessity for integrating it with an unglazed BIPVT collector. An ideal heat pump model was assumed, calculations for the same will be presented later in chapter 7. Working of a heat pump has been discussed earlier in section 2.4.1. Ideal heat pump equations are listed below, derived from Bouteiller et al. [9] & [3]. Figure 5.5 provides an illustration of the heat flows occurring within a heat pump. Q_C refers to the heat extracted from the cold reservoir, or in the case of this project, the heat extracted from the BIPVT. Q_H depicts the heat delivered to the hot reservoir, or the condenser delivering heat to the thermal storage tank. W depicts the work carried within the heat pump, referred to as the energy required by the compressor.

$$COP = \frac{Q_H}{W} \tag{5.36}$$

The coefficient of performance for a heat pump is described as the ratio between energy transferred for heating, to the input electric energy used in the process. It can be defined with the help of equation 5.36. While assuming an ideal heat pump in action, an average COP for the same can be assumed as well. Thus, for further calculations, a COP of 4 will be assumed for the heat pump. With the help of this basic assumption, the collector loop inlet temperature for the storage tank can be measured, by using equation 5.38.

$$Q_C = m\rho_{htf}c_p\left(T_{w,out} - T_{w,in}\right) \tag{5.37}$$

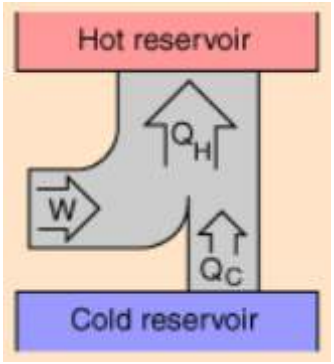

Figure 5.5: Heat flow within a Heat pump [3]

$$T_5 = (T_{w,out} - T_{w,in}) \times COP \tag{5.38}$$

Temperatures T_5 & T_6 were mentioned earlier in section 4.5. m_{Ref} & $c_{p,ref}$ refer to the mass flow rate of the heat pump, & the specific heat capacity of the refrigerant used. Q_C is calculated using equation 5.37. Once T_5 has been calculated with the help of equation 5.38, its values can be substituted in equation 5.39, to ascertain Q_H. In doing so, another assumption needs to be made for T_6, i.e. the collector loop outlet temperature from the storage tank. Illustrated in figure 4.13, T_6 can be assumed to be equivalent to T_8, i.e. the demand loop outlet temperature, sourced from the mains.

$$Q_H = Q_C + W = m_{Ref}\rho_{ref}c_{p,ref}\left(T_5 - T_6\right) \tag{5.39}$$

5.7.2 Multinodel model for stratified thermal storage tanks

Chapter 2 mentioned various thermal storage options, as well as their importance. No thermal system can exist without a storage solution. Let's consider any type of tank, be it a water tank, or a petrol tank, etc. Any such tank having a continuous inflow and outflow of fluids at different temperatures will be unable to maintain a constant temperature for itself. Understanding this, the thermal storage mentioned in section 4.13 follows the same principle as well, with constantly varying temperatures at each time step. Thus, in order to comprehend these varying temperatures and to obtain a clearer picture of the storage tank's performance, a multinodel numerical model was implemented, that can effectively calculate these varying temperatures, by diving the thermal tank into segments. Thus the following section will present this model, for stratified thermal storage tanks, extracted from Santbergen [54], Duffie and Beckman [18] & Kleinbach et al. [44].

In the mutlinodel approach, N number of fully mixed volume segments, also called as nodes, form a stratified thermal storage tank. Each segment is considered to have a uniform, yet different temperature, denoted by T_i. Where, i depicts the node, i.e. i = 1.....N segments. The top segment for the tank stands at i=1, at T_1, with the highest tank temperature (thus, lowest density). Altering the values of N, or the number of nodes for the tank, alters it's stratification degree. With a higher amount of nodes giving a higher degree of stratification. Figure 5.6 illustrates a thermal storage tank with nodes up till N. Temperatures denoted from T_5 to T_8 were mentioned in section 4.5. Understandable from the figure, two main flows control the thermal tank stratification and temperatures. That is, the collector loop flow arriving from the heat pump's condenser, and the demand loop flowing towards a household. T_5 is considered the collector loop inlet, with its flow rate denoted by m_c, while T_7 is the demand loop inlet, with the flow rate denoted by m_d. T_8 represents the fresh water inlet from the mains, and is assumed to have a temperature of 10^oC. It is also the demand loop inlet for the storage tank, while T_6 is the collector loop outlet for the tank, going back to the condenser. The mains inlet T_8 enters the tank from the bottom, while collector loop outlet, T_6 exits from the bottom as well.

Owing to buoyancy effects taking place in the tank, water entering the tank will try and match the density and

temperature of the water already present, and in doing so, rise or descend accordingly. For ease of calculation, the model assumes best matching temperatures for the water entering the tank.

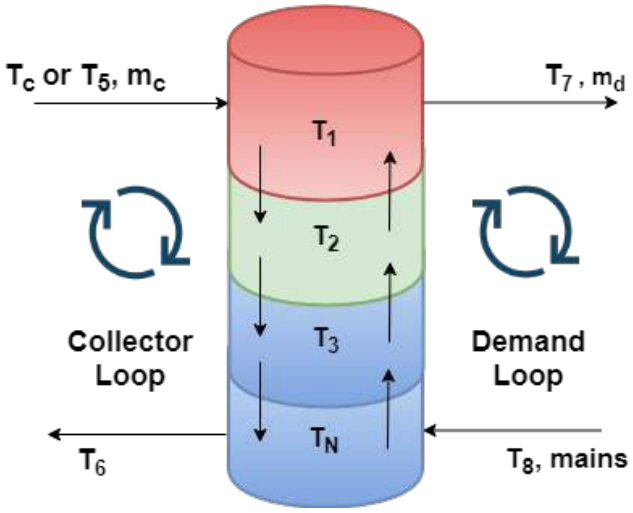

Figure 5.6: Overview of a stratified thermal tank

The energy balance for the stratified tank is discussed in appendix C. The equation responsible for the same is defined in C.1. After which, the FOM, or figure of merit & it's relevance was discussed as well. Equation C.1, represented as a first order differential equation, can be solved for i=1....N number of segments, determining temperature of each segment at t>0. The final result yields equation 5.40 below [54].

$$T_i(t) = T_c + \sum_{j=0}^{i-1} \frac{1}{j!} \left(\frac{t}{\tau}\right)^j (T_0 - T_c)\, e^{\frac{-t}{\tau}} \tag{5.40}$$

Where, $T_i(t)$ refers to the temperature at segment temperature i, in time step t. T_c is better known as T_5, mentioned earlier. j is considered for referring to the previous segment, that is, *i-1*. T_0, discussed in Appendix C as well, is considered as the starting temperature point of the thermal tank, at 0^{th} time step. The segment turnover time is denoted by $\tau = \mathrm{M}/m_c$. With M representing the flow rate of the storage tank. While, t is referred as the tank turnover time, calculated by $\mathrm{t} = \mathrm{N}/\tau$. T_e is the mean collector temperature, such that, $\bar{T_e} = \sum T_i/\mathrm{N}$.

As the number of segments, or N, decide the degree of stratification of the modelled tank, it is important to keep a good estimate for the same. With N=1 corresponding to a fully mixed tank tank, with an FOM of 0.63. While, $\mathrm{N} \to \infty$ is the limiting case for the segments, with a perfectly stratified tank, having an FOM = 1. Between these two cases, a consideration of three stratified segments, i.e. N = 3, represents a good balance and a reasonable compromise between complexity and performance. An N = 3, corresponds to a FOM of 0.78 [54].

Chapter 6

Model Validation

This chapter will provide further insight into experimental data, it's filtering, various test procedures, general assumptions made for the calculations, and the validation of the thermal model presented in section 5.2. The analysis procedures and assumptions stated below correspond to all three models described previously in chapter 5 unless otherwise stated.

6.1 Parametric assumptions

This section aims to describe various parameter assumptions and constants considered for the models described in chapter 5. ISO norm 9806 [4] characteristically lists out various quantity measurements required for model calculations, along with permitted deviations for measuring periods.

Steady-state thermal model

A solar thermal collector can be evaluated with the help of the steady-state thermal model only when the collector is operating in a steady-state condition. Thus, a collector is considered to be operating in steady-state conditions over a period of time if none of the experimental parameters deviate more than the limits of their mean values. These limits have been thoroughly described in NEN [4]. Include experimental parameters such as solar irradiance ($\pm 50 W/m^2$) , ambient air temperatures ($\pm 1.5K$), mass flow rate ($\pm 1\%$), fluid inlet temperature ($\pm 0.1K$), and a few others. Although these deviations were not accounted for in the model calculations, the system was assumed to be operating in steady state conditions.

Quasi-dynamic thermal model

The experimental parameter deviations mentioned earlier for the steady-state model are used for quasi-dynamic testing as well although out of scope for the calculations for this project. NEN [4] states that solar thermal collectors with a concentration ratio less than 20 are mandated to consider coefficients c_1, c_2 & c_5 for the calculations. Further information regarding the same is presented in appendix B. Whereas, the remaining collector terms, such as c_3, c_4, & c_6 are only included in the final calculations if they contain statistical significance. The statistical significance of terms is determined by there *'t-value'*. Which is defined as a ratio of the parameter value by the standard deviation of the parameter value. Recommended by NEN [4], a parameter should be considered only if it's t-value is above three.

A later part of this chapter will present the respective model coefficients, illustrated in table 6.2, determined for each analysis. This table illustrates the various coefficients determined for analysing the quasi-dynamic performance model. Note that coefficients c_2 & c_4 where not considered for the final calculations. This is because, even though coefficient c_2 should be mandatory for performance calculations, it should also depict a positive value to be included in the same. While c_4 is not mandatory to be included, its statistical significance (t-value) was found to be lower than 3, thus being omitted from the final calculations.

A simple thermal model for concentrating PV-Thermal collectors

Two main assumptions that can be considered for the simple thermal model, in order to simplify its thermal efficiency equation 5.14 were discussed earlier in section 5.2. These assumptions rely solely on the heat transfer coefficients and the thermal adjustment length. Since the model has been designed to fit concentrating collectors, certain designs can attain a higher heat transfer coefficient from cell to fluid ($h_{cw} \gg h_{ca}$). However, this is not the case for unglazed, non-insulated designs, which will always concur a significant amount of heat loss to the ambient. Owing to which, this simplification cannot be assumed.

The thermal adjustment length (l) described for a simple thermal model previously in chapter 5 is used to determine the time taken for the fluid flowing within a thermal absorber to reach its stagnation temperature. The stagnation temperature was determined for the experimental setup using equation 5.10. If an adequately high flow rate is assumed, such that l greatly exceeds the thermal absorber length (l $\gg$ L), the curly brackets containing an exponential term in equation 5.14 can be simplified to L/l. Carrying out presumptive analysis for the collector, the thermal adjustment length was found to be significantly higher than the length of the thermal absorbers. Thus, this particular assumption was presumed for determining heat loss coefficients, and expressed the simplified thermal efficiency, by equation 5.15.

6.2 Filtering data

The measured data presented here were collected between the 1^{st} of July 2018, till the 30^{th} of September 2018. The raw experimental data extracted from various sensors mentioned in section 4.2.2, was obtained using the data acquisition (DAQ) servers mentioned in section 4.4. The DAQ recorded data every ten seconds, which was averaged out over every minute. The randomness of this raw data is illustrated in figure 6.2. In order to make better sense of the obtained data, it had to be averaged out even further. EN 12975 standards [45], recommend using an averaging period of five to ten minutes. Figure 6.1 illustrates the variation of heat transfer coefficients for the simple thermal model. With averages ranging from a minute up til sixty minutes. It was observed that this averaging did not make a significant impact on the regression results. Thus, in order to maintain a relatively large set of data points, an averaging time period of fifteen minutes was considered for all the models.

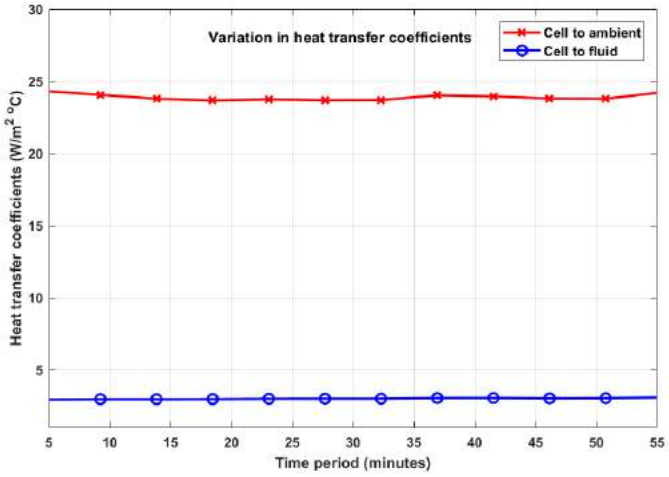

Figure 6.1: Heat transfer coefficient variation with changing averaging periods

The thermal efficiency data points against respective reduced temperatures can be found in figure 6.2 below. With the blue points illustrating the averaged out data for every 15 minutes. This average was carried out with the help of a mean filter function created on MATLAB. The extracted raw data consisted of data points spanning over three months, i.e. July, August, & September. Comprising of **132480** such data points, for each minute. After averaging out the same, the analyses for all the thermal models was carried out on **8832** such data points.

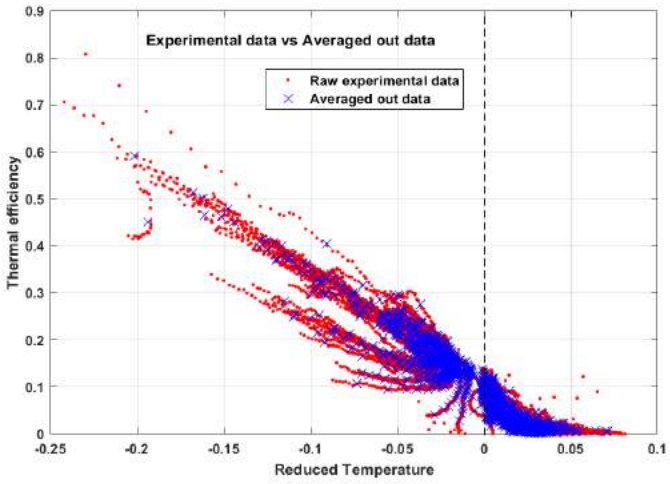

Figure 6.2: Raw experimental data vs. Averaged out data

In line with ISO 9806 [4], the limiting range of operating irradiances for the three models can be found in table 6.1 below. Since diffuse irradiation is out of the scope of this project, solar irradiance for all three models was corrected for long-wave irradiance measured using the pyrgeometer present on the demo roof, discussed in section 4.2.2. Equation 5.19 was used to correct for the same. It is evident from table 5.19 below, that testing procedure for the steady-state model is reasonably rigorous.

Model	**Minimum** (W/m^2)	**Maximum** (W/m^2)
Quasi-dynamic	300	1100
Steady-state	600	-
Simple model	300	1100

Table 6.1: Limiting irradiance for analysis

6.3 Linear Regression

Linear regression is a basic and commonly used type of predictive analysis. The three major use cases for the same include, (1) forecasting an effect, (2) trend forecasting, & (3) determining the strength of predictors. Its overall idea is to examine two important criterion. One, if a set of predictor variables do a good job in predicting the outcome, or the dependent variable. Two, which of the variables in question are relevant predictors of the outcome variable. Estimations in linear regression are used to explain the relationships of usually one dependent variable, and one or more independent variables. The simplest form for the same utilises one dependent and one independent variable. Solved with the help of the following regression equation $y = mx + c$. Where y refers to the estimated dependent score, x is the score for the independent variable. While, m depicts a regression coefficient or slope, and c is considered a constant, or y-intercept [2]. The various coefficients for the models described in sections 5.2, 5.3, & 5.4 were calculated using Ordinary Least Squares (OLS) method of linear regression. More information about OLS can be found in a book written by Craven and Islam [14]. The models were analysed on MATLAB 2017 edition, with the help of its inbuilt linear regression model. Accessed by the function **fitlm**. OLS employs a simple form of a linear regression model, aiming to reduce the square of the difference between measured values, and the predicted values, for a given data set. The interpolated linear curve, along with the fitted curve for the thermal model is illustrated in figure 6.3. While utilising the 'fitlm' linear regression function of MATLAB, the robust fit option for the same was utilised as well, in order to fit a robust linear curve in the particular data points. While the curve fitting tool inbuilt into MATLAB libraries was used as well. This curve fitting tool was accessed with the help of a 'cftool' command and provides a flexible interface for interacting with fitting curves or surfaces. With the help of this toolbox, a linear curve fit was chosen with the particular data points, while a custom equation was input for each thermal model being analysed. An estimate of these

coefficients was then saved and utilised later for fitting respective linear curves.

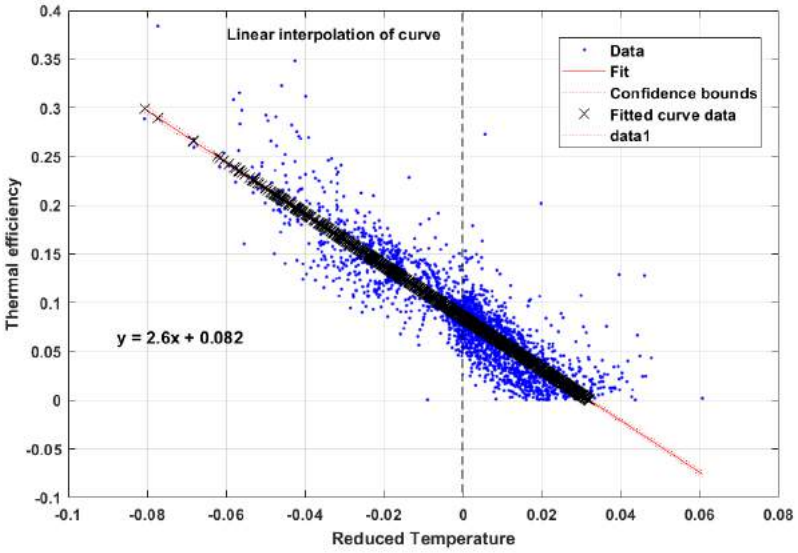

Figure 6.3: Linear interpolation of curve & Curve fitting

6.4 Calculated coefficients

The table 6.2 below will provide an overview of the various coefficients obtained for all three models from the linear regression discussed in section 6.3. It is important to note that the quasi-dynamic coefficients listed below, were obtained with the help of the analysis performed by SEAC.

Thermal model	Coefficients	Values
A simple thermal model	η_0	8.73 (%)
	h_{ca}	23.6 $(W/(m^{2o}C))$
	h_{cw}	3.07 $(W/(m^{2o}C))$
Steady-state model	η_0	9.14 (%)
	b_1	-2.63 $(W/(m^{2o}C))$
	b_2	-0.1664 $(J/(m^{3o}C))$
	b_u	-0.02 (s/m)
Quasi-dynamic model	η_0	11 (%)
	c_1	-2.35 $(W/(m^{2o}C))$
	c_2	-
	c_3	-0.165 $(J/(m^{3o}C))$
	c_4	-
	c_5	2809 $(J/(m^{2o}C))$
	c_6	-0.01 (s/m)

Table 6.2: Respective Thermal model coefficients

The low zero-loss efficiency values obtained from the models can be attributed to the poor thermal contact between the PV and the thermal absorbers. Decreasing the thermal resistance between the PV and the thermal absorbers can lead to a better zero-loss efficiency. Ways to improve this will be mentioned later on in section 8.2. Heat loss coefficient terms and their significance for steady-state and quasi-dynamic thermal models have been described previously in sections 5.3 & 5.4. Parameter c_3 describes the heat loss due to wind speed, while parameter c_4 describes the sky temperature dependence for heat loss. The dynamic behaviour of the thermal collector is demonstrated by coefficient c_5, using dT_m/dt term. Owing to the wide range of considerations for

the quasi-dynamic performance model, a few collector coefficients of the steady-state model are comparable with the other. The coefficients b_1, b_2 & b_u corresponding to the steady state model are analogous to c_1, c_3 & c_6 coefficients of the quasi-dynamic model. Comparing the same in table 6.2, show a close agreement between the two. Coefficients b_1 & c_1 representing heat loss can also be compared against the h_{ca} coefficient of the simple thermal model. Although the differences between the first two are quite similar, the difference between the heat loss coefficient of the simple model is quite large. This can be attributed to the fact that the steady-state and quasi-dynamic model, in particular, consider more coefficients affecting the thermal performance. Thus, in the simple thermal model, the entirety of the thermal losses for the system are combined into one convenient coefficient. Also, the slight difference in values for steady-state & quasi-dynamic models can be attributed to a lack of data for the steady-state analysis, as it applies for only a limited irradiance range. Which was presented in table 6.1.

6.5 Varying data

Mentioned in section 6.2 previously, the thermal model calculations were performed via data that was obtained between the months of July, August & September of 2018. Section 5.1 mentioned that the main parameters affecting system performance were the solar irradiance, the inlet flow temperature for the collector and the flow rate of the same. As it is an outdoor setup, incident solar irradiance is out of control. However, the inlet flow rate and temperature are the two main parameters that are controlled, in order to obtain a better understanding of how the system will perform under varying conditions. Thus, over the course of the three months, these two parameters were altered. The thermal efficiency curve for the setup illustrated in figure 6.3 was a result of this variation, and the coefficients obtained present an average of these varying values. Tables 6.3 and 6.4 provide the inlet temperature and and mass flow rate variations observed, respectively.

Month	**Day**	$T_{w,in}$ in ^oC
July	01 - 02	40 ± 2
	03 - 05	30 ± 2
	06 - 12	25 ± 2
	13 - 15	20 ± 2
	16 - 31	10 ± 2
August	01 - 31	40 ± 2
September	01 - 27	20 ± 2
	27 - 30	30 ± 2

Table 6.3: Varying inlet temperatures over the course of the experiment

Month	**Day**	**m in l/h**
July	01 - 02	110 ± 5
	03 - 31	100 ± 5
August	01 - 05	100 ± 5
	06 - 27	95 ± 5
	27 - 31	85 ± 5
September	01 - 03	85 ± 5
	04 - 30	95 ± 5

Table 6.4: Varying mass flow rates over the course of the experiment

6.6 Validating the model

Mentioned earlier, figure 6.2 provided a basic curve fitted model validation for a simple thermal model. The experimental data points were plotted against fitted data points obtained from the thermal model. Yielding a near perfect fit for the same. This, however, can only be deemed as a fitted curve validation for the model.

Thermal Model	η_{avg} (%)	Difference (%)
Simple thermal	8.3	-
Steady-state	8.16	1.65
Quasi-dynamic	7.53	9.21

Table 6.5: Comparing the thermal models

In order to further validate the same, the thermal efficiency curves obtained from two other thermal models were juxtaposed with the simple thermal model, buttressing its validity. The average thermal efficiencies calculated by the models were observed, as well as the percentage difference for the same, between the simple model and the other two models. Figure 6.4 illustrates a juxtaposed plot comprising the thermal efficiency curves of all three thermal models. This figure provides a better understanding of how the simple thermal model performs, side by side with the steady-state and quasi-dynamic models. All three models showcase a similar trend and similar slope, with only marginal differences between them.

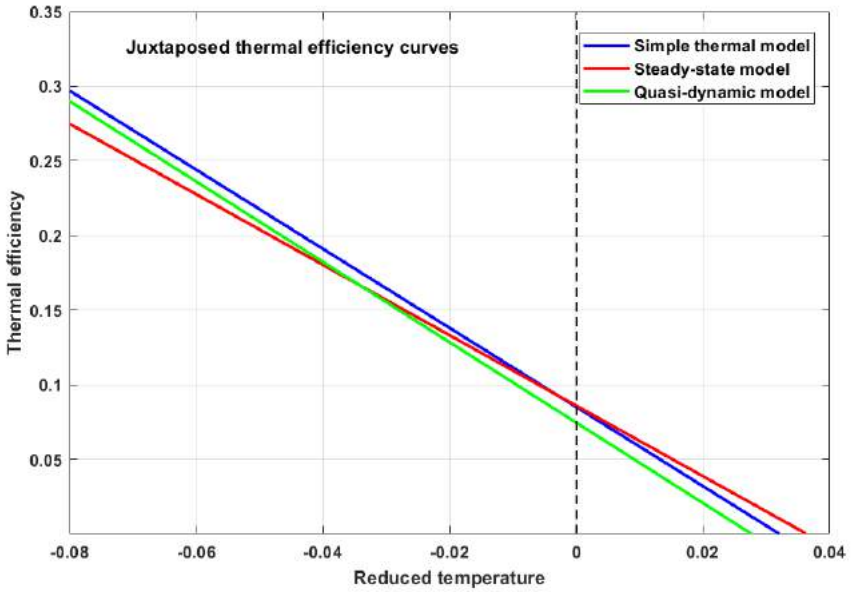

Figure 6.4: Juxtaposed model efficiency curves

The marginally higher slope for the simple thermal model can be attributed to the fact that it considers fewer coefficients affecting design performance. Another major attribute for this is the varying definitions of reduced temperatures for the three models. While the simple model considers reduced temperature as a temperature gradient between the collector inlet temperature and the ambient air temperature, illustrated in equation 5.4, the steady-state and quasi-dynamic models consider reduced temperature as the temperature gradient between the mean collector temperature and the ambient air temperature, illustrated by equation 5.21.

The entire premise of the model described in section 5.2 being termed '**A simple thermal model for concentrating PV-Thermal collectors**' is based on the fact that even though it takes only two coefficients into consideration, namely the heat transfer from cell to ambient (h_{ca}) and fluid (h_{cw}), it is able to effectively approximate a thermal efficiency curve for a non-concentrating, unglazed, BIPVT system. Concurring only a marginal amount of error in the process. The model was able to calculate an average thermal efficiency for the system, at **8.3 %**, with an error of **1.65 %** from the steady-state model's calculated efficiency, and an error of **9.21 %** against the quasi-dynamic model. The tabulated results can be found in table 6.5.

Chapter 7

Results & Discussions

This chapter will provide a concise evaluation of the results obtained from the experimental setup discussed in chapter 4, and the thermal models discussed in chapter 5.

7.1 Electrical Performance

Evaluating electrical performance characteristics for the BIPVT experimental setup was deemed essential. With the setup described in-depth in chapter 4. The DC voltage and current were recorded each minute for the setup, following which the results were averaged out over 15-minute time intervals.

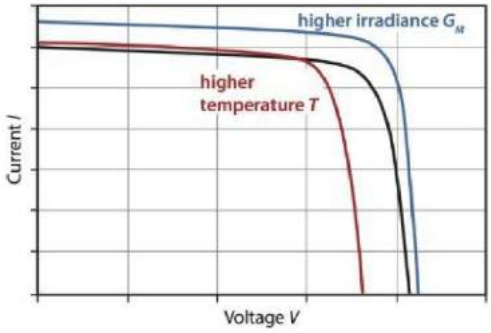

Figure 7.1: Effect of temperature on PV Module performance [42]

Increased photovoltaic cell temperatures can have a significant impact on module performance. Figure 7.1 illustrates the impact that they can have, resulting in reduced maximum operating points. A slight increase in temperature leads to a slight increase in the generated current, owing to a moderate increase in the photo-generated current, caused due to an increased number of thermally-generated charge carriers. However, higher temperatures lead to a decrease in open circuit voltage (V_{OC}), outweighing the increase in short circuit current (I_{SC}) that it results in as well. This results in an overall decrease in power at high temperatures, and a reduced efficiency. An in-depth review of this decrease in performance can be found in section 20 of the book Isabella O. [42]. While a datasheet for the 50W panels utilised can also be found in appendix E, figure E.1 that illustrates it's various thermal coefficients (in %/K) as well.

Figure 7.2 depicts the electrical output and combined panel efficiency, plotted alongside solar irradiance, for the experimental setup. The figure supports the claims made earlier about decreasing power output with increasing temperatures. It clearly showcases a decreasing power output for the system with increasing irradiance. Even though the panel efficiency increases almost linearly with the increase in irradiance, the power output consistently reduces. Figure 7.3 provides a better understanding of how the electrical efficiency of the panels, witnesses a linear reduction with increasing temperatures.

Performance Ratio

Performance ratio is a measure of the quality of a photovoltaic plant or system. It is often described as a quality factor as it is independent of the plant location. Stated as a percentage, it signifies the relationship between the

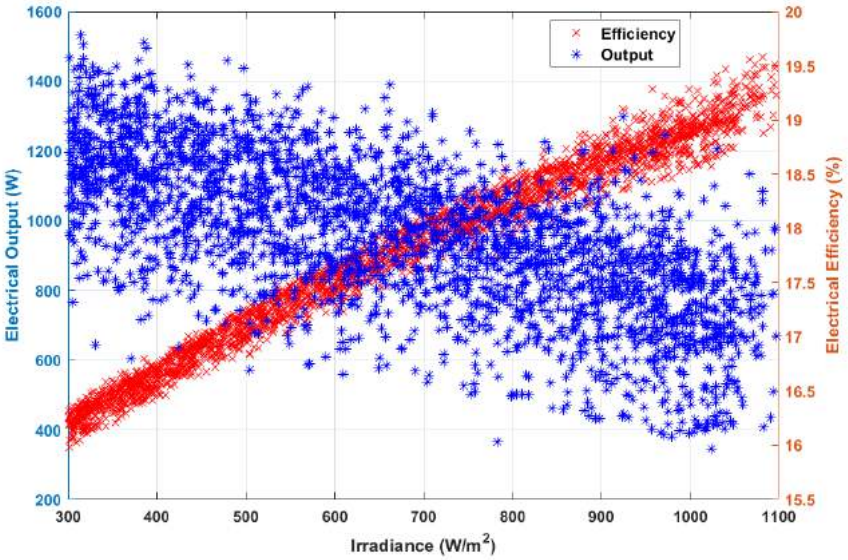

Figure 7.2: Effect of irradiance on electrical output & panel efficiency

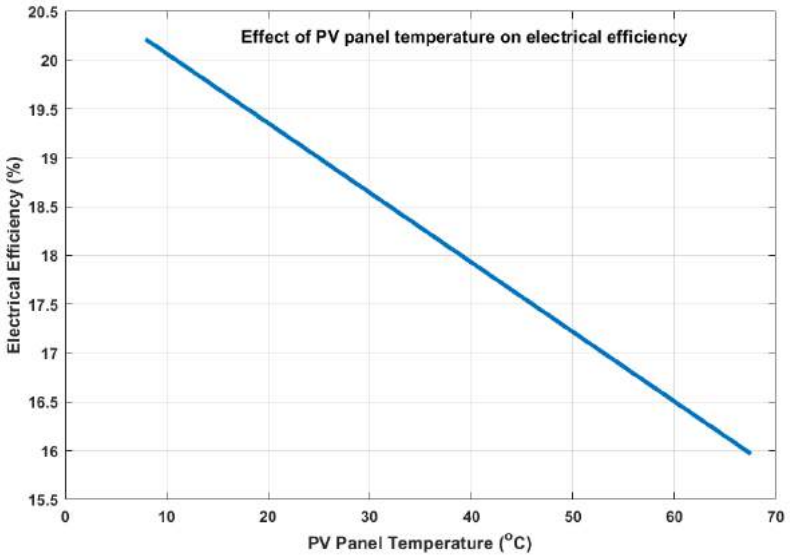

Figure 7.3: Effect of PV Cell temperatures on panel efficiency

actual power output of a plant, and the theoretical rated energy output recorded at STC conditions. Thus, it showcases actual energy production that can be transported to the grid. It helps inform the consumer about a system's operating efficiency and reliability [17]. It can be described by equation 5.30 discussed in chapter 5. One year of data is considered as the optimal period for calculating the performance ratio for a system. However, as the experimental setup was installed this year itself, one year of data was unavailable. On average, a performance ratio of **82.54 %** was observed for the experimental setup, within the time frame mentioned in section 6.2.

Figure 7.4a illustrates a scatter cloud of incident radiation versus performance ratio for the experimental setup. The results can be considered in line with the electrical output versus incident irradiance plot seen earlier in figure 7.2. Since performance ratio is defined with the help of equation 5.30, as the irradiance increases, module temperatures increase, lowering the electrical output. There-by reducing the performance ratio as well.

Figure 7.4b on the other hand, provides a better understanding of the effect of increasing PV cell temperatures

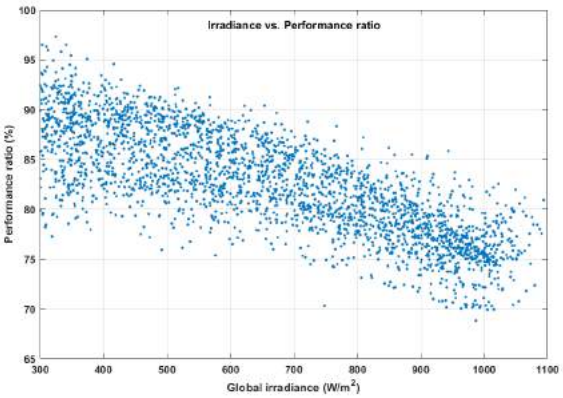

(a) Effect of irradiance on performance ratio

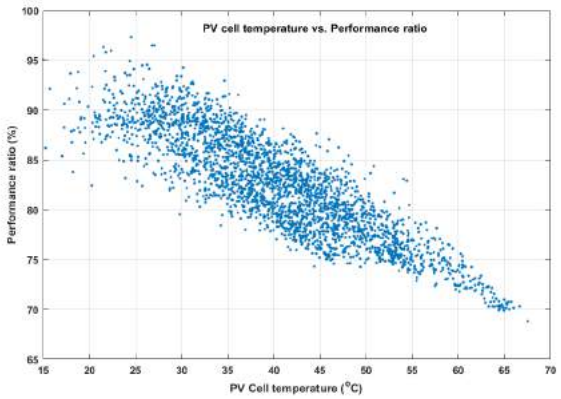

(b) Effect of PV Cell temperature on performance ratio

Figure 7.4: Performance ratio analysis

on the performance ratio. Mentioned in section 4.2.2, a thermal temperature probe was attached to the back of a PV panel, recording its temperature. Data from this probe was plotted against the calculated performance ratio, with expected results. Increased panel temperatures lowered the performance ratio, based on the same principle on which it lowered the system's energy output and panel efficiencies.

7.2 System Characterisation

The following section will illustrate various results of the experimental setup, followed by yearly characterisation for a square meter design of the same.

7.2.1 Setup Characteristics

An overview of the thermal & electrical energy output for the setup, plotted alongside the experimental time step is depicted in figure 7.5, averaged out for every 15-minute time interval. The energy data acquired between the measuring period, was smoothed out by running it through a move mean function in MATLAB, with a step of 50 data-points.

The thermal efficiency curve for the setup was presented first in chapter 6. An easier to comprehend version of the same can be found in figure 7.6. The plot takes into account negative reduced temperatures until -0.08 $((m^2{}^oC)/W)$. Such reduced temperatures are only reached with relatively low fluid inlet temperatures and high ambient air temperatures. These values do not define the average operating range within which the system usually performs. For the same, the average operating range for the system has been highlighted in figure 7.6 as well. Table 7.1 puts the values for the experimental setup into perspective. It tabulates the setup's characteristics, such as the collector area (m^2), and the length of the thermal absorber. It also tabulates the performance ratio, along with the heat transfer coefficients for the system, obtained for the simple thermal model. It also portrays the zero-loss efficiency for the system, as well as it's average thermal, electrical & combined efficiencies.

Figure 7.7 provides an overview of the inlet $(T_{w,in})$, outlet $(T_{w,out})$ water temperatures, and ambient air temperature (T_{amb}) against averaged out thermal & electrical efficiencies for the system, along the course of the of the acquired experimental data.

Mentioned earlier in section 5.1, unglazed PVT systems perform best under relatively low ambient air, and inlet temperatures. Figure 7.7 further bolsters these claims, as the thermal efficiency is found to reach its peak towards the end of July, recording low inlet temperatures averaging around 10 ^oC, and relatively low ambient air

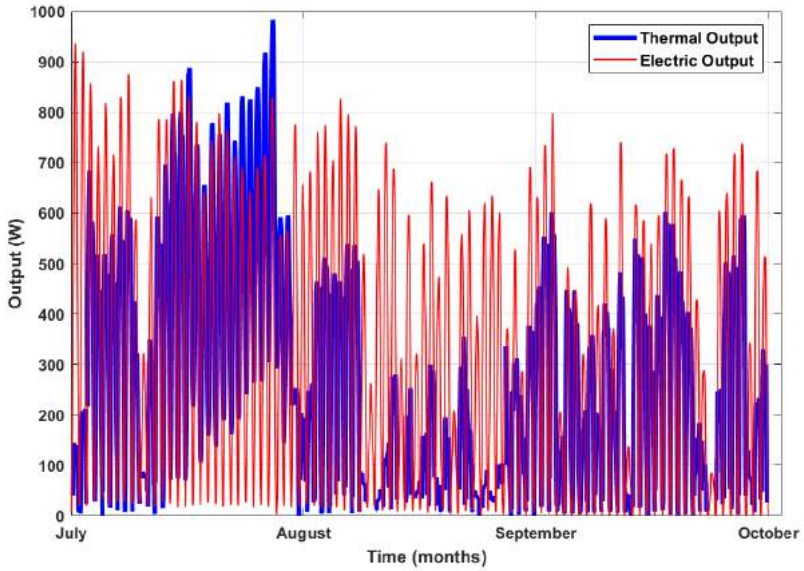

Figure 7.5: Thermal & Electrical Energy output for the experimental setup

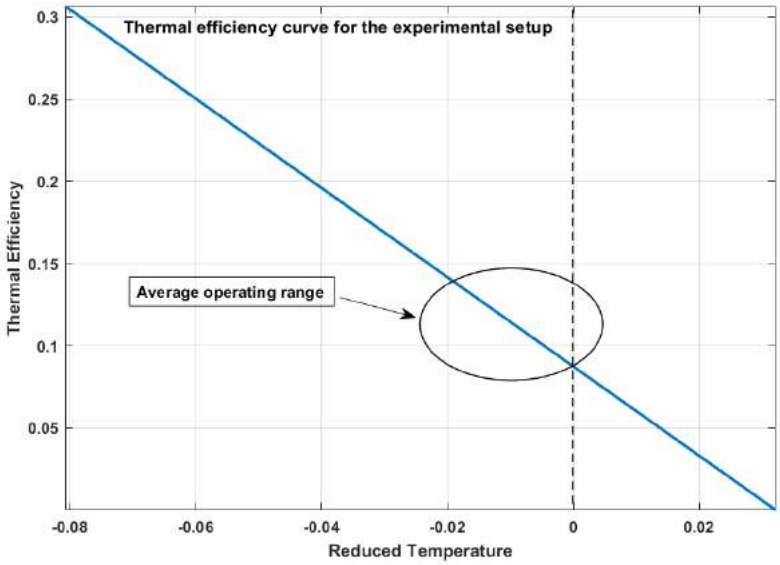

Figure 7.6: Thermal efficiency curve for the experimental setup

temperatures. It is seen that the efficiency of the system takes a severe hit as we move further down the time steps, owing to higher water inlet temperatures averaging around 40^oC.

Figure 7.8 depicts the power curve for the BIPVT setup, i.e. the output power plotted against a temperature gradient between the inlet fluid and ambient air temperatures. The figure provides an idea of the system performance with regards to changing ambient air temperatures. Performing at its peak with ambient air temperatures higher than fluid inlet temperatures, and vice-versa.

Parameter	Denotation	Value	Unit
Setup characteristics			
Collector area	A	8.87	m^2
Collector length	L	30	m
Setup calculations			
Performance ratio	Pr	82.54	%
Cell to ambient	h_{ca}	23.6	$W/m^{2o}C$
Cell to fluid	h_{cw}	3.07	$W/m^{2o}C$
Setup efficiencies			
Zero-loss efficiency	η_0	8.73	%
Thermal efficiency	η_T	8.3	%
Electrical efficiency	η_E	18.9	%
Combined efficiency	η_C	27.2	%

Table 7.1: Setup's calculated characteristics

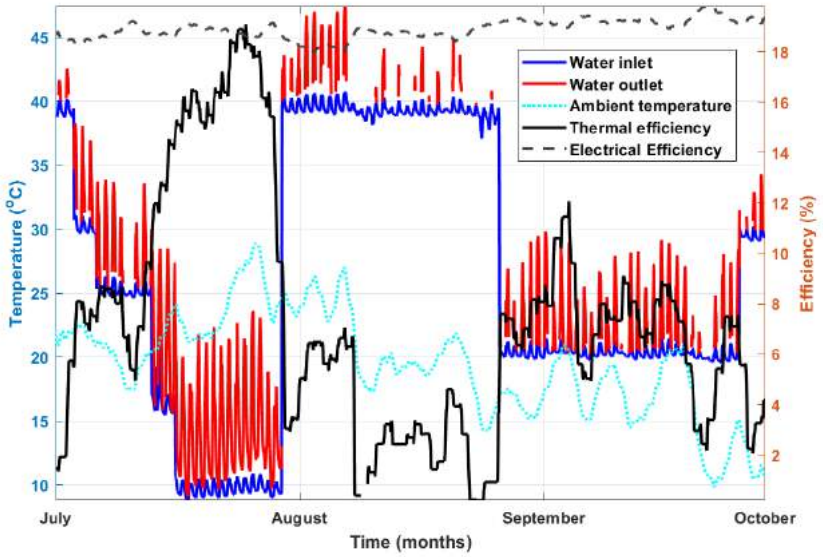

Figure 7.7: Water temperature against thermal efficiency

7.2.2 Yearly Characterisation

This section will dive into characterising the BIPVT design on an annual basis, in order to ascertain its performance. Before that, an important note is that the results presented below were calculated per meter square of the collector area.

With the simple thermal model validated in chapter 6, the model was applied for characterising the BIPVT design for the entirety of a year, helping it predict it's performance. The model has been described in-depth in chapter 5, wherein it displays its versatility by predicting not only the electrical output of a system but also the stagnation, fluid & cell temperatures for each segment of the thermal absorber. The yearly system characteristic was carried out with the help of irradiation data obtained from the software, **Meteonorm**.

Before the system is characterised for the year, a few general design characteristics & parameter assumptions were made in order to perform this analysis. These assumptions are tabulated in table 7.2. The table displays design characteristics, such as collector area (considered for $1m^2$), it's thermal absorber length calculated at roughly 3.3 meters, per meter square area, and each segment length considered at 0.1 meters. As each panel covers an area of (0.82×0.33) roughly $0.27m^2$, four such panels need to be combined, amassing $1m^2$ of collector area, requiring

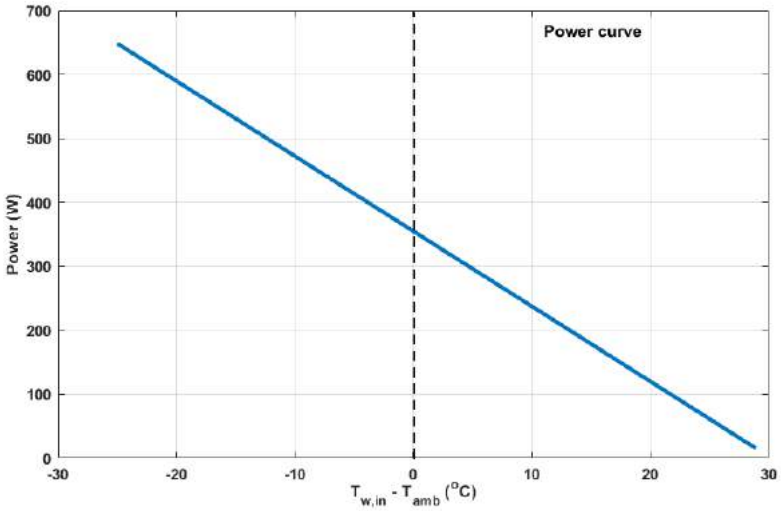

Figure 7.8: Power curve for the thermal collector

a 3.3-meter long thermal absorber. Thus, for the analysis, a constant flow rate (m) of 0.03 kg/s was assumed, along with a constant water inlet temperature ($T_{w,in}$) of 10^oC, arriving from the evaporator side of a heat pump. A performance ratio of 82.54 % was considered, calculated previously in section 7.1. The heat loss and heat gain coefficients, tabulated in table 6.2, calculated from the experiments were assumed for the yearly characterisation as well. The values mentioned above have also been tabulated in table 7.1. No wind speed assumption was considered as the simple thermal model does not take into account wind dependent losses.

Parameter	**Denotation**	**Value**	**Unit**
Collector characteristics			
Collector area	A	1	m^2
Collector length	L	3.3	m
Segment length	x	0.1	m
Parameter assumptions			
Flow rate	m	0.03	kg/s
Water inlet	$T_{w,in}$	10	^oC
Performance ratio	Pr	82.54	%
Cell to ambient	h_{ca}	23.6	$W/m^{2o}C$
Cell to fluid	h_{cw}	3.07	$W/m^{2o}C$

Table 7.2: Parameter assumptions for yearly characterisation

Figure 7.9 illustrates the yearly thermal curve for a square meter of the BIPVT design, illustrating the average operating range of the design as well, marked by an ellipse. As the fluid inlet temperature is kept constant for this analysis, naturally, for unglazed systems without insulation, the design performs best with higher ambient air temperatures.

Figure 7.10a illustrates the yearly energy output for the collector. Four of the solar panels mentioned in chapter 3 were used, for the BIPVT design to amass a square meter of area. Each panel rated at 50W, four such panels would produce a rated power of **200 W**. The irradiance limitations for the calculations mentioned earlier in section 6.2 are assumed for this scenario as well. Wherein, irradiance values below 300 & above 1100 (W/m^2) are not considered. Owing to which, almost negligible energy production is witnessed in the winter months. However, which isn't so, as solar panels are capable of outputting an electric current in irradiances as low as 50 Wh/m^2.

Figure 7.10b illustrates the yearly efficiency trend for the collector design, depicting averaged out thermal and electrical efficiencies over the year, against averaged out ambient air temperatures. With negligible performance in the winter months, owing to strict boundary conditions (section 6.2). The electrical efficiency trend further bolster

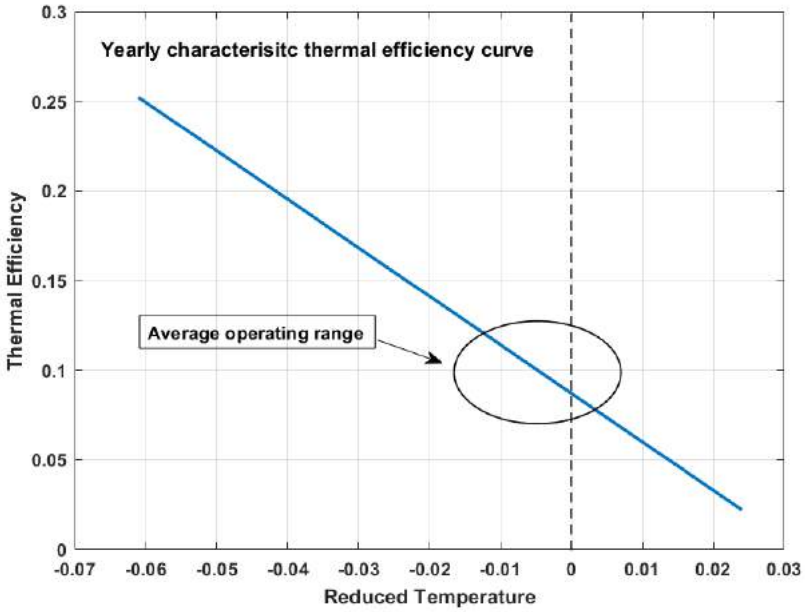

Figure 7.9: Yearly thermal efficiency characteristic curve

Parameter	Denotation	Value	Unit
Yearly energy output			
Thermal	Q	89	kWh
Electrical	E	109	kWh
Combined	C	198	kWh
Efficiency			
Thermal	η_T	12.73	%
Electrical	η_E	18.61	%
Combined	η_C	31.35	%

Table 7.3: Yearly output & efficiencies

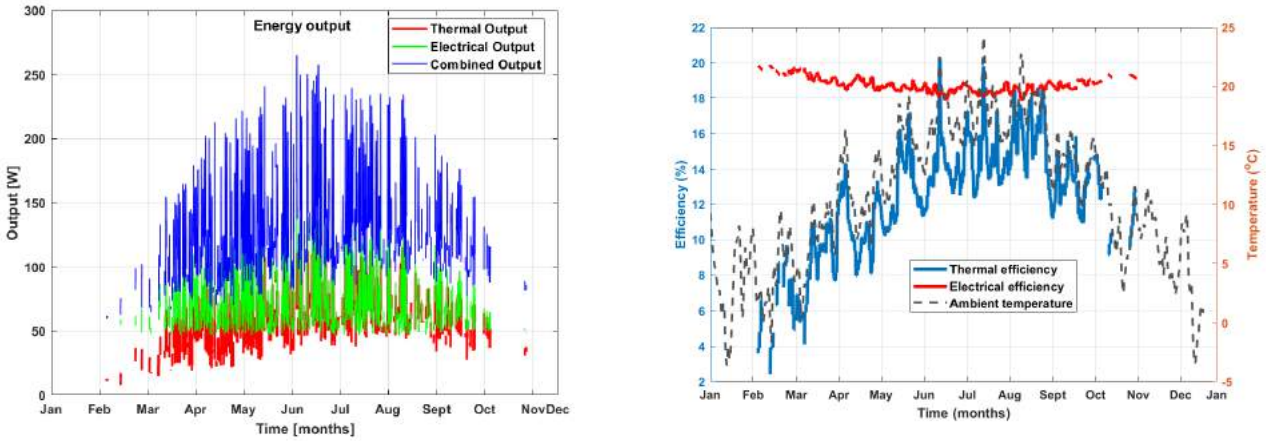

(a) Yearly energy output

(b) Yearly efficiency trend

Figure 7.10: Yearly design performance

the statements made earlier about efficiencies dropping in the summer months owing to higher PV temperatures.

However, the panels maintain a relatively minimal deviation from their rated efficiency of 19 %. This electrical efficiency was calculated using equation 5.16. While the predicted thermal efficiency was calculated using equation 5.13. The thermal efficiency seems to be following a similar trends with ambient air temperatures plotted alongside. As temperatures increase over the months, thermal efficiency increases with it, reaching its peak alongside the peak for ambient air temperatures. Using a moving average, figure 7.10b helps understand annual efficiency trends, while figure 7.10a illustrates the predicted annual output. Table 7.3 summarises the collector's performance, with an area of one square meter. Annually, a square meter of the collector is able to produce *89 kWh* of thermal energy, almost *109 kWh* of electrical energy, yielding a combined energy output of *198 kWh*. On average, the system recorded a combined efficiency of **31.35 %**, with electrical efficiency averaging at **18.61 %**, and thermal efficiency at **12.73 %**. These efficiencies suggest that with an incident irradiance of 1000 Wh/m^2, a square meter of the collector would produce roughly **127 Wh** of thermal energy.

7.3 Simulations for a household

Once the BIPVT's initial characterisations had been carried out, the design's performance was evaluated for a demo house. A CAD model for this demo house can be found in figure 3.5. Figure 3.5 displays a house roof with 10×9 panels (90) installed, each panel rated for a 50W output. Table 7.4 provides roof dimensions and the collector's characteristics. It also includes various parameter assumptions considered for this demo house, in order to calculate it's performance for a year. Note, that these parameters remain the same as tabulated earlier in table 7.2, with the addition of an assumed coefficient of performance for a heat pump to be attached in conjunction with the BIPVT system. An overview of such a system was presented earlier in figure 4.13. The demo house consists of a 30 m^2 roof, deploying an effective aperture area of 23.25 m^2 for the thermal absorbers. Table 7.2 includes the length of the thermal absorber pipe as well, along with the considered length for each segment of the BIPVT.

Parameter	**Denotation**	**Value**	**Unit**
Collector characteristics			
Roof area	-	30	m^2
Collector area	A	23.25	m^2
Collector length	L	72	m
Segment length	x	0.5	m
Rated electric output	P_{rated}	4.5	kW
Parameter assumptions			
Flow rate	m	0.03	kg/s
Water inlet	$T_{w,in}$	10	^oC
Performance ratio	Pr	82.54	%
Cell to ambient	h_{ca}	23.6	$W/m^{2o}C$
Cell to fluid	h_{cw}	3.07	$W/m^{2o}C$
Coefficient of performance	COP	4	-

Table 7.4: Assumptions for house characterisation

7.3.1 System Characteristics

Figure 7.11 illustrates the yearly thermal curve for the BIPVT design installed on a demo house, depicting the average operating range of the design, marked by an ellipse. With the fluid inlet temperature assumed constant for this analysis, the unglazed system, although larger in size performs similarly to the results described earlier for a square meter of this design. With it, performing best with higher ambient air temperatures. The collector does witness a drop in performance from a square meter of the same design. Which can be explained by the larger surface area for the house, accounting for higher thermal losses to the ambient.

Figure 7.12a illustrates the yearly energy output for the house. Electric output of this installation was rated at 4.5

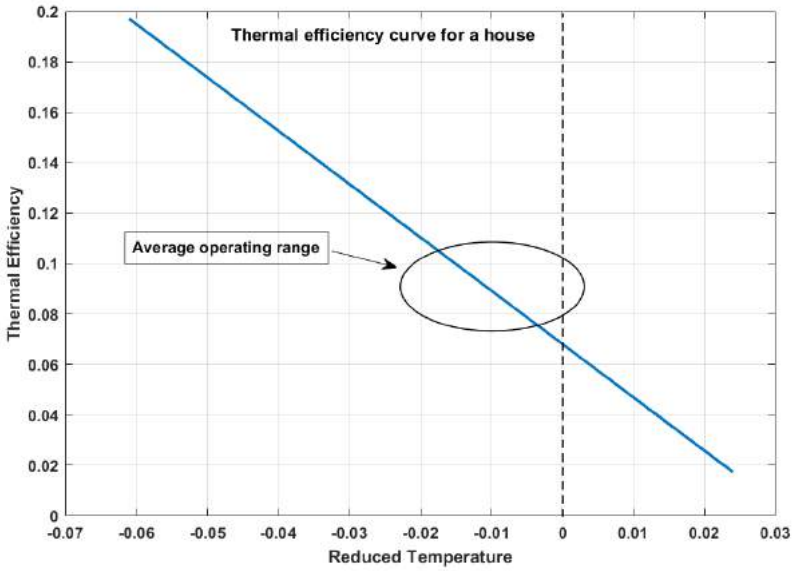

Figure 7.11: Thermal efficiency curve for a house

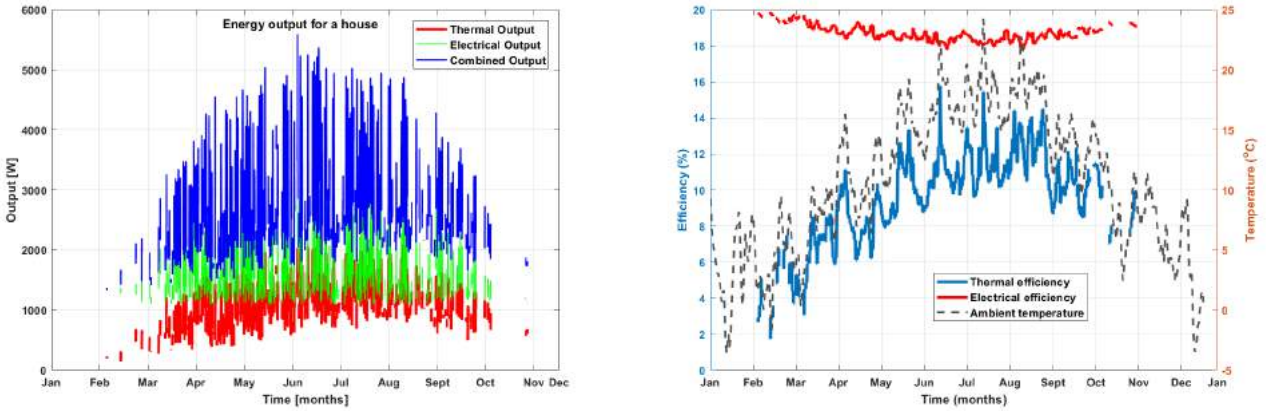

(a) Energy output for a house

(b) Yearly efficiency trend

Figure 7.12: Yearly performance analysis for a house

Parameter	Denotation	Value	Unit
Yearly energy output			
Thermal	Q	1.62	MWh/y
Electrical	E	2.52	MWh/y
Combined	C	4.14	MWh/y
Efficiency			
Thermal	η_T	10	%
Electrical	η_E	18.56	%
Combined	η_C	28.54	%

Table 7.5: Yearly output & efficiencies

kW, to be generated from 90 solar panels. Solar irradiance limitations mentioned in section 6.2 were assumed for this calculation as well, owing to which, an almost negligible energy production is visible for the winter months. Figure 7.12b illustrates the system's annual efficiency trend for the house, depicting the averaged out thermal and electrical efficiencies over the year, against averaged out yearly ambient air temperatures. With negligible

performance recorded for the winter months. Electrical efficiency followed the same trend as seen earlier in figure 7.10b, dropping in the summer months owing to higher PV temperatures. The thermal efficiency followed a similar trend as seen earlier in figure 7.10b as well, increasing for the summer months, with higher ambient air temperatures. Table 7.5 helps summarise the performance for the house. With an effective absorption area of 23.25 m^2, the system was able to produce a respectable thermal output of *1.62 MWh*, as well as *2.52 MWh* of electrical energy. Delivering a combined annual output of *4.14 MWh*. On average, the system recorded a combined efficiency of **28.54 %**, with electrical efficiency averaging at **18.56 %**, and thermal efficiency at roughly **10 %**. These values suggest that with an incident irradiance of 1000 Wh/m^2, the household would be able to produce approximately **2.325 kWh** of thermal energy, at standard testing conditions.

7.3.2 Heat pump integration

Once the system was characterised for a household, ideal heat pump calculations could be carried out for the same. An important research question that this project had set out to answer was whether heat pump integration would be required for an unglazed BIPVT system. Considering the hot water demand for a household of four, discussed in section 4.5.1, a demand of *2960 kWh/y* or 2.96 MWh/y needs to be met. Referring to table 7.5, the stand-alone BIPVT system is able to produce 1.62 MWh/y of thermal energy, falling short of *1.37 MWh*, or roughly **46 %** of the required load. However, for a stand-alone, unglazed, & non-insulated system, matching even **55 %** of the annual thermal demand for domestic hot water can be considered reasonable. The demand matching figure of 55% is also broadly known as the solar fraction (section 5.6), particularly for domestic hot water demand. Various solar fractions and annual system efficiencies will be discussed further in section 7.3.3.

For any household, specifically located in northern Europe, domestic hot water demands are not the only thermal energy requirements. The annual space heating demand, mentioned in section 4.5.1, amounts to *2990 kWh/y*, or 2.99 MWh/y. With that in mind, the cumulative thermal energy demand for a house stands at *5950 kWh/y* or 5.95 MWh/y. The stand-alone system producing 1.62 MWh/y, can match **27 %** of the same. This necessitates the requirement of an integrated heat pump, along with an auxiliary heater that can meet space heating demands during peak winter months, when the thermal system has negligible production. However, a benefit of the BIPVT system is that it can produce electricity as well, powering an auxiliary heater in order to meet excessive demand loads.

Figure 7.13 predicts the thermal output of the BIPVT system (Q_C), as well as the heat pump (Q_H), against the annual domestic hot water & space heating load demand curve. With an integrated heat pump, performing at an average COP of 4, the system is able to output **2.16 MWh/y** of thermal energy, with it's compressor requiring an input of **0.54 MWh/y** of electrical input to achieve the same. Mentioned earlier as well, the solar panel installation rated at 4.5 kW_p, is able to produce 2.52 MWh/y of electrical energy, supplementing the demand required by the compressor. Thus, with the integrated heat pump, the system is able to match over **36 %** of the entire thermal demand for a household. Figure 7.13 showcases that the system is undersized. Wherein it produces more thermal energy than required during the summer months, yet it is unable to match thermal energy requirements for the winter months. As negligible energy is produced during the winter months, the excess heat can possibly be stored in a large sized, insulated tank for seasonal storage, to be used for the winter months. According to thermal energy calculations, with the stand-alone system, **4.29 MWh/y** of thermal energy is not supplied, owing to peak thermal loads occurring during winter months. However, this figure reduces to **3.75 MWh/y** of excess thermal energy that will be required for heating a household. Comparing the heat pump's thermal output with the annual domestic hot water demand, the integrated system is able to match almost **73 %** of the same.

7.3.3 Solar fraction & Annual system efficiencies

Solar fraction (SF), annual thermal (η_{th}^{sys}) & electrical (η_{e}^{sys}) system efficiencies were defined earlier in section 5.6. Annual thermal energy contributions for a stand-alone and heat pump integrated system have been mentioned in the previous sections, along with annual domestic hot water and space heating requirements. To get a better sense of the system's performance, stand-alone and integrated with a heat pump, four relevant solar fractions were calculated, listed below.

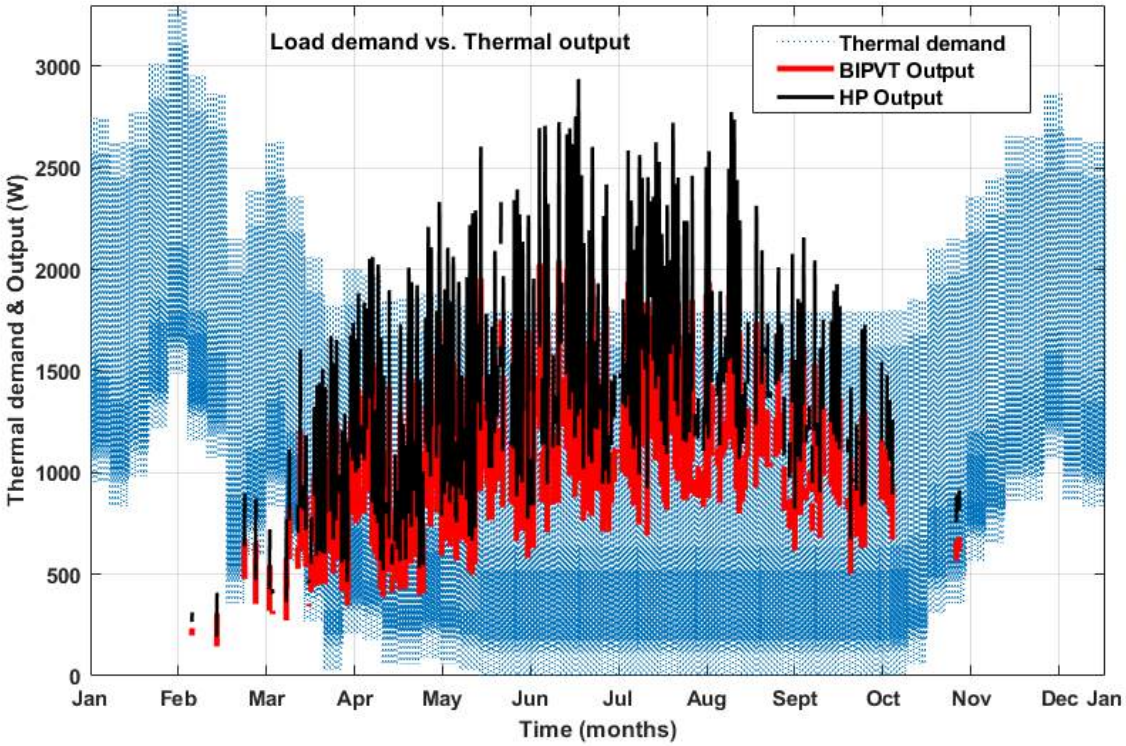

Figure 7.13: Load demand vs. Thermal output for the BIPVT & Heat pump

1. $SF_{PVT,DHW}$: SF for stand-alone BIPVT, supplying domestic hot water demand.
2. $SF_{PVT,TD}$: SF for stand-alone BIPVT, supplying the complete thermal demand.
3. $SF_{HP,DHW}$: SF for an integrated heat pump, supplying domestic hot water demand.
4. $SF_{HP,TD}$: SF for an integrated heat pump, supplying the entire thermal demand.

Table 7.6 concisely depicts the calculated solar fractions for the stand-alone and heat pump integrated systems, matching the domestic hot water demand, or the total thermal load demand (domestic hot water + space heating demand). The simulated household comprised of an effective collector area of $23.25m^2$, with an incident irradiation of 692.2 $kWh/y/m^2$. Thus, amounting to **16.09 MWh/y** for the simulated household. Utilising this value, table 7.6 also depicts the measured annual thermal, electrical & combined system efficiencies.

Parameter	**Denotation**	**Value (%)**
Solar Fraction		
PVT,DHW	$SF_{PVT,DHW}$	55
PVT,TD	$SF_{PVT,TD}$	27
HP,DHW	$SF_{HP,DHW}$	73
HP,TD	$SF_{HP,TD}$	36
Annual system efficiencies		
Thermal	η_{th}^{sys}	10.12
Electrical	η_{e}^{sys}	15.75
Combined	η_{comb}^{sys}	25.9

Table 7.6: Solar fraction & annual system efficiencies

It is important to note that the annual electrical system efficiency stated in table 7.6 is confined to strict solar radiation limits, between 300 & 1100 Wh/m^2, and will be higher for an actual system in place, since the working

range for solar panels is much wider than for solar thermal systems. Another important figure to note, is the annual thermal system efficiency, with an integrated heat pump, calculated to be **13.5 %**.

7.3.4 Stratified thermal storage tank

The multinodel numerical model for stratified thermal storage tanks was discussed in section 5.7.2. Keeping in mind the assumptions discussed in the same, three segments for stratification were chosen for this case. With a similar design as the one illustrated in figure 5.6. The sizing for the storage tank was discussed in section 4.5.2.

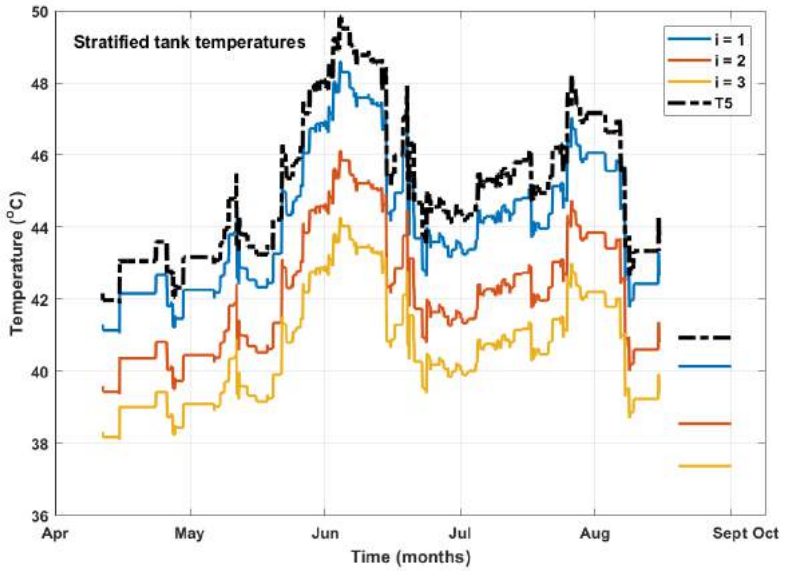

Figure 7.14: Averaged stratified tank temperatures over the year

Figure 7.14 depicts the temperature analysis for the stratified tank model. It is important to note that the temperatures depicted in the figure correspond to averaged out collector and tank values, achieved by a moving average. The collector loop inlet temperature, depicted by T_5 defines the inlet for the tank, operating at strict temperature conditions. The tank's stratification temperatures are also affected by the applied control strategy, described in section 4.5.2. The heat pump is only able to charge the thermal tank within a temperature range of 40 to 95 ^oC. As seen in the figure, no temperature enters the tank below 40 ^oC. The rest of the curves, labelled from i = 1, 2, 3, illustrate the stratified levels of a thermal storage tank. From the missing monthly data between September & April depicted in figure 7.14, we understand that the heat pump, operating within a strict temperature range, is able to charge the thermal storage tank only between the months of high solar irradiance, as expected. That is, between April & August, roughly five months of the entire year.

7.4 Varying system Performance

Chapter 5 defined equation 5.13 for the simple thermal model, in order to ascertain the thermal efficiency of the collector design in question. A deeper look into this equation reveals the two main components that can be varied and have a drastic effect on the system's performance. These are the inlet water temperature for the collector (T_{in}), and the mass flow rate for the system (m). Thus, both these components were varied, within their specific ranges to get a better sense of how the system would perform accordingly. Following which, daily performance variations for the system will be discussed as well. It is important to note that the results provided below were calculated keeping the demo house in mind, that was simulated earlier in section 7.3. Thus, the parameter assumptions considered in table 7.4 apply for the following set of results. Except for the flow rate & inlet temperatures, respectively. Before the varying system performance is discussed, it is important to note that

moving averages of the obtained results are depicted below, in order to ascertain a better sense of their juxtaposed performance.

7.4.1 Varying flow rates

Flow variation's performance analysis was carried out considering the set of flow rates provided in table 7.7.

Flow rate	Value in kg/s
m_1	0.01
m_2	0.02
m_3	0.03
m_4	0.04
m_5	0.05
m_6	0.075
m_7	0.10

Table 7.7: Range of flow rate variation

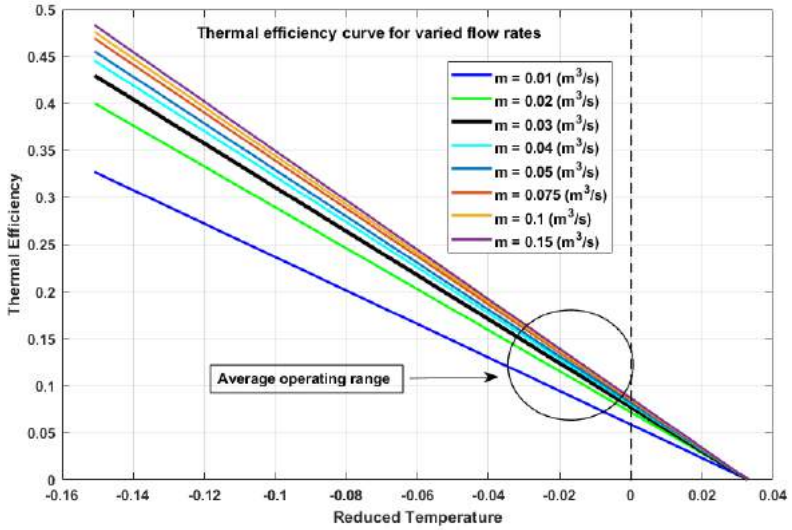

Figure 7.15: Characteristic thermal curve for varying flow rates

Figure 7.15 illustrates the varying thermal efficiency curves for the respective flow rates mentioned in table 7.7. The figure also depicts the average efficiency operating range for the system. With the increasing flow rates, an increase in the slope, as well as thermal performance for the collector, is witnessed. Although a sharp rise in performance is witnessed while moving from 0.01 (kg/s) to 0.02 (kg/s), the rise in performance becomes quite gradual after a flow rate of 0.03 (kg/s). While the system performance starts saturating with flow rates upwards of 0.075 (kg/s). For previous performance calculations, a flow rate of 0.03 (kg/s) has been assumed. Equation 5.13 clearly depicts thermal efficiency linearly proportional to the mass flow rate, further explaining the results obtained.

Although from a performance point of view, it makes sense to increase the flow rates to attain higher thermal efficiency, it doesn't work so in practice. This is because the increase in flow rate is directly proportional to the power consumed by a pump, to pump the required thermal fluid through the system. Thus, unnecessarily increasing the power consumption for the pump, for a marginal increase in performance. Equation 7.1 clearly depicts the linear correlation between the two.

$$P_h = q_p \rho_p g h \tag{7.1}$$

Where, P_h depicts the hydraulic power required by the pump (in kW), q_p is the flow capacity or flow rate of the pump (in m^3/h or kg/s), ρ_p being the density of the fluid pumped (in kg/m^3), g being earth's gravity with a constant value of 9.81 (in m/s^2), & h representing the differential head to be covered by the pump (in m) [Pum].

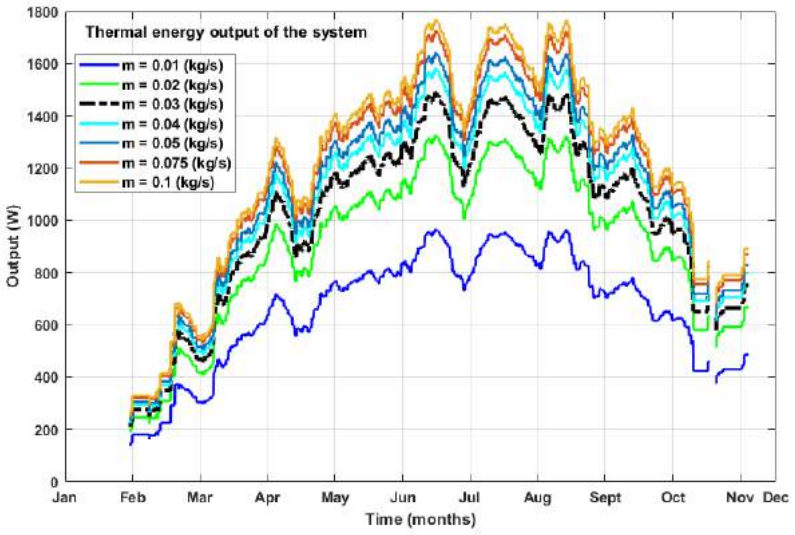

Figure 7.16: Characteristic thermal output for varying flow rates

Figure 7.16 depicts the averaged out thermal output for the system for the course of a year, with similar results as the ones obtained for the thermal efficiency. Equation 5.37 defines the energy generated by the BIPVT, with the flow rate being directly proportional to the same. Similar results as found in figure 7.15 are observed, with increasing thermal output at the flow rate increases. However, a saturation is observed with their performance, with flow rates increasing higher than 0.04 (kg/s). The same limiting conditions for the flow rate apply here as well, that increasing flow rates cause a proportionally increasing power demand from the pump.

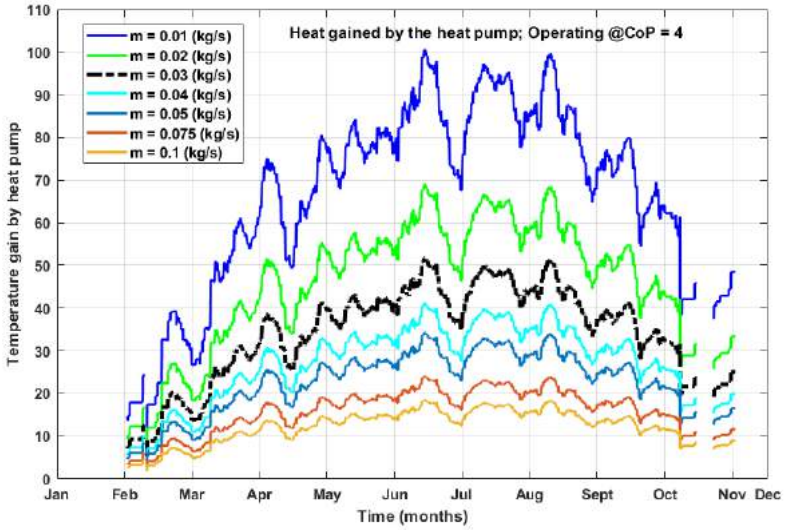

Figure 7.17: Heat gained by the heat pump at varying flow rates, operating at COP = 4

Figure 7.17 depicts heat gain by the heat pump, operating at a COP of 4. This figure provides interesting results, wherein, we see the negative effects of considering a higher flow rate, with the temperatures gained by the heat pump reducing as the flow rate is increased. This reverse behaviour can be understood by the fact that with lower flow rates, the thermal fluid is able to travel longer in the thermal absorbers, thus, absorbing more heat and providing the heat pump with a higher temperature gradient than what is possible with a higher flow rate.

With higher flow rates, the fluid flows too quickly through the absorbers and is unable to absorb enough heat from the solar panels.

Thus, keeping the results discussed above in mind, it is crucial to maintaining a balance of the flow rate for the system. Even though a higher flow rate may result in a better thermal yield for the BIPVT, it causes a proportional increase in the power required to pump the fluid through the system. At the same time, the system is unable to maintain a steady temperature gradient for the evaporator side of a heat pump. This temperature gradient is essential for the evaporator's operation, without which, it will be unable to maintain it's COP, concur a drop in efficiency, as well as a drop in the amount of heat supplied to the attached thermal storage tank. The electric output for the system was plotted against the time as well, in order to determine its change, however as the correlation between the two is almost insignificant, no deviation was recorded.

7.4.2 Varying inlet temperatures

The inlet temperature variation analysis for the system was performed considered the set of temperatures provided in table 7.8.

Inlet temperature	**Value in ^oC**
$T_{in,1}$	-10
$T_{in,2}$	-5
$T_{in,3}$	0
$T_{in,4}$	5
$T_{in,5}$	10
$T_{in,6}$	15
$T_{in,7}$	20
$T_{in,8}$	25
$T_{in,9}$	30
$T_{in,10}$	40

Table 7.8: Range of inlet temperature variation

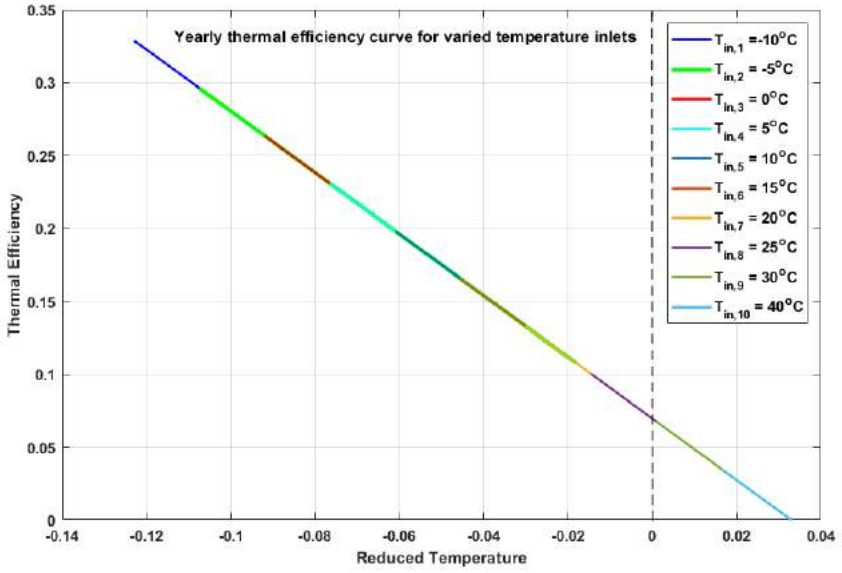

Figure 7.18: Thermal efficiency curves with varying inlet temperatures

Figure 7.18 depicts thermal efficiency curve variations, with varying inlet temperatures. The illustrated curves may seem the same at first, as they lie atop each other. However, that is not so. Although the curves maintain the

same slope, their peak thermal efficiency outputs reduce with each increase in collector inlet. Unglazed systems perform optimally under low collector inlets and high ambient temperatures. Thus, with the higher the inlet temperature goes, the lower it's performance. A 5^oC inlet reaches a peak efficiency of almost **24 %**. Whereas with an inlet of 40 ^oC, the system maxed out at a peak efficiency of just **4 %**. For the performance calculations performed earlier, a constant inlet of 10^oC was assumed, peaking at roughly **20 %**.

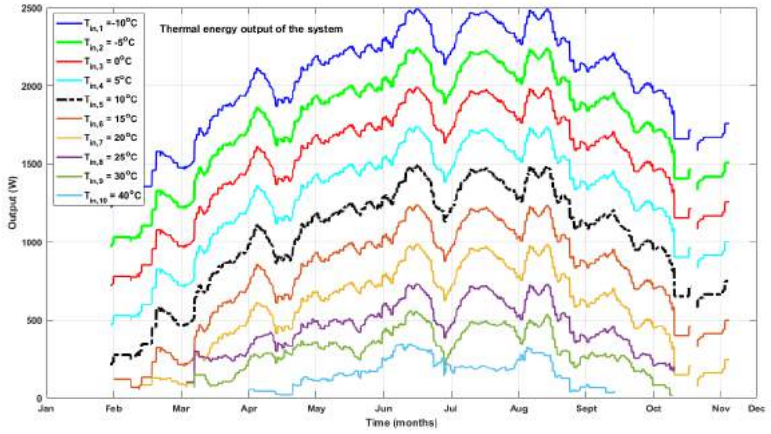

Figure 7.19: Characteristic thermal output for varying inlet temperatures

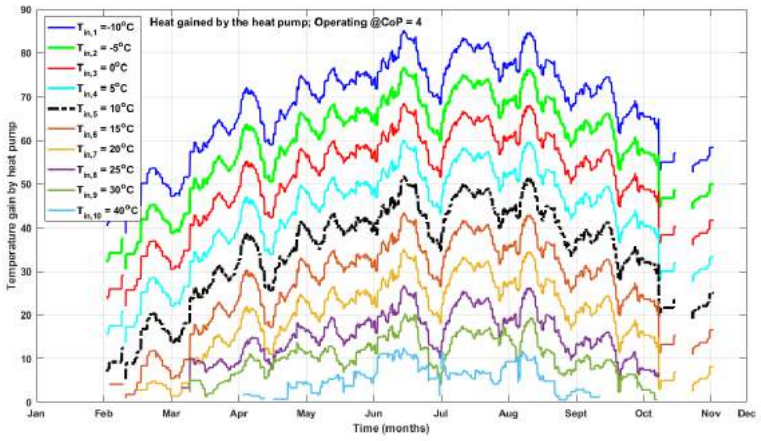

Figure 7.20: Heat gained by the heat pump at varying water inlet temperatures, operating at COP = 4

Figures 7.19 & 7.20 depict the thermal output and temperature gain by the heat pump for the system. With both plots following the similar trend of decreasing thermal output & heat gain, with increasing collector inlet temperatures. Mentioned earlier as well, unglazed systems perform best under low collector inlet temperatures. As is visible in figure 7.19 as well, the collector is able to increase its output with lower inlet temperatures. Similar case with 7.20 as well, with lower inlet temperatures, the amount of absorbed heat by the system is higher, resulting in a higher temperature gradient supplied to the heat pump.

Naturally, system operations at lower inlet temperatures provide great performance. However, the caveat is in maintaining these temperatures. From a practical point of view, the collector inlet temperature is never constant and varies based on the amount of heat absorbed by the heat pump, ambient temperatures, and other parameters. It usually fluctuates within a range of 5^oC to 25^oC, for winter or summer months respectively.

7.4.3 Daily Variation

Over the course of a year

Figure 7.21 depicts the thermal & electrical energy output variations for the system, on specific days spread across the year. The summer solstice on 21^{st} of June, winter solstice on 21^{st} of December, & the vernal equinox on 21^{st} of March for the northern hemisphere, were chosen for the predictions. It is important to note that the empty spaces on the edges of each curve depict a negligible output. As expected, the system, for both electrical and thermal outputs, performs best in the summer days, i.e. for June 21st. It shows a reasonable level of performance for March as well. Although, as expected, with almost negligible performance in the winter months, i.e. for December.

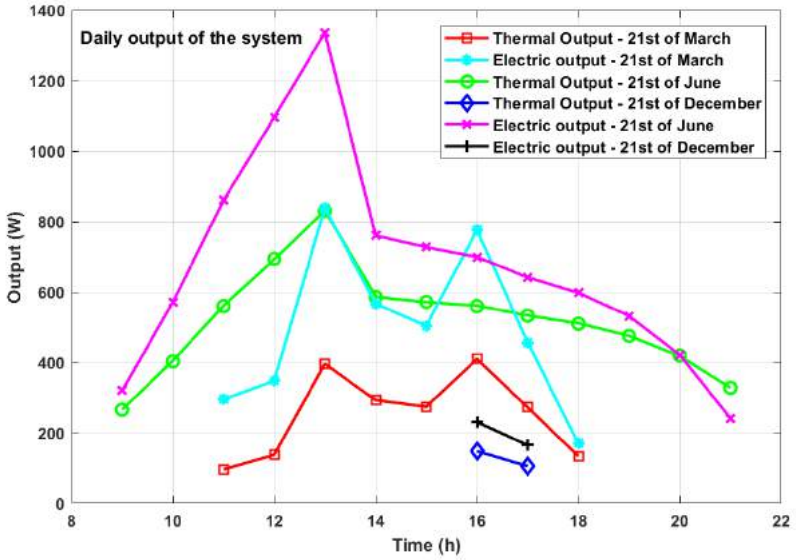

Figure 7.21: Energy output variation at specific days

August 21^{st}

Chapter 5 discussed how the simple thermal model segregates the thermal absorber into various segments of length x. In doing so, it is able to predict PV cell temperatures and fluid temperatures over the course of the thermal absorber's length. Utilising equations 5.9 & 5.11 respectively. Using these equations, the cell and fluid temperatures were predicted for a random day, August 21^{st} of a year. The electrical efficiency of the system, altering with regards to cell temperatures was also calculated using equation 5.16. With the help of these equations, figure 7.22 predicts the dynamic behaviour of fluid temperatures (depicted in blue), cell temperatures (depicted in green), and the system's electrical efficiency (depicted in brown) over the course of a day.

Figure 7.22 depicts how increasing cell temperatures cause a rise in fluid temperatures, as is expected from any PVT system. With the fluid extracting more and more heat from the cells as the temperatures rise. A similarly expected trend is witnessed for the electrical efficiency, with it reducing for increasing cell temperatures. The three components presented in figure 7.22 are predicted for each hour and each length of a segment x, forming a matrix of the size [(length of time step) $\times$ (number of segments)]. Making it harder to be predicted on a 2D plot, i.e. figure 7.22. Thus, figure 7.23 depicts averaged out matrix values for cell temperatures, fluid temperatures & electrical efficiency, over the course of a day. Making it easier to decipher there average values.

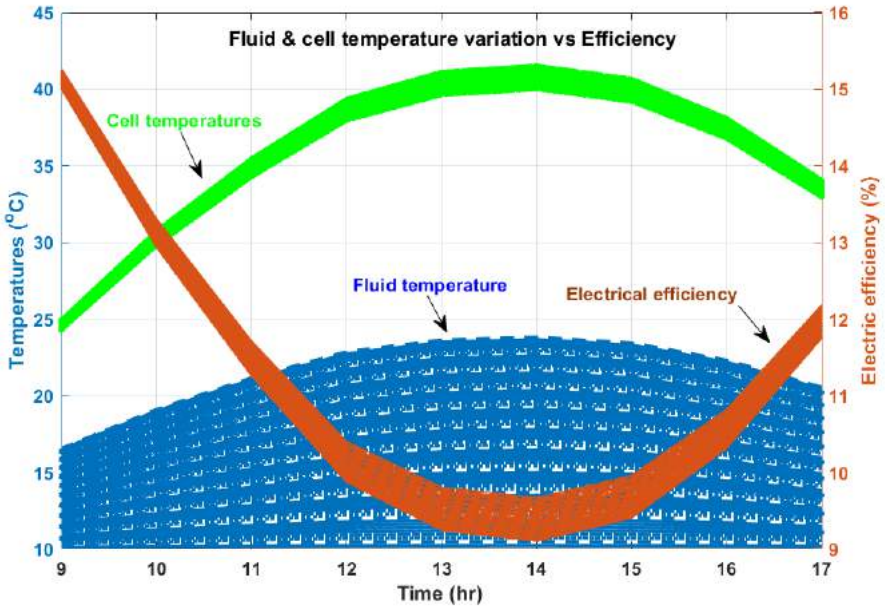

Figure 7.22: Fluid & cell temperature variations throughout the day, against electrical efficiency

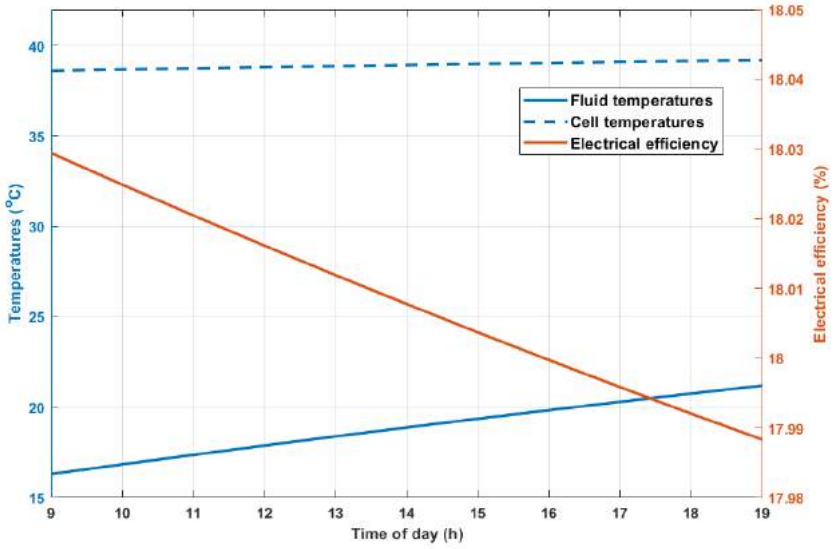

Figure 7.23: Averaged out fluid & cell temperature variations throughout the day, against electrical efficiency

Chapter 8

Conclusions & Recommendations

The following chapter will conclude this project with a discussion on the obtained results. Followed by design recommendations, and possible system optimisations.

8.1 Conclusions

8.1.1 Model validation

The simple thermal model, currently under development at the TU Delft has been described in-depth in chapter 5, alongside the steady-state and quasi-dynamic thermal models, defined in ISO norms [4]. They have been applied widely to determine the performance of a wide variety of solar thermal collectors. Thus, it was imperative to understand how the simple thermal model performed, in comparison with the other two.

Utilising the data obtained from the experimental setup, chapter 6 presented the validation by juxtaposing the thermal efficiency curves obtained for each model in a single plot. The juxtaposed curves, illustrated in figure 6.4, showcase the simple thermal model performing almost on par with the other two widely validated models. The simple thermal model calculated the average thermal efficiency of the setup at 8.3%, while the steady-state & quasi-dynamic models calculated the same at 8.16% & 7.53% respectively. With relatively similar figures, the simple model recorded an error of 1.65% with the steady-state model and 9.21% with the quasi-dynamic model.

These errors were considered within the confined limitations for validating the simple thermal model. This is because thermal models in general, can be quite complex, with a myriad of limiting parameters and conditions. For example, the steady-state model takes wind speed dependence and it's heat loss into consideration, while the quasi-dynamic model considers wind speed, incident angle modifier and a plethora of other heat-loss coefficients into consideration. In doing so, the models are able to ascertain a more accurate performance of the design being evaluated, while adding to their complexities in doing so. The simple thermal model, on the other hand, considers two main heat loss coefficients, the heat lost from the PV cell to ambient, and the heat gained from the PV Cell to water. Combining a plethora of heat loss coefficients into two easily determinable and understandable coefficients.

8.1.2 Performance analysis

The performance analysis carried out for the setup was discussed in section 7.2. Experimental setup, covering a roof area of $8.8m^2$, and having a thermal absorber length of 30 m, recorded a zero-loss efficiency of 8.73 %, with an averaging thermal efficiency of 8.3 %. With the PV panels in conjunction, the system recorded a combined energy efficiency of 27.2 %.

The BIPVT design's yearly performance was tested for a square meter area of the collector, comprising of a 3-meter long thermal absorber. Table 7.2 depicted the various parameter assumptions considered for this analysis, with the coefficients obtained from the experimental setup used for same. The analysis showcased the design performing at an average thermal efficiency of 12.73 %, with a combined thermal efficiency of 31.35 %.

Once the system characterisation was complete, the BIPVT design was simulated for demo household of four people, comprising a roof area of $30m^2$. Parametric assumptions for the same can be found in table 7.4. Simula-

tions for the demo house showcased an average thermal efficiency of 10 % for the system, along with a combined thermal and electrical efficiency of 28.54 %. A drop from the square meter analysis was witnessed due to a longer thermal absorber, resulting in higher cell to ambient losses.

Simulations were also performed considering an integrated heat pump, assumed to be operating at an average COP of 4. The stand-alone system was able to cover 55 % of the domestic hot water load demand. While with an integrated heat pump, the system was able to cover almost 80 % of the annual domestic hot water demand. With the space heating demand included, the stand-alone system was able to cover almost 27 % of the entire load. With the heat pump attached, the system was able to meet almost 36 % of this demand.

These figures further validate the necessity of an integrated heat pump with the BIPVT. Figure 7.13 illustrated the thermal output for the system, clearly depicting that the system produces excess thermal energy during hot summer months. This excess thermal output can be stored in a domestic hot water tank, sized at 250 l for a house of four, matching hot water demand needs throughout the day. While further excess thermal energy can be stored in a large $40m^3$ storage tank underground, to be utilised for matching space heating demands during the winter months. Although, such a storage solution for space heating can be expensive and optional for the end consumer, who can also utilise an auxiliary (electric) heater to match demand more efficaciously.

8.1.3 Varying system performance

The BIPVT design's performance analysis for varied inlet flow rates and collector temperatures was discussed in section 7.4, with interesting results. The system's performance analysis considered a constant inlet temperature of 10^oC and a constant flow rate of 0.03 kg/s. Whereas the varying performance analysis was carried out incorporating a wide range of inlet conditions, tabulated in tables 6.4 & 6.3.

As expected, increased flow rates resulted in higher thermal efficiencies and a higher thermal output. However, increasing them beyond a certain point was not beneficial for two reasons. One, a very high flow rate requires significant pumping power. Second, its beneficial thermal effect acts negatively for the performance of the heat pump. This is because if the flow rate is very high, it is not able to absorb enough thermal heat from the PV cells. Thus, not being able to supply a high enough temperature gradient for the heat pump to perform effectively. The system should maintain a flow rate between 0.02 & 0.04 kg/s. By doing so, it can maintain a decent thermal efficiency, while supplying an effective temperature gradient to the heat pump.

It has been mentioned earlier as well that unglazed systems perform best at low collector inlets and relatively higher ambient temperatures. Thus, similarly predictable results were obtained when varying collector inlet temperatures were implemented. Although the various inlet temperatures maintained the same effective slope for their thermal efficiency curves, higher temperatures saw reduced thermal efficiency peaks and outputs. With similar results for the heat pump temperature gain as well, an almost negligible gain was realised for higher inlet temperatures. Thus, it is best to maintain low collector inlet temperatures, but not the most convenient. Inlet temperatures rely largely on the heat extracted by the evaporator of a heat pump, along with the incident solar radiation and ambient air temperatures. They generally fluctuate between 5 to 25 ^oC, between winter/summer months respectively.

8.2 Recommendations

With any novel technology and a new design, there's always room for improvement and growth. With a calculated average design efficiency of 12.73 % per square meter, further optimisations can be carried out to improve this efficiency figure. Mentioned in section 1.2, this project has been a part of a larger project consortium, the PVT inSHape project, which aims to realise zero-energy buildings. The next stage of this project includes a specialised heat pump integration, designed specifically for PVT systems, currently under development at NRGTEQ. Along with the heat pump integration at the SolarBEAT, further design studies and system characterisation will be carried out at TU Eindhoven. A test setup has been prepared at the Mechanical Engineering faculty of TU/e, where further indoor testing for the BIPVT system will take place. A few key optimisation techniques will be tested out in order to improve the system's performance. Largely related to improving the thermal contact between the PV and the absorber pipes. The improved thermal contact will be achieved using a myriad of configurations.

The first such configuration will apply thermal paste between the PV and the current thermal absorber pipes mentioned in chapter 4. Application of the thermal paste will definitely help with an improved heat transfer between the two. The second configuration will apply the same thermal paste, while replacing the current absorber pipes with copper, as they provide a significantly higher thermal conductivity, of roughly 385 W/mK at room temperatures. The third configuration will utilise the current absorber pipes, while incorporating a thin strip of copper, running the entire length of the panel, with a width similar to that of the mounting structure present below it. These copper strips will be bonded to the back of glass-glass Exasun modules, along with the thermal paste between them and the absorber pipe. Owing to a large amount of heat loss to the ambient from the back of the solar panel, the fourth configuration will also measure performance results by incorporating a simple insulation material such as thermocol or polystyrene, for trapping the heat within the system. The last and final configuration will aim to evaluate the system's performance by effectively doubling the length of the current thermal absorbers present below the BIPVT.

Further possibilities for future work with such systems can be the implementation of a thorough control strategy for a PVT integrated with a heat pump, combined with two thermal storage options, for daily and seasonal requirements. The daily storage would effectively supply domestic hot water needs for a household, whereas the seasonal storage would conserve excess thermal energy for the summer months, to be used later during the winter months. Another study could be performed pertaining to the effectiveness of an expensive seasonal storage system, and whether an auxiliary electric heater would be a better and more effective alternative.

Bibliography

[Pum] Pump power calculator. https://www.engineeringtoolbox.com/pumps-power-d_505.html. (Accessed on 10/27/2018).

[2] (2013). What is linear regression? - statistics solutions. http://www.statisticssolutions.com/what-is-linear-regression/. (Accessed on 10/18/2018).

[3] (2015). Heat pump. http://hyperphysics.phy-astr.gsu.edu/hbase/thermo/heatpump.html. (Accessed on 10/25/2018).

[4] (2017). Nen-en-iso 9806:2017. https://www.nen.nl/NEN-Shop/Norm/NENENISO-98062017-en.htm. (Accessed on 10/18/2018).

[5] Al-Waeli, A. H., Chaichan, M. T., Kazem, H. A., and Sopian, K. (2017). Comparative study to use nano-(al2o3, cuo, and sic) with water to enhance photovoltaic thermal pv/t collectors. *Energy Conversion and Management*, 148:963–973.

[6] Amin, N., Lung, C. W., and Sopian, K. (2009). A practical field study of various solar cells on their performance in malaysia. *Renewable Energy*, 34(8):1939–1946.

[7] Aste, N., del Pero, C., and Leonforte, F. (2014). Water flat plate pv–thermal collectors: a review. *Solar Energy*, 102:98–115.

[8] Boersma, T. (2016). The end of Dutch natural gas production as we know it. [Online; accessed 26-Sept-2018].

[9] Bouteiller, P., Terrier, M.-F., and Tobaly, P. (2017). Experimental study of heat pump thermodynamic cycles using co2 based mixtures-methodology and first results. In *AIP Conference Proceedings*, volume 1814, page 020052. AIP Publishing.

[10] Cattaneo, G., Faes, A., Li, H.-Y., Galliano, F., Gragert, M., Yao, Y., Grischke, R., Söderström, T., Despeisse, M., Ballif, C., et al. (2015). Lamination process and encapsulation materials for glass-glass pv module design. *Photovoltaics International*, 3(15):1–8.

[11] Chol, S. and Estman, J. (1995). Enhancing thermal conductivity of fluids with nanoparticles. *ASME-Publications-Fed*, 231:99–106.

[12] Clement, F., Neidert, M., Henning, A., Mohr, C., Zhang, W., Thaidigsmann, B., Hoenig, R., Fellmeth, T., Spribille, A., Lohmueller, E., et al. (2010). Processing of highly-efficient mwt silicon solar cells. In *25th European Photovoltaic Solar Energy Conference and Exhibition, Valencia, Spain.*

[13] CONDITIONING, H. H. . A. (2015). Geo Thermal Heat Pump Systems. http://www.hollidayheating.com/geo-thermal/. [Online; accessed 03-Sept-2018].

[14] Craven, B. and Islam, S. (2011). *Ordinary least-squares regression.* Sage Publications.

[15] de Jong, C. K. J. B. M. (2017). Pvt benchmark. (Grant Agreement no.: 642242). https://www.seac.cc/en/seac-presents-a-new-market-survey-pvt-products/.

[16] Debbarma, M., Sudhakar, K., and Baredar, P. (2016). Comparison of bipv and bipvt: a review. *Resource-Efficient Technologies.*

[17] Degli Uberti, F., Faranda, R., Leva, S., and Ogliari, E. (2010). Performance ratio of a pv power plant: different panel technologies comparison. In *Proc. Solar Energy Tech Workshop*, volume 8.

[18] Duffie, J. A. and Beckman, W. A. (2013). *Solar engineering of thermal processes.* John Wiley & Sons.

[Education.org] Education.org, P. Module Materials. https://www.pveducation.org/pvcdrom/modules/module-materials. [Online; accessed 06-Sept-2018].

[20] Emmi, G., Tisato, C., Zarrella, A., and De Carli, M. (2016). Multi-source heat pump coupled with a photovoltaic thermal (pvt) hybrid solar collectors technology: A case study in residential application. *International Journal of Energy Production and Management*, 1(4):382–392.

[Energy] Energy, F. Heat Pumps. `http://free-energy.ws/heat-pumps/`. [Online; accessed 03-Sept-2018].

[22] et al., C. R. J. D. D. L. (201). High performance flat plate solar thermal collector evaluation. *National Renewable Energy Labratory*, (Grant Agreement no.: 642242).

[23] Eurostat. Complete energy balances - annnual data. [Online; accessed 26-Sept-2018].

[24] Eurostat. Energy consumption in households. [Online; accessed 26-Sept-2018].

[25] Faninger, G. (2007). Sensible heat storage. *Sustainable Solar Housing*, 2:215.

[26] Fischer, S., Heidemann, W., Müller-Steinhagen, H., Perers, B., Bergquist, P., and Hellström, B. (2004). Collector test method under quasi-dynamic conditions according to the european standard en 12975-2. *Solar Energy*, 76(1-3):117–123.

[27] for Storage of Energy, E. A. (2016). Thermal energy storage. `http://ease-storage.eu/wp-content/uploads/2016/03/EASE_TD_HotWater.pdf`. [Online; accessed 10-Sept-2018].

[28] Fraisse, G., Ménézo, C., and Johannes, K. (2007). Energy performance of water hybrid pv/t collectors applied to combisystems of direct solar floor type. *Solar Energy*, 81(11):1426–1438.

[29] Gabriel Bachner, Andreas Tuerk, K. W. K. S. (2017). Economic costs and benefits of renewables deployment in the eu. *CARISMA Innnovation for Cliamte Change Mitigation*, (Grant Agreement no.: 642242).

[30] Gang, P., Huide, F., Tao, Z., and Jie, J. (2011). A numerical and experimental study on a heat pipe pv/t system. *Solar energy*, 85(5):911–921.

[31] Garg, H. and Adhikari, R. S. (1997). Conventional hybrid photovoltaic/thermal (pv/t) air heating collectors: steady-state simulation. *Renewable energy*, 11(3):363–385.

[32] Ghadiri, M., Sardarabadi, M., Pasandideh-fard, M., and Moghadam, A. J. (2015). Experimental investigation of a pvt system performance using nano ferrofluids. *Energy Conversion and Management*, 103:468–476.

[33] harkin, S. (2014). The future of the French and Dutch heating markets: How will they evolve? [Online; accessed 26-Sept-2018].

[34] Hasan, A., McCormack, S., Huang, M., and Norton, B. (2010). Evaluation of phase change materials for thermal regulation enhancement of building integrated photovoltaics. *Solar Energy*, 84(9):1601–1612.

[35] Hasnain, S. (1998). Review on sustainable thermal energy storage technologies, part i: heat storage materials and techniques. *Energy conversion and management*, 39(11):1127–1138.

[36] Hersch, P. and Zweibel, K. (1982). Basic photovoltaic principles and methods. Technical report, Solar Energy Research Inst., Golden, CO (USA).

[37] Huang, M., Eames, P., and Norton, B. (2004). Thermal regulation of building-integrated photovoltaics using phase change materials. *International Journal of heat and mass transfer*, 47(12-13):2715–2733.

[38] Huang, M., Eames, P., and Norton, B. (2006). Phase change materials for limiting temperature rise in building integrated photovoltaics. *Solar Energy*, 80(9):1121–1130.

[39] Hub, R. E. History behind solar thermal and solar water heating technology. Retrieved from: https://www.renewableenergyhub.co.uk/solar-thermal-information/the-history-of-solar-thermal-technology.html.

[40] Hub, T. R. E. Thermodynamic Panels. `https://www.renewableenergyhub.co.uk/thermodynamic-panels/`. [Online; accessed 09-Sept-2018].

[41] IRENA (2017). Renewable power generation costs in 2017.

[42] Isabella O., Jager K., S. A. v. S. R. Z. M. (2016). *Solar Energy: the physics and engineering of photovoltaic conversion technologies and systems,*. UIT Cambridge Ltd., Cambridge, UK.

[43] Jarimi, H., Bakar, M. N. A., Othman, M., and Din, M. H. (2016). Bi-fluid photovoltaic/thermal (pv/t) solar collector: Experimental validation of a 2-d theoretical model. *Renewable Energy*, 85:1052–1067.

[44] Kleinbach, E. M., Beckman, W., and Klein, S. (1993). Performance study of one-dimensional models for stratified thermal storage tanks. *Solar energy*, 50(2):155–166.

[45] Kovacs, P. (2012). Quality assurance in solar heating and cooling technology: Report of project achievements.

[46] Krauter, S., Pénidon, R., Hanusch, B. L. M., and Grunow, P. (2011). Pv module lamination durability. In *ISES. ISES Solar World Congress*, pages 2011–02.

[47] Lee, H. S. (2010). *Thermal design: heat sinks, thermoelectrics, heat pipes, compact heat exchangers, and solar cells*. John Wiley & Sons.

[Nave] Nave, C. Thermal conductivity. `http://hyperphysics.phy-astr.gsu.edu/hbase/Tables/thrcn.html`. [Online; accessed 26-Sept-2018].

[of Energy] of Energy, U. D. Heat transfer fluids for solar water heating systems | department of energy. `https://www.energy.gov/energysaver/solar-water-heaters/heat-transfer-fluids-solar-water-heating-systems`. (Accessed on 08/28/2018).

[50] Office of Energy Efficiency & Renewable Energy, F. B. (2015). Heat Pump Systems. `https://www.energy.gov/energysaver/heat-and-cool/heat-pump-systems`. [Online; accessed 03-Sept-2018].

[51] Patterson, J. E., Miers, R. J., and Carolina, N. (2009). The thermal conductivity of common tubing materials applied in a solar water heater collector. *Western Carolina University, Cullowhee, North Carolina*.

[52] Rodríguez-Hidalgo, M. d. C., Rodríguez-Aumente, P. A., Lecuona, A., Legrand, M., and Ventas, R. (2012). Domestic hot water consumption vs. solar thermal energy storage: The optimum size of the storage tank. *Applied Energy*, 97:897–906.

[53] Rosenthal, A. H., Gonçalves, B. P., Beckwith, J., Gulati, R., Compere, M. D., and Boetcher, S. K. (2015). Phase-change material to thermally regulate photovoltaic panels to improve solar to electric efficiency. In *ASME 2015 International Mechanical Engineering Congress and Exposition*, pages V08BT10A009–V08BT10A009. American Society of Mechanical Engineers.

[54] Santbergen, R. (2008). *Optical absorption factor of solar cells for PVT systems*. PhD thesis, TUE : Department of Mechanical Engineering.

[55] Sathe, T. M. and Dhoble, A. (2017). A review on recent advancements in photovoltaic thermal techniques. *Renewable and Sustainable Energy Reviews*, 76:645–672.

[56] Struckmann, F. (2008). Analysis of a flat-plate solar collector. *Heat and Mass Transport, Project Report, 2008MVK160*.

[57] Tonui, J. and Tripanagnostopoulos, Y. (2007). Air-cooled pv/t solar collectors with low cost performance improvements. *Solar energy*, 81(4):498–511.

[58] (US), E. I. A. and Office, G. P. (2016). *International Energy Outlook 2016: With Projections to 2040*. Government Printing Office.

[59] Walker, A. (2012). Solar water heating, nrel (national renewable energy laboratory). `https://www.nrel.gov/docs/fy13osti/56706.pdf`. (Accessed on 10/13/2018).

[60] Wei Long, H. L. (2014). Manufacturing cost reduction roadmap for mwt modules. *Back-contact Workshop, Shanghai*.

[61] Wolf, M. (1976). Performance analyses of combined heating and photovoltaic power systems for residences. *Energy Conversion*, 16(1-2):79–90.

[62] Yazdanifard, F., Ebrahimnia-Bajestan, E., and Ameri, M. (2016). Investigating the performance of a water-

based photovoltaic/thermal (pv/t) collector in laminar and turbulent flow regime. *Renewable Energy*, 99:295–306.

[63] Zondag, H., Van Helden, W., Elswijk, M., and Bakker, M. (2004). Pv-thermal collector development–an overview of the lessons learnt. In *19th European PV Solar Energy Conference and Exhibition, Paris, France*, pages 7–11.

[64] Zondag, H. A., Jong, M. J., and Helden, W. G. J. (2001). *Development and applications for PV thermal*. Energy research Centre of the Netherlands ECN.

Appendix A

Hottel-Whillier-Bliss Equation

In continuation of the heat flow through the BIPVT described in section 5.1. The heat removal factor for the collectors is depicted in equation A.1.

$$F_R = \frac{mc_p \left(T_{w,out} - T_{w,in}\right)}{A \left[G_{sun} \left(\tau\alpha\right) - U_L \left(T_{w,in} - T_{amb}\right)\right]} \tag{A.1}$$

The maximum possible temperature gain occurs when the entirety of the solar collector is at its inlet fluid temperature. Keeping this in mind, the actual useful temperature gain is found by multiplying equation 5.3, with the collector's heat removal factor, expressed in equation A.1. The actual useful energy gain is depicted in equation A.2 below.

$$Q_u = F_R A \left[G_{sun} \left(\tau\alpha\right) - U_L \left(T_{w,in} - T_{amb}\right)\right] \tag{A.2}$$

Equation A.2, is also known as the **"Hottel-Whillier-Bliss equation"**. Used widely for measuring collector energy gain. The collector's instantaneous thermal efficiency can be used as a measure of the collector's thermal performance. It can be defined as a ratio between useful energy gain (Q_u) and the product of irradiance incident on the collector and its surface area. Expressed further in equation

$$\eta = F_R\tau\alpha - F_R U_L \left(\frac{T_{w,in} - T_{amb}}{G_{sun}}\right) \tag{A.3}$$

Considering terms F_R, α, τ, & U_L^2 as constants for the collector in question, then the instantaneous efficiency defined in equation A.3, can be considered a linear function of three important parameters. Which are, the solar irradiance (G_{sun}), fluid inlet temperature ($T_{w,in}$), and the ambient air temperature (T_{amb}). Thus, a flat-plate collector's performance can be approximated with the help of these three parameters. However, it is important to note that U_L is not actually constant and that it will increase as the collector temperature rises above ambient, and fall when it drops below.

Appendix B

ISO Norm 9806:2017 Collector parameters

B.1 Steady-state testing method

Stated in ISO norms 9806 [4], the extracted power (Q) for the steady state testing method can be modelled with the help of equation B.1.

$$Q_{SS} = A_G[\eta_0 G_b - a_1(T_m - T_{amb}) - a_2(T_m - T_{amb})^2 - a_3 u(T_m - T_{amb}) + a_4(E_L - \sigma(T_{amb})^4) - a_6 u G_b - a_7 u(E_L - \sigma(T_{amb})^4) - a_8(T_m - T_{amb}^4)] \quad \text{(B.1)}$$

Where,

$$a_4 = \eta_0 \frac{\epsilon}{\alpha} \qquad and \qquad a_6 = \eta_0 b_u \qquad and \qquad a_7 = \eta_0 b_u \frac{\epsilon}{\alpha} \quad \text{(B.2)}$$

Most of the coefficients described above have been mentioned earlier in chapter 5. Coefficients *'a'* in equation B.1 refer to parameter coefficients *'b'* presented in equation 5.18.

B.2 Quasi-dynamic testing method

ISO norms 9806 [4]model the extracted power for the quasi-dynamic testing methods with the help of equation B.3.

$$Q = A_G[\eta_o K_b(\theta_L, \theta_T) G_b + \eta_0 K_d G_d - a_1(T_m - T_{amb}) - a_2(T_m - T_{amb})^2 - a_3 u(T_m - T_{amb}) + a_4(E_L - \sigma(T_{amb})^4) - a_5(\frac{dT_m}{dt}) - a_6 u G_b - a_7 u(E_L - \sigma(T_{amb})^4) - a_8(T_m - T_{amb})^4] \quad \text{(B.3)}$$

Majority of the coefficients illustrated in equation B.3 have been presented earlier in chapter 5, in equation 5.22. However, the parametric coefficients presented as *'a'* in equation B.3 refer to coefficients *'c'* in equation 5.22. ISO norms state that for collectors with a concentration ratio less than 20, the use of η_0, $K_b(\theta_L, \theta_T)$, K_d, and coefficients a_1, a_2. & a_5 are mandatory. They need to be identified, whereas parameter a_8 can be set to 0 [4].

The incidence angle modifier (IAM), depicted as $K_b(\theta_L, \theta_T)$, is best defined as the ratio of peak efficiency at a given angle of incidence, and the peak efficiency at normal incidence. Further calculations for IAM and respective incidence angles can be found in NEN [4].

$$\eta_0 = F^{'} (\tau\alpha)_{en} \quad \text{(B.4)}$$

$$K_{\theta b}(\theta) = 1 - b_o \left(\frac{1}{cos\theta - 1} \right) \quad \text{(B.5)}$$

Equation B.4 defines the zero-loss efficiency for the model. The parameter b_o in equation B.5 is for the characterisation of the incident angle modifier of the beam irradiance.

Appendix C

Stratified thermal storage tank model

C.1 Energy balance

$$Mc_p\frac{dT_i}{dt} = \alpha_i m_c c_p(T_c - T_i) + \beta_i m_d c_p(T_{mains} - T_i) + \delta_i\gamma_i c_p(T_{i-1} - T_i) + (1-\delta_i)\gamma_i c_p(T_i - T_{i+1}) - h_{env}(T_i - T_{env}) \quad \text{(C.1)}$$

Equation C.1 denoted above, represents the energy balance for the i^{th} segment of a stratified thermal storage tank, derived from Kleinbach et al. [44]. M depicts the mass of the water for each segment, with c_p depicting the specific heat of water. h_{env} is the heat loss coefficient of the segment to the environment, & T_{env} being the temperature of the tank's environment. Other notations used in the same are listed below.

- $\alpha_i = 1$, if T_c best matches T_i, otherwise it is considered 0.
- $\beta_i = 1$, if T_{mains} is best matched by T_i, considered 0 otherwise.
- $\gamma_i = m_c \sum_{j=1}^{i-1} \alpha_j$ - $m_d \sum_{j=i+1}^{N} \beta_j$
- $\delta_i = 1$, if $\gamma_i > 0$, otherwise considered 0.

The terms mentioned on the right hand side of equation C.1 will be described briefly. The α_i term represents the water inflow entering from the collector side loop into the segment of best matching temperature. The β_i term represents the T_8 inflow, or the inflow of cold water from the mains, into its segment of best matching temperature. δ_i term represents the resultant internodal flow into segment i, arriving from the segment above, i.e. *i - 1*. The fourth, or the $(1 - \delta_i)$ term represents the resultant internodal flow, flowing from a lower segment i, towards a higher segment, *i+1*. The last term of equation C.1, depicts the heat loss to the environment. It is important to note that γ_i is considered the resultant internodal flow. Which can be determined on addition of the various flows induced by the demand & collector loop. Equation C.1 represents a set of N, first order differential equations, which can further be solved for N segments of a storage tank, as a function of time t.

C.2 Figure of Merit (FOM)

Multinodel model for stratified thermal storage tanks discussed briefly in section **??**, uses a figure of merit for indicating the degree of stratification for a thermal storage tank [54]. Figure of merit, denoted by FOM, can be defined as the ratio between the actual energy stored in a tank, by the maximum possible energy that can be stored in the same, within a single charging cycle. Depicted by equation C.2 below. For FOM calculations, an initial, or starting tank temperature must be assumed. Denoted as T_0 in equation C.2, where T_c, also denoted as T_5 in section 5.7, represents the collector inlet temperature, & T_e is defined as the mean collector temperature for the storage tank.

$$FOM \equiv \frac{\overline{T_e} - T_0}{T_c - T_0} \quad \text{(C.2)}$$

Depicted by figure 5.6 as well, T_5 or T_c enters the tank at the top, displacing the water below, that leave the tank. Perfect stratification is a situation considered when there is no mixing of the energy stored within the tank,

and the entire tank is at one exact temperature. That is, all the water flowed out and was replaced by only the maximum possible inlet temperature, throughout the tank. In such a situation, the tank is considered to have a FOM = 1. Thus, as mixing does occur, FOM defined by equation C.2 is always less than one.

Appendix D

Computer Aided Renders

Before the experimental setup could be installed, Computer Aided Design (CAD) models for the same were prepared using SolidWorks, in order to attain accurate dimensions. The models were created keeping the roof dimensions from figure 4.2b in mind. Figure D.3 depicts the final computer aided render for the installation, including the entirety of the panels, pipe assembly and alucobond fixtures involved. Figure D.2 depicts a CAD render of the base of the test roof, depicting the aluminium mounting blocks, as well as the thermal absorber (pipe) schematic for the system. Figure D.1 helps depict a zoomed in view of the top portion of the setup, without alucobond panels.

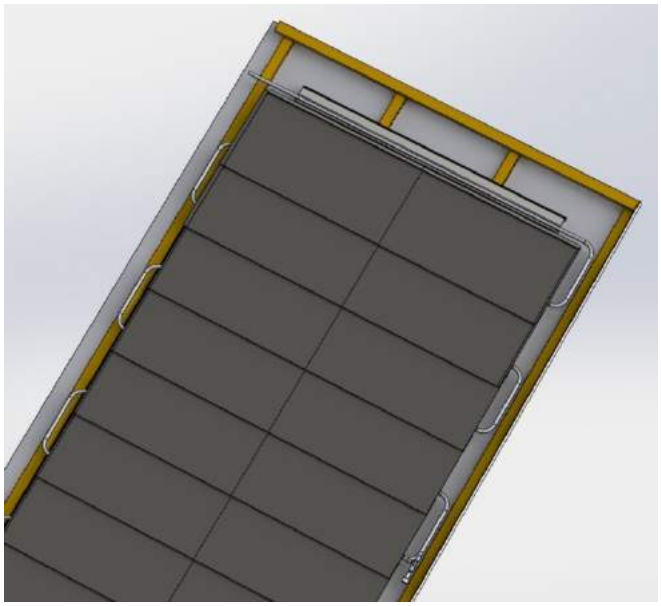

Figure D.1: Top view render with solar panels

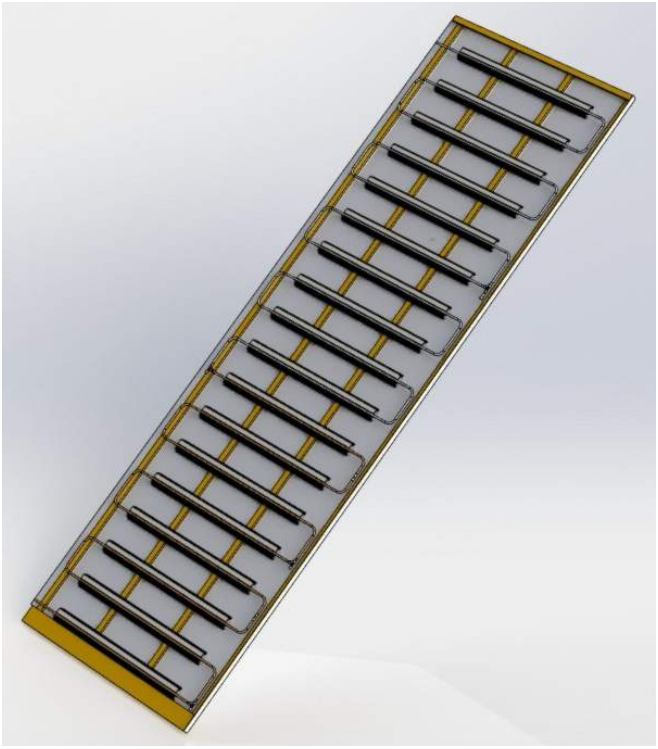

Figure D.2: Test roof base schematic

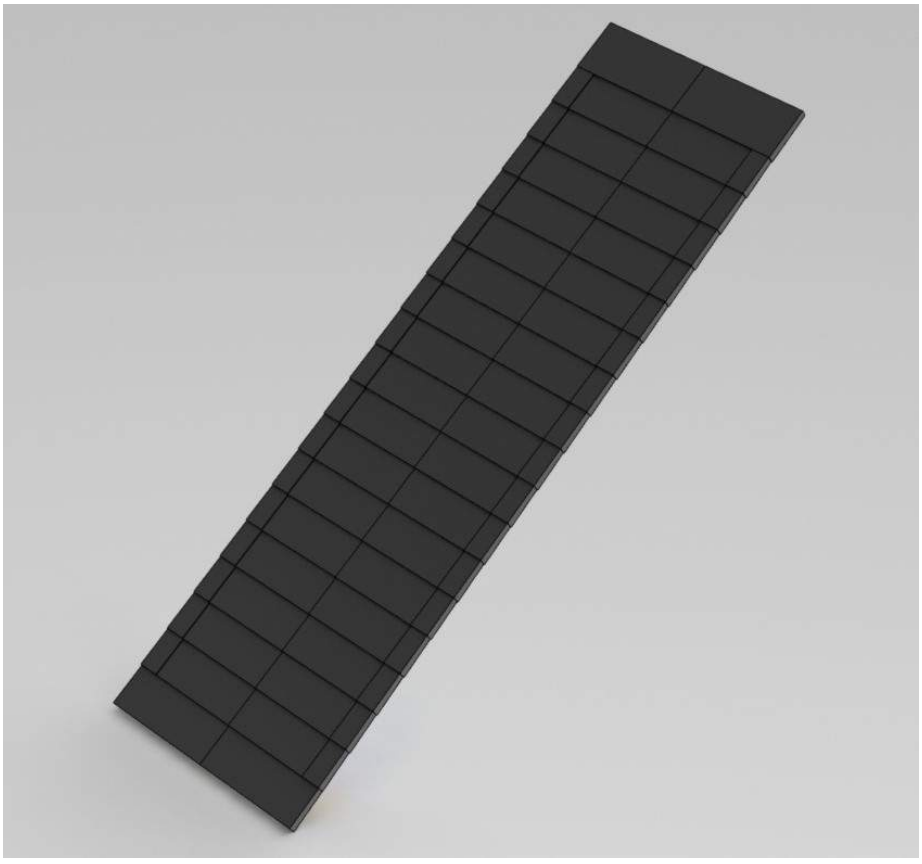

Figure D.3: Final CAD render

Appendix E

Datasheets

PV-T Panel™ EXASUN

MODULE SPECIFICATIONS		PV-T PANEL
Number of cells		10
		50 [W_p]
ELECTRICAL PERFORMANCE (STC)		
Module Efficiency	N_m [%]	18.5 %
Peak Power Output	P_{max} [W_p]	50
Maximum Power Voltage	V_{mpp} [V]	5.3
Maximum Power Current	I_{mpp} [A]	9.4
Open Circuit Voltage	V_{oc} [V]	6.7
Short Circuit Current	I_{sc} [A]	9.9
STC: Irradiance at 1000W/m2; Cell temp. 25 C, AM 1.5spectrum according to EN 60904-3		
ELECTRICAL PERFORMANCE (NOCT)		
Maximum Power	P_{max} [W_p]	37.1
Maximum Power Voltage	V_{mpp} [V]	4.6
Maximum Power Current	I_{mpp} [A]	8.1
NOCT: Irradiance at 800W/m2; Ambient Temp. 20. Wind speed 1.0 m/s		
COMPONENTS & DIMENSIONS		
Cell Type		PERC - Monocrystalline Silicon - Metal Wrap Through
Dimensions	mm	156.75 x 156.75
Module		Frameless BIPV Glass-Glass module
Dimensions	mm	820 x 430 (functional 820 x 330-350)
Weight	kg	6
Mounting		Rear side Mounting system
Frontside Glass		3.2 hardened ultra-clear glass (EN1863) AR coated & Structured
Back Side Glass		3.2 mm hardened glass
Diodes		1
Connector		MC 4
OPERATING CONDITIONS		
Max. Static Load Front	Snow	5400 Pa
Max. Static Load Back	Wind	2400 Pa
Max Hailstone Impact	mm at m/s	75 mm at 39.5 [m/s]
Temp Coefficient Power	P_{max}	-0.375 [%/K]
Temp Coefficient Voltage	V_{oc}	-0.294 [%/K]
Temp Coefficient Current	I_{sc}	+0.041 [%/K]
Operating Temperature range	°C	- 40 °C to 85 °C
Max System Voltage	V_{DC}	1000
Max Series Fuse Rating	A	12

Figure E.1: Exasun PVT Panel Datasheet

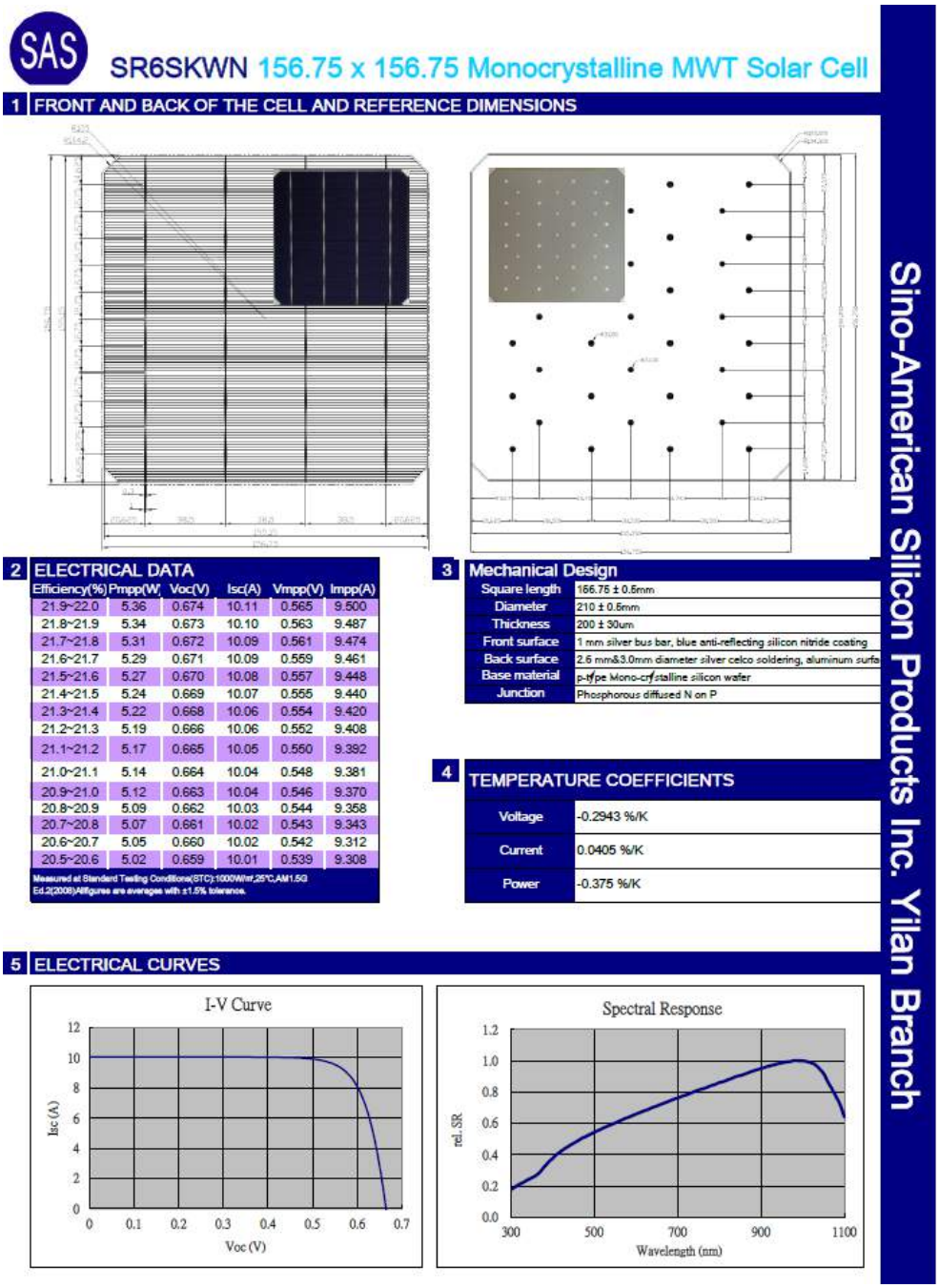

Figure E.2: MWT PERC Cell Datasheet

HENCO Multilayer Pipe PE-Xc/Aluminium/PE-Xc

HENCO with all the advantages of plastic and metal

- Butt welded aluminium pipe
- 100% oxygen-tight and water vapour diffusion tight
- Low coefficient of linear expansion, similar to metal pipe
- Entirely corrosion-resistant, also resistant against chemicals and electrochemicals
- Sound-insulation similar to entirely plastic pipe
- Electron beam crosslinked inner and outer pipe
- High resistance to pressure and temperature
- Smooth surface, less loss of pressure
- Light as plastic piping
- Flexible, easy to bend even at low temperatures, retains shape after bending

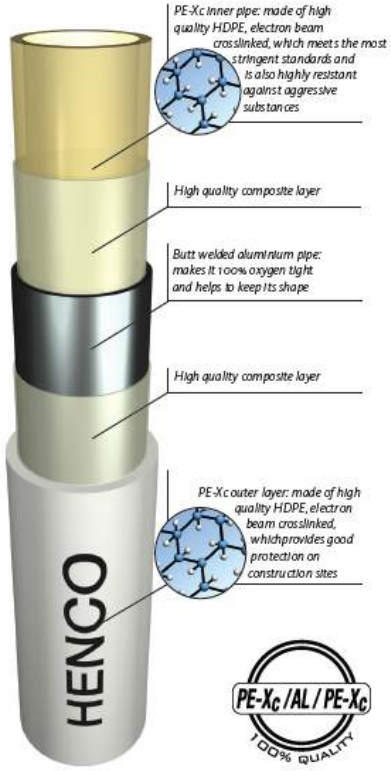

Technical Profile Henco Multilayer Pipe

Diameter (mm)	12	14	16	16 RIXc	18	18 RIXc	20	20 RIXc	26	26 RIXc	32	40	50	63	75	90
Inner diameter (mm)	8,8	10	12	12	14	14	16	16	20	20	26	33	42	54	63	76
Wall thickness (mm)	1,6	2	2	2	2	2	2	2	3	3	3	3,5	4,0	4,5	6	7
Max. working temperature (°C)	60	95	95	95	95	95	95	95	95	95	95	95	95	95	95	95
Max. working pressure (bar)	6	10	16	10	10	10	16	10	16	10	16	10	10	10	10	10
Thermal conduction (W/mK)	0,43	0,43	0,43	0,43	0,43	0,43	0,43	0,43	0,43	0,43	0,43	0,43	0,43	0,43	0,43	0,43
Linear expansion (mm/mK)	0,025	0,025	0,025	0,025	0,025	0,025	0,025	0,025	0,025	0,025	0,025	0,025	0,025	0,025	0,025	0,025
Minimum tensile strength of adhesive layer (N/10mm)	30	30	30	30	30	30	30	30	30	30	30	30	30	30	30	30
Surface roughness of inner pipe (µ)	7	7	7	7	7	7	7	7	7	7	7	7	7	7	7	7
Oxygen diffusion (mg/l)	0	0	0	0	0	0	0	0	0	0	0	0	0	0	0	0
Min. bending radius, manual/external spiral spring (mm)	5XDu	5XDu	5XDu	5XDu	5XDu	5XDu	5XDu	5XDu	5XDu	5XDu	*	*	*	*	*	*
Min. bending radius, manual/internal spiral spring (mm)	3XDu	3XDu	3XDu	3XDu	3XDu	3XDu	3XDu	3XDu	3XDu	3XDu	*	*	*	*	*	*
Degree of crosslinking (%)	60	60	60	60	60	60	60	60	60	60	60	60	60	60	60	60
Weight (kg/m)	0,084	0,108	0,125	0,101	0,132	0,118	0,147	0,129	0,261	0,252	0,39	0,528	0,766	1,155	1,516	2,155
Volume (l/m)	0,061	0,079	0,113	0,113	0,154	0,154	0,201	0,201	0,314	0,314	0,531	0,855	1,385	2,29	3,117	4,536

Figure E.3: HENCO Pipe Datasheet

Thermophysical properties of TYFOCOR® LS®
as a function of temperature

T [°C]	Density [kg/m³]	Specific heat capacity [kJ/kg·K]	Thermal conductivity [W/m·K]	Kinematic viscosity [mm²/s]	Cubic expansion coefficient [•10⁻⁵/K]	Vapour pressure [bar]
200	-	-	-	-	-	14.9
190	-	-	-	-	-	12.0
180	-	-	-	-	-	9.20
170	-	-	-	-	-	7.10
160	-	-	-	-	-	5.60
150	-	-	-	-	-	4.20
140	-	-	-	-	-	3.20
130	-	-	-	-	-	2.50
120	959	3.990	0.483	0.50	87	1.80
110	969	3.960	0.476	0.63	84	1.40
100	977	3.920	0.469	0.76	81	0.90
90	986	3.880	0.462	0.91	78	0.62
80	993	3.840	0.456	1.08	75	0.42
70	1001	3.800	0.449	1.32	72	0.29
60	1008	3.760	0.442	1.66	69	0.19
50	1015	3.720	0.434	1.91	66	0.12
40	1021	3.680	0.427	2.52	63	0.07
30	1029	3.640	0.420	3.40	59	0.04
20	1034	3.600	0.413	4.95	56	-
10	1040	3.560	0.406	7.90	53	-
0	1045	3.520	0.399	14.5	49	-
–10	1049	3.480	0.392	26.9	46	-
–20	1053	3.440	0.385	57.1	43	-

Figure E.4: TYFOCOR LS HTF Thermophysical properties

Thickness		Standards	Unit	3 mm	4 mm
Thickness of Aluminium Layers			[mm]	0.5	
Weight			[kg/m²]	5.9	7.6
Width			[mm]	1250 / 1500	
Technical properties					
Section modulus	W	DIN 53293	[cm³/m]	1.25	1.75
Rigidity	E·J	DIN 53293	[kNcm²/m]	1250	2400
Alloy / Temper of Aluminium Layers		EN 573-3 EN 515		EN AW 5005A (AlMg1) H22 / H42	
Modulus of Elasticity		EN 1999 1-1	[N/mm²]	70'000	
Tensile Strength of Aluminium		EN 485-2	[N/mm²]	$R_m \geq 130$	
0.2 % Proof Stress		EN 485-2	[N/mm²]	$R_{p0,2} \geq 90$	
Elongation		EN 485-2	[%]	$A_{50} \geq 5$	
Linear Thermal Expansion		EN 1999 1-1		2.4 mm/m at 100°C temperature difference	
Core					
Mineral-filled core with polymer adhesives					

Figure E.5: Tehnical Datasheet for ALUCOBOND A2

solaredge

SolarEdge Power Optimizer

Module Add-On for North America

P320 / P370 / P400 / P405 / P505

OPTIMIZER MODEL (typical module compatibility)	P320 (for high-power 60-cell modules)	P370 (for higher-power 60 and 72-cell modules)	P400 (for 72 & 96-cell modules)	P405 (for thin film modules)	P505 (for higher current modules)	
INPUT						
Rated Input DC Power[1]	320	370	400	405	505	W
Absolute Maximum Input Voltage (Voc at lowest temperature)	48	60	80	125	83	Vdc
MPPT Operating Range	8 - 48	8 - 60	8 - 80	12.5 - 105	12.5 - 83	Vdc
Maximum Short Circuit Current (Isc)	11		10.1		14	Adc
Maximum DC Input Current	13.75		12.63		17.5	Adc
Maximum Efficiency	99.5					%
Weighted Efficiency	98.8				98.6	%
Overvoltage Category	II					
OUTPUT DURING OPERATION (POWER OPTIMIZER CONNECTED TO OPERATING SOLAREDGE INVERTER)						
Maximum Output Current	15					Adc
Maximum Output Voltage	60			85		Vdc
OUTPUT DURING STANDBY (POWER OPTIMIZER DISCONNECTED FROM SOLAREDGE INVERTER OR SOLAREDGE INVERTER OFF)						
Safety Output Voltage per Power Optimizer	1 ± 0.1					Vdc
STANDARD COMPLIANCE						
EMC	FCC Part15 Class B, IEC61000-6-2, IEC61000-6-3					
Safety	IEC62109-1 (class II safety), UL1741					
RoHS	Yes					
INSTALLATION SPECIFICATIONS						
Maximum Allowed System Voltage	1000					Vdc
Compatible inverters	All SolarEdge Single Phase and Three Phase inverters					
Dimensions (W x L x H)	128 x 152 x 28 / 5 x 5.97 x 1.1		128 x 152 x 36 / 5 x 5.97 x 1.42	128 x 152 x 50 / 5 x 5.97 x 1.96	128 x 152 x 59 / 5 x 5.97 x 2.32	mm / in
Weight (including cables)	630 / 1.4		750 / 1.7	845 / 1.9	1064 / 2.3	gr / lb
Input Connector	MC4[2]					
Output Wire Type / Connector	Double Insulated; MC4					
Output Wire Length	0.95 / 3.0	1.2 / 3.9				m / ft
Operating Temperature Range	-40 - +85 / -40 - +185					°C / °F
Protection Rating	IP68 / NEMA6P					
Relative Humidity	0 - 100					%

[1] Rated STC power of the module. Module of up to +5% power tolerance allowed.
[2] For other connector types please contact SolarEdge

PV SYSTEM DESIGN USING A SOLAREDGE INVERTER[3][4]		SINGLE PHASE HD-WAVE	SINGLE PHASE	THREE PHASE 208V	THREE PHASE 480V	
Minimum String Length (Power Optimizers)	P320, P370, P400	8		10	18	
	P405 / P505	6		8	14	
Maximum String Length (Power Optimizers)		25		25	50[5]	
Maximum Power per String		5700 (6000 with SE7600H-US, SE10000H-US)	5250	6000	12750	W
Parallel Strings of Different Lengths or Orientations		Yes				

[3] For detailed string sizing information refer to: http://www.solaredge.com/sites/default/files/string_sizing_na.pdf.
[4] It is not allowed to mix P405/P505 with P320/P370/P400/P600/P700/P800 in one string.
[5] A string with more than 30 optimizers does not meet NEC rapid shutdown requirements; safety voltage will be above the 30V requirement

Figure E.6: Tehnical Datasheet for Solar Edge P405 Power Optimiser

Appendix F

Model Validation

F.1 Linear Curve interpolation

Figure F.1 below, provides the linear curve interpolation plot used for estimating the thermal coefficients for the steady-state and quasi-dynamic models.

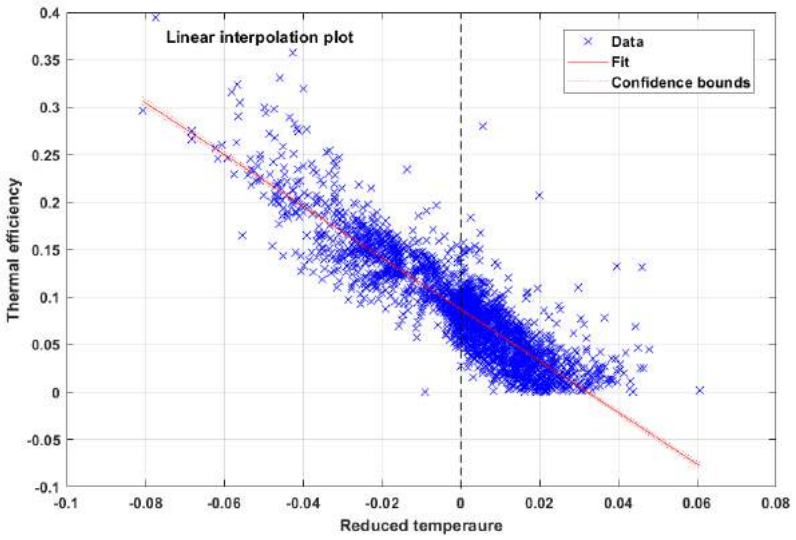

Figure F.1: Linear curve interpolation for Steady-state & Quasi-dynamic thermal models

Appendix G

Experimental Setup

G.1 Tools used for the experimental setup

- 2 x Drill with charger and spare battery
- 1 x Jigsaw
- 1 x Grinder
- 2 x Glue clamps
- 1 x Spirit level
- 1 x Pipe bender
- 2 x Saw
- 3 x Safety gloves & glasses
- 2 x Hammer
- 1 x Crow bar
- 1 x T-square
- 1 x Pipe cutter
- 2 x Measuring tape
- 1 x Vernier caliper
- Various screws & respective screw heads